LOW-LEVEL THERMODYNAMIC, KINEMATIC, AND REFLECTIVITY FIELDS OF HURRICANE BONNIE (1998) AT LANDFALL

A THESIS SUBMITTED TO THE GRADUATE DIVISION
OF THE UNIVERSITY OF HAWAI'I IN PARTIAL FULFILLMENT
OF THE REQUIREMENTS FOR THE DEGREE OF

MASTER OF SCIENCE

IN

METEOROLOGY

MAY 2004

By
Rebecca S. Schneider

Thesis Committee:

Gary M. Barnes, Chairperson
Thomas A. Schroeder
Yuqing Wang

ACKNOWLEDGMENTS

I am grateful to Dr. Gary Barnes, my advisor, for his insight and direction throughout this study. His enthusiasm for the project and the many hours he was available for discussion are greatly appreciated. I would also like to thank Dr. Schroeder and Dr. Wang for their comments and suggestions which helped improve this thesis. Steve Feuer, Peter Dodge, and Paul Leighton of the Hurricane Research Division (HRD) aided me greatly in accessing the dropwindsondes and the radar images. Shirley Murillo, also of HRD, has been a constant source of support. I am also indebted to Sam Houston for both his review of this manuscript and his guidance. Thank you to Jamie Rhome for his editorial comments when I had just begun to write, and for his support.

A special thank you is extended to my parents, Stewart and Frankie, and my sister, Jessica, and her husband, Petter. I wish to thank my fellow graduate students, Klaus Dolling, Eric Lau, Bunmei Taguchi, Luis Bejarano, and Chueh-hsin Chang for their friendship and support. A final thank you goes out to all my friends who made my stay in Honolulu that much more memorable.

ABSTRACT

Eighty-five dropwindsondes were deployed from two NOAA WP-3D aircraft over nearly eleven hours on August 26th, 1998, prior to and during Hurricane Bonnie's landfall. During this study Bonnie's MSLP did not vary by more than 3 hPa from 964 hPa. The dropwindsondes are used to establish storm-relative composites of temperature, humidity, equivalent potential temperature, radial winds, and tangential winds at various horizontal levels from 10 m to 2 km altitude. Aircraft radar as well as the WSR-88Ds at Morehead City and Wilmington, North Carolina provide reflectivity fields.

The low-level kinematic, thermodynamic, and reflectivity fields are examined to determine if the hurricane structure is affected by the proximity of land. The greatest asymmetries in thermodynamics are found at large radii from storm center (~1.5 degrees latitude) where the offshore flow is warmer, drier, and more stable than the onshore flow. Closer to storm center the fields are more symmetric. The radial winds indicate strong inflow to the southwest of storm center, with outflow to the northeast from the surface upward. Bonnie's tangential winds reveal a large radius of maximum winds, averaging just under 80 km. Reflectivity fields change little in the onshore flow, yet a suppression of high reflectivity is evident beyond the eyewall in the offshore flow.

I will use the thermodynamic, kinematic, and reflectivity fields to infer that Bonnie's outer portions were affected by the proximity to land yet her intensity did not change as the flow became more homogenized near the eyewall.

TABLE OF CONTENTS

LIST OF FIGURES

LIST OF APPENDICES

CHAPTER 1:

INTRODUCTION

1.1 Background

A tropical cyclone's (TC) survival depends on the surface sensible and latent heat fluxes it receives into its boundary layer from the ocean. Once a TC makes landfall, these fluxes are greatly reduced, boundary layer energy diminishes, and the TC decays. Changing the underlying surface from sea to land has a strong negative impact on the intensity of the TC circulation. This invites a question – does the nearness of land affect a hurricane prior to landfall?

Little is known about how the proximity to land affects the TC's boundary layer since it cannot be routinely observed due to the complications of flying at low altitudes, especially over land. Coastal observation stations are also frequently disabled by the high winds and heavy rains of an impending TC. Offsetting this data shortage are the Global Positioning System (GPS) dropwindsondes, developed by the National Center for Atmospheric Research (NCAR), the National Oceanic and Atmospheric Administration (NOAA), and the German Aerospace Research Establishment, which collect data down to the ocean surface. These instruments may be deployed directly off the coast, but are not ordinarily released over land. The dropwindsondes are a new tool in identifying how the TC boundary layer responds to the proximity of land.

On August 26th, 1998, while Hurricane Bonnie was offshore of the Carolinas, two research flights from NOAA's Hurricane Research Division (HRD) were deployed. Spiral flight patterns were designed to document the hurricane's inflow in the first flight. There were 45 successful dropwindsondes, released from 1220 Z to 1800 Z. Capturing

the onshore and offshore flow along the coast was part of the second flight's mission. Forty dropwindsondes from this flight were successful. This second flight overlapped slightly with the earlier flight as data collection began at 1630 Z and ended at 2300 Z. According to Best Track (Jarvinen et al. 1984), which defines landfall when the eye crosses the coast, Bonnie made landfall near Wilmington, North Carolina at 0330 Z on August 27th. Additional data were provided by two coastal WSR-88Ds (Weather Surveillance Radar 88 Doppler) as well as from lower fuselage radar on both aircraft. The dropwindsonde and radar data will be used to identify the thermodynamic and kinematic structure of the hurricane as well as differences between the onshore and offshore flows within 300 km of the TC circulation center. This is the portion of the TC where the highest winds occur, and where changes in the thermodynamics might affect TC intensity.

1.2 Previous Work

Miller (1964) was the first to publish evidence that the primary mechanism for TC decay over land was not increased friction but loss of sensible and latent heat. Hurricane Donna's (1960) landfall in South Florida was well documented by a dense network of rawinsonde stations, aircraft flights at three levels and aircraft radar. Miller detected a 3 °C cooling within the storm center, and a 0.6 °C warming outside of a 40 nm radius as Hurricane Donna made landfall. Simultaneously, Hurricane Donna's pressure increased within the storm center and decreased slightly outside of a 40 nm radius. This revealed a change in the distribution of mass of the storm, as the warm air once concentrated near the core spread out over a larger area. Miller concluded that although increased surface roughness at landfall did reduce the circulation's surface winds, its decay was caused by

the loss of the ocean as a moisture and heat source. Dunion et al.'s (2003) reanalysis of Hurricane Donna's surface winds found that after landfall the storm's peak one-minute sustained surface winds were lower than those available in the National Hurricane Center's hurricane database archive. Houston and Powell's (2003) reanalysis of Hurricane Donna's landfall also noted that Miller did not adjust his wind observations to a common height, exposure, and averaging time. While these new studies question Miller's surface wind analysis, his argument that loss of sensible and latent heat causes TC decay prevails.

Previous studies have examined the thermodynamics and kinematics in the boundary layer of TCs over the ocean and have found these fields to be fairly symmetric about the circulation center. Barnes and Bogner (2001) used 130 Omega dropwindsondes (ODWs) from six Atlantic hurricanes to examine the surface (5 m) temperature fields. The dropwindsondes were nearly evenly distributed, with a slight favoring of the left front quadrant. They created a 5 m composite temperature and found the temperature field to be symmetric about the circulation center. Barnes and Bogner also composited hurricane temperature at upper levels (100 m, 200 m, 500 m, 1 km, 1.5 km, and 2 km) and found that the fields continued to be symmetric.

Bogner et al. (2000) suggested that over the ocean a hurricane has a fairly axisymmetric surface wind field at ranges beyond 75 km from the inner core. They analyzed the conditional instability and shear for six Atlantic hurricanes with the data set as described above for Barnes and Bogner (2001). They did not have surface observations since the ODWs cannot record wind speeds within 400 m of the sea surface. Bogner et al. adopted the work of Powell (1980) and assumed the 10-m wind is 80 % of

that found at 500 m. They found that shear values over the ocean from 1500 m to the surface were half of those over land, when compared to the previous studies of shear over land by Novlan and Gray (1974), and McCaul (1991). Shear within the lowest 1500 m increased with decreasing radius to the circulation center, from 2 m s^{-1} at 500 km to 8.5 m s^{-1} at 75 km. Bogner et al. noted that there was little difference in shear (1500 m to the surface) between quadrants, emphasizing the symmetry of the hurricane's wind field over the ocean.

Black and Holland (1995) examined the thermodynamics and kinematics of TC Kerry's (1979) boundary layer when it was over the Coral Sea and found that these fields were asymmetric. They concluded that these asymmetries were primarily due to the TC interacting with the environmental flow as well as to a cold tongue of SST created by the translating storm. TC Kerry was a slow-mover in the midst of a clockwise loop when it was observed. Black and Holland argued that asymmetries in both thermodynamics and kinematics may exist in the boundary layer of a TC over the ocean given certain conditions.

Powell (1982) studied Hurricane Frederic (1979) as it came ashore on the Alabama-Mississippi Gulf Coast. Winds were altered at the surface (10 m), but the winds at 500 m showed little change. The result is that shear was modified substantially by the presence of land. At landfall Powell also found enhanced convergence to the right of track and enhanced divergence to the left of track. These asymmetries indicate that the land surface modified the hurricane's circulation.

Powell (1987) found asymmetries in the surface wind field of Hurricane Alicia (1983) when she made landfall in the Galveston area. Analysis of aircraft, surface station

and buoy data revealed that Alicia exhibited surface convergence, an inflow maximum, and a rainfall maximum in the offshore flow. The location of the inflow maximum may be explained by the southwesterly environmental flow, which paralleled the southwest-northeast orientation of the coastline. Powell argued that many factors including environmental flow, land-sea surface roughness difference and storm translation were responsible for the asymmetries in Alicia's surface wind field.

Powell et al. (1991) examined the asymmetries in Hurricane Hugo's (1989) surface wind field at landfall upon the South Carolina coast. They created two storm-relative analyses of Hurricane Hugo's surface winds at landfall: one over the ocean, and the other over land. The winds over the ocean came from flight level winds reduced to the surface, and oceanic platforms. The winds over land came from the few available surface stations, and flight level winds reduced to the surface where land stations were sparse. The wind reduction from flight level to the surface differed over land and over ocean. Merging the two analyses identified a discontinuity at the coastline. Hurricane Andrew's (1992) landfall in South Florida revealed a similar discontinuity in surface winds (Powell and Houston 1996). This discontinuity marks a transition zone where the oceanic flow adjusts to the land surface, and the land flow adjusts to the ocean surface. The width of this zone remains unknown. A similar discontinuity was observed in Hurricane Belle (1976) as she made landfall across Long Island (Sethu Raman 1979). Prior to landfall the hurricane was already weakening. Three observing stations located 100 m inland, 10 km inland, and 18 km inland, collected data as Belle made landfall. These surface stations revealed that the mean onshore wind speed at the coast was four times greater than that 18 km inland. All of these studies identified a difference in wind

speed from over the ocean to over land, indicating that land has produced these asymmetries.

Numerical studies have been used to examine the landfall and decay of TCs. Tuleya and Kurihara (1978) examined the effect land has on a mature TC making landfall. Their definition of landfall is the instant when the center of a TC encounters land. They used a three-dimensional, primitive equation model with 11 levels, four of which were located in the boundary layer. The basic landfall experiment excluded any topography or evaporation over land. The model neglected any advection of cold or dry air from the land. After landfall the radial winds increased between a height of 100 and 900 m, while the tangential winds decreased. The TC's most rapid filling did not occur at the time of landfall, but five hours later.

Later Tuleya (1994) used a triply nested version of the Geophysical Fluid Dynamics Laboratory (GFDL) model to determine why TCs do not form over land, and what causes their decay. He isolated the effects of surface wetness, surface roughness and subsurface thermal property. The model was initialized based on the development of Hurricane Gloria (1985) with low-level winds of 28 m s^{-1} and a central surface pressure of 996 hPa. A land-only simulation with high vorticity, low surface roughness and wet surface conditions failed to develop a tropical storm when a realistic soil subsurface moisture content was introduced. The land-only simulation revealed that neither surface roughness nor surface dryness could explain why a storm could not develop over land. In this simulation a cool pool of surface air developed near the TC's core associated with the model's cool ground temperature. This resulted in a decrease in evaporation which prevented storm development over land. The landfall simulation came to this same

conclusion. Tuleya's work supports the findings of Miller (1964) who argued that lack of evaporation was the cause of Hurricane Donna's (1960) dissipation.

Kepert (2002) analyzed 30 dropwindsondes released in 1998 in Hurricane Mitch while the storm was 85 km offshore. Mitch displayed large asymmetries in the near eyewall region (15 to 40 km radius from the storm center). The strongest inflow existed in the left rear quadrant in the lowest 1.2 km. The strongest tangential winds at any level were found one quadrant downstream of the strongest inflow. Kepert concluded that these asymmetries were largely due to the proximity of land. This agreed with a model run whereby the inclusion of land (increased friction) led to the wind asymmetries observed in Mitch. His finding indicates that a hurricane's wind field may be impacted by a land surface even while it is offshore. Kepert's work supports that of Powell (1982, 1987), Powell et al. (1991), and Powell and Houston (1996), who found asymmetries in the wind field as a hurricane neared the shore or made landfall.

1.3 Goals

I will examine the GPS dropwindsondes released during two flights on August 26th, 1998 as Hurricane Bonnie made landfall on the North Carolina coastline. The dropwindsonde observations will enable me to produce composite maps of the hurricane's thermodynamics and kinematics at multiple levels. The lower fuselage and land station radar provide short-term evolution of given features. The composite maps will determine the degree of asymmetry in the lowest 2 km that Bonnie experienced at landfall and to what depth this asymmetry existed. I have chosen a 2 km depth to represent the boundary layer because this depth includes any surface and mixed layers as

well as the bulk of the inflow layer found in a hurricane. I will also examine the synoptic conditions over land as Bonnie nears the coast.

To the author's knowledge this study marks one of the first times that multiple fields of thermodynamic and kinematic variables of a TC at landfall have been produced. Asymmetries produced by the proximity of land have the potential to modify the intensity, rainfall patterns, and wind fields beyond the eyewall. Increasing our knowledge of how a TC responds to the nearness of land will provide forecasters with a greater understanding of what to expect once the TC makes landfall.

CHAPTER 2:
DATA AND METHODS

2.1 Experimental Design

2.1.1 Flight Plan

The first aircraft (42RF) flew at 3.7 km and released dropwindsondes in curved paths that mimic inflow trajectories to the eyewall (Fig. 1). Fifty-five dropwindsondes were released from 1220 Z to 1759 Z, and 45 of these were successful. Numerous dropwindsonde failures occurred during a fourth spiral flight pattern in the northeast quadrant of the storm. The flight pattern for the second WP-3D (43RF) was designed to capture the boundary layer wind structure for both the onshore and offshore flow. This aircraft flew at 2.5 km. The dropwindsondes were released in flight legs parallel to the coast to best document the winds on either side of the storm track (Fig. 2). Forty dropwindsondes released from the 43RF from 1628 Z to 2259 Z were successful.

2.1.2. Dropwindsonde Classification

Each dropwindsonde was classified as part of the onshore or offshore flow. This was determined by creating a storm-relative streamline analysis of the winds and then by adjusting the location of the storm center for each dropwindsonde. The streamline analysis was first conducted at 50 m to determine the most likely trajectory for each dropwindsonde at this lower level. Trajectories were determined to establish how long a dropwindsonde had been over the ocean or over land. Streamlines and trajectories are distinct, but when the storm is both steady and stationary the two become equivalent. During the experiment Bonnie did maintain a mean sea level pressure (MSLP) of ~ 964 hPa but was moving at about 4 m s^{-1}. This implies that with time, the streamlines will

depart more and more from a trajectory. Still, over short periods the streamlines provide the most likely trajectory of the air parcels.

In this scheme the dropwindsonde location at the 50 m level is moved upwind and parallel to the nearby streamlines to determine the path of the flow. The scheme cannot pinpoint the exact trajectory of the air parcels but can at least provide guidance as to where the air was. I use this analysis to estimate if a dropwindsonde is part of the onshore or offshore flow. A second streamline analysis conducted at 1 km yielded similar results to those at 50 m.

In a few cases the streamline analysis revealed that a dropwindsonde, which initially appeared to be part of the offshore flow, was actually part of the onshore flow that wrapped around the circulation center, without traveling over land. Figure 3 indicates if the air was part of the onshore flow, offshore flow, or neither.

2.1.3. Data Treatment

The composite method assumes that the storm remains in a near steady state. The dropwindsondes in this study were released from 1220 Z to 2259 Z on August 26th, 1998. During these 11 hours Bonnie's MSLP (from Best Track) did not vary more than 3 hPa, averaging 964 hPa. Bonnie's speed was approximately 4 m s^{-1} heading toward the NNW for the first seven hours of the experiment, then to the NNE for the remaining four hours. Compositing with respect to the moving circulation center was necessary to provide enough data for analysis. The dropwindsondes were composited with respect to storm center at 1730 Z, which is the mid-point of the dropwindsonde releases. At this time Bonnie was centered at 33.26 °N, 77.90 °W. Powell (1987) analyzed Hurricane Alicia's landfall using three eight-hour periods that represented before, during, and post-landfall.

Post-landfall the storm's pressure changes were not near steady-state, yet the wind and precipitation structure changed little. Bonnie's precipitation structure evolved slowly over the 11-hour composite, yet the pressure changes were minimal.

The dropwindsondes provided data for calculations of radial and tangential winds as well as numerous thermodynamic variables. The radial and tangential winds were computed as follows:

$$v_r = u_{rel} \cos\theta + v_{rel} \sin\theta$$

$$v_t = -u_{rel} \sin\theta + v_{rel} \cos\theta$$

Note that $u_{rel} = u_{sonde} - u_{storm}$, $v_{rel} = v_{sonde} - v_{storm}$.

Both the u and v components of the storm were determined by nine aircraft fixes from 0050 Z on August 26th to 0325 Z on the following day (Section 2.4.2). Positive radial wind (v_r) is away from storm center (outflow) and positive tangential wind (v_t) is cyclonic. Theta (θ) is the angle between the original coordinate system and the rotated coordinate system (Fig. 4). The thermodynamic variables are computed following the work of Bolton (1980).

2.2 Global Positioning System (GPS) Dropwindsonde

The GPS dropwindsonde was designed to provide better atmospheric measurements over data sparse regions. This instrument has a mass of almost 400 g, a 7 cm diameter and a 41 cm length. It is equipped with a pyramid-shaped parachute that opens once the dropwindsonde is released from the aircraft. The parachute stabilizes the instrument and slows its descent. The dropwindsonde's fall velocity is a function of pressure and slows to about 12 m s^{-1} by 1000 hPa.

Compared to the Omega dropwindsonde (ODW), the previous generation airborne instrument to vertically sample the atmosphere, the GPS dropwindsonde has many advantages. While the ODW could not estimate winds below 400 m, the GPS dropwindsonde provides winds down to the surface (Hock and Franklin 1999). The ODW could only achieve a vertical resolution of 150 m but the GPS dropwindsonde provides measurements every 7 m.

The GPS dropwindsonde is equipped with three state sensors. The Barocap, with 0.5 hPa accuracy, measures pressure via a silicon diaphragm through a change in capacitance which results in a pressure change. The humidity sensor, the H-Humicap, consists of two relative humidity capacitors and has an accuracy of 2 %. Temperature is measured by the Thermocap, a slow-responding sensor which causes a lag in temperature data. The Thermocap is accurate to 0.2 °C. Faster-responding temperature sensors were too fragile for the GPS dropwindsonde. The temperature lag is easily corrected in post-processing. To calculate velocity the dropwindsonde triangulates its position relative to many different GPS satellites in orbit. Typical errors for pressure and temperature measurements are 1.0 hPa and 0.2 °C, respectively. Errors for humidity usually average 2 %. Wind errors are 0.5 m s^{-1}.

2.2.1 Dropwindsonde Quality Control

The Atmospheric Sounding Processing Environment (ASPEN) program was used to process the dropwindsonde data. This software, developed at NCAR, accepts raw data from the dropwindsonde in the form of AVAPS (Airborne Vertical Atmosphere Profiling System) files. The Bonnie dropwindsondes were processed using the 2.2.1. ASPEN Version (18 July 2001). ASPEN is a recent development in dropwindsonde processors.

It was evaluated next to Editsonde, the Hurricane Research Division (HRD) dropwindsonde processor. The quality controlled data from ASPEN were similar to those from Editsonde. ASPEN produces x-y graphs with the raw data, the quality-controlled data, or both. Skew-T diagrams can also be produced.

ASPEN considers all variables separately for quality control. The exception is the GPS derived winds which are separated into u and v components. Should one of the two fail the quality control tests, both are discarded. ASPEN also requires a minimum of three satellites to compute wind observations. All of the variables pass through buddy checks, outlier checks, filter checks and smoothing. Details of these and the wavelengths used in the filter checks and smoothing are found in the ASPEN User Manual (http://www.atd.ucar.edu/rtf/facilities/software/aspen/AspenManual.pdf). The Thermocap's temperature time lag is also automatically corrected in ASPEN.

Despite the filtering of the raw data the corrections are not so exhaustive as to discard all suspicious data. Like Editsonde, ASPEN also produces some questionable post-processed data. One such error can occur in the lower levels of Skew-T diagrams where the air is saturated yet the lapse rate is dry adiabatic. Figure 5 demonstrates this effect in the layer from the bottom of the Skew-T diagram (973 hPa) to approximately 950 hPa. This error is likely due to the humidity sensor remaining wet after passing through cloud (Bogner et al. 2000). This can cause faulty relative humidity readings, which would result in spuriously high specific humidities as well as incorrect values of equivalent potential temperature. To determine how great of an impact these false readings might have I re-examined specific humidity and equivalent potential temperature at 200 m and below, where it is possible that the dropwindsonde is no longer

in cloud. I replaced all relative humidities of 100 percent (most of which were found in the core of the storm) with values of 95 percent, which may be considered a conservative value for the mixed layer. Then, I re-calculated specific humidity and equivalent potential temperature. The new values of specific humidity were approximately 1 g kg^{-1} lower than the original values while the values of equivalent potential temperature were 3 to 4 K lower than the original values. I will use the modified values of specific humidity and equivalent potential temperature in this thesis.

2.3 Aircraft and Land-based Radars

Both WP-3D aircraft have lower fuselage radar. The lower fuselage radar scans horizontally with a wavelength of 5.6 cm (C-band) and provides plan views of the hurricane. Its beam width is 1.1° in the horizontal and 4.1° in the vertical. This large vertical beam width often causes inadequate beam filling, especially at ranges greater than 60-90 km (Marks, 1985). Radar snapshots are also plagued by attenuation and aircraft pitch and roll. Compositing lessens these effects to provide a more complete view of the storm. Still, composites must be scrutinized as a cell moving at a speed of 40 m s^{-1} over 15 minutes will have traveled 36 km. In this experiment fifteen minute composites were assembled from the plan views of the lower fuselage radar. This period is short enough to avoid excessive stretching of convective scale features into the mesoscale.

Two Weather Surveillance Radar (WSR) 88Ds, at Wilmington (KLTX) and Morehead City (KMHX) (Figs.1 and 2) collected images as Bonnie neared landfall. These Doppler radars have a wavelength of 11.1 cm (S-band) and a beam width of 0.93°.

The radar pictures can be used to study the evolution of the TC, both on a storm-scale and a convective scale. Radar also provides a broad view of where the dropwindsonde traveled on its descent, and if it entered or exited a given feature (e.g., the eye, eyewall, or rainband). These images may also be used to dispute or accept questionable data collected by a dropwindsonde.

2.4 Hurricane Bonnie

2.4.1. Overview

Hurricane Bonnie began as a tropical wave passing over Dakar, Senegal on August 14th, 1998. The tropical wave moved west-southwesterly and became a tropical depression at 1200 Z on August 19th. Twenty-four hours later the system strengthened and became Tropical Storm Bonnie. Tropical Storm Bonnie traveled along a west-northwesterly track and became a hurricane at 0600 Z on August 22nd. Hurricane Bonnie's complete track is shown in Figure 6. The hurricane's MSLP of 954 hPa was recorded 280 km east of San Salvador in the Bahamas at 0000 Z on the 24th of August with winds of 50 m s^{-1}.

Bonnie's eye passed east of Cape Fear, North Carolina (34.3 °N, 77.9 °W) at 2130 Z on August 26th. By this time the hurricane had slowed down and taken a more northeastward path. According to Best Track, Bonnie made landfall at 0330 Z near Wilmington, North Carolina (34.4 °N, 77.7 °W) with maximum 1-minute surface winds of 48 m s^{-1}.

2.4.2 Track

Nine aircraft fixes of the hurricane's center from 0050 Z on August 26th until 0325 Z on the 27th reveal Bonnie's track. At the beginning of the study the circulation center was approximately 153 km offshore. Best Track, as seen in Figure 6, could not be used to plot the hurricane's path for this thesis as it is only available every six hours and the dropwindsondes were deployed over 11 hours. Plotting the fixes versus time (Fig. 7) indicate that the storm's meridional speed (v) was constant at 4.0 m s^{-1} while its zonal speed (u) changed from easterly to westerly as the storm neared the coast. The hurricane's zonal speed varied from -1.3 m s^{-1} at the time of the first dropwindsonde release to +0.8 m s^{-1} at the release of the last dropwindsonde. The change from a northwesterly to a northeasterly route occurred at approximately 1900 Z on August 26th. At this time the storm center was closest to the coastline, only 50 km offshore.

Despite choosing the best fit for the storm track, four dropwindsondes close to the circulation center were revealed to be in the wrong storm-relative quadrant. Their position errors ranged from 3 km to 18 km. The two dropwindsondes with the largest position errors (17 and 18 km, respectively) were deployed just after the 16 hour mark from the first aircraft fix of Bonnie's track (Fig. 7). As shown on Figure 7 the closest aircraft fix to the time of these two dropwindsonde releases was at least three hours. It is possible that Bonnie's actual path departed from the best fit track that I used during this time, resulting in the larger position errors for these two dropwindsondes near the circulation center. Kepert (2002) exposed the perils of misplaced dropwindsondes when calculating radial winds. His example involved a dropwindsonde located at a 25 km radius with tangential winds of 75 m s^{-1}. A mere 2 km position error resulted in a bogus

radial wind of 6 m s^{-1}. As such, these misplaced dropwindsondes have been eliminated from the analysis.

CHAPTER 3:

RESULTS

3.1 Reflectivity Structure

Bonnie exhibited a large eyewall (~ 80 km) that often merged with surrounding rainbands. The storm's eyewall is collocated with the RMW, based on aircraft wind observations. Samsury and Zipser's (1995) analysis of 787 radial legs flown in 20 Atlantic tropical cyclones revealed a mean RMW of 37.2 km. Bonnie's RMW is twice as large. Bonnie also featured cells in the eye with high reflectivities (> 38 dBZ) that reached heights of 16 km. Animation of the WSR-88D images indicated that cells entered Bonnie's eye after breaking off from the inner eyewall. The cells in Bonnie's eye and the large RMW are apparent in the hourly radar snapshots taken by the Wilmington and Morehead City WSR-88Ds (Figs. 8a-g).

The 1400 Z radar image (Fig. 8a) reveals that Bonnie's northernmost eyewall was over land at this time. This occurs 13 hours earlier than Best Track's landfall of the storm (0330 Z on Aug. 27). Best Track defines landfall at the time the storm center crosses the coast. The 1400 Z radar picture reveals that Bonnie has a greater number of rainbands to the north of the circulation center than to the south.

The remaining radar pictures (Figs. 8b-g) also reveal the asymmetry in rainbands as the northern half of the storm persistently features more rainbands than the southern half. The 1500 Z and 1759 Z pictures (Figs. 8b, e) also indicate several convective cells over land that do not move off the coast into the over ocean flow. These convective cells appear in radar images prior to 1400 Z. This series of radar pictures also demonstrate that as the rainbands come ashore neither their intensities nor their orientations change.

An aircraft radar composite (Fig. 9), which spans 30 minutes, reveals similar traits to those radar pictures taken by the WSR-88Ds. The top half of the figure is the 1815 to 1830 Z composite, the bottom half is the 1830 to 1845 composite. This combined composite provides a full view of the storm. (In the earlier composite the aircraft was flying in the northern part of the storm, while in the later composite it was flying in the southern portion.) The composite highlights the difficulty distinguishing between the eyewall and the rainbands. The northern half of the storm is much more convectively active with reflectivities of 45 dBz, than the southern half. The lack of reflectivity to the far southwest of the storm (Figs. 8a-g), is also evident. None of the echoes in the onshore flow are affected in intensity or orientation by crossing the coastline.

3.1.1 Changes in the eyewall

Figure 10 demonstrates that as Hurricane Bonnie approached land the eyewall radius decreased. The correlation coefficient (R^2) for a linear regression is 0.87. The figure includes measurements of Bonnie's eyewall from two WSR-88Ds (Wilmington and Morehead City) which provide data from 1100 Z to 2000 Z. The lower fuselage radar on the aircraft also provides data from approximately 1820 Z to 2100 Z. All three independent radars reveal a similar trend, as Bonnie's eyewall decreases from approximately 92 km at 1115 Z to 64 km by 2037 Z. This is a decrease of 2.5 km per hour.

The last WSR-88D radar snapshot is at 1957 Z and the last lower fuselage composite runs from 2245 to 2300 Z. During the period for which radar pictures are available this trend, of a decreasing eyewall, persists. One cannot conclude that the storm's proximity to land was responsible for this shrinking without examining earlier

radar pictures. It is clear, however, that the shrinking began before Bonnie's eyewall was ashore, which occurred at approximately 1400 Z.

Bonnie's MSLP (964 hPa) did not vary more than 3 hPa throughout the analysis. During this time the cells that break off from the inner eyewall do not form a new eyewall. As such, Bonnie's shrinking eyewall does not seem to follow Willoughby et al.'s (1982) concentric ring model.

3.2 Thermodynamic Structure

3.2.1 Temperature

Storm-relative composites of Hurricane Bonnie's temperature at 10 m, 500 m, and 2 km are seen in Figures 11-13. Given that these composites are with respect to the storm center the coastline has been omitted to avoid the impression of analyzing fields over land. Note that the Carolina coastline runs approximately southwest to northeast. At 10 m (Fig. 11) Bonnie's large warm eye is evident, with temperatures of at least 27 °C. Outside of the eye there is a region of cooler air, especially to the southwest of the circulation center, noted by a 25.5 °C contour. This is coincident with the location of the eyewall less than 80 km to the southwest of the circulation center. The total wind vectors on this figure reveal that some of this cooler air is being drawn toward the circulation center. Bonnie also features an atmospheric wake which is apparent in the right rear quadrant of the storm where temperatures fall below 25 °C. This region is collocated with the wake in sea surface temperature (Appendix A). Temperatures to the far southwest and far northeast (~1.5 degrees latitude radius) of the storm tend to increase. Bonnie's low-level inflow is not isothermal, which agrees with the work of both Cione et

al. (2000) and Barnes and Bogner (2001). The 50 m temperature plot (Appendix B.1.1.) supports the observations at 10 m.

By 500 m (Fig. 12) maximum temperatures in the eye are just over 25 °C. As at 50 m, the warm contours surrounding the circulation center have shrunk even more. The cool region around the circulation center persists (note the 22 °C contour to the southwest) and temperatures increase to the northeast and southwest of the storm. In contrast to the lower levels, the cool wake can no longer be detected and has likely blended with the cooler region surrounding the storm center.

The temperature at 2 km (Fig. 13) reveals that although the warm eye is visible, there is no cool region surrounding the circulation center or a cool wake to the right rear quadrant of the storm. There is also no indication of warmer temperatures to the far northeast and far southwest of the circulation center. Instead, slight cooling is seen to the far northeast of the storm center, with temperatures falling below 14 °C.

The cooling that was seen around the circulation center is limited to the lowest 1 km. This cooling is collocated with the position of the eyewall and rainbands, as identified on the WSR-88Ds. This infers that the cooling may be attributed to downdrafts.

If downdrafts are responsible for the cooling around the circulation center one must consider that the lower the cloud base, the weaker the potential cooling. Typical cloud base heights may be 300 m or lower in the eyewall of the hurricane. Assuming the parcel is brought down moist adiabatically (~ 6.5 °C km^{-1}), the parcel will have cooled by 2 °C. From cloud base to the surface the environmental temperature (following a dry adiabat) will have cooled off by 3 °C, giving a 1 °C gradient. This is sufficient for the

cooling seen around the circulation center of the storm. Downdrafts likely play a role in the cooling seen in the region surrounding the storm's center, yet are they solely responsible for this cooling?

The evaporation of sea spray is ruled out as a factor responsible for any cooling around Bonnie's circulation center since the average relative humidity in this region exceeds 90%. Andreas (1995) performed model calculations of the evaporating temperature of a spray droplet as a function of its initial radius, the surface-water salinity and the ambient temperature and relative humidity. He demonstrates that the evaporating temperature of the spray droplet is very close to the ambient temperature (30 °C) at high relative humidities (> 90%) (his Figure 2). Even if evaporation was possible in this cool region, the cooling effect would be negligible. Cooling by evaporation of sea spray may play a role in other regions of the storm.

At 10 m temperatures in Bonnie's offshore flow fall from 28 °C to 26 °C as one moves closer to the storm center (Fig. 11). Relative humidities (%) in this region range from the upper sixties to the upper eighties. Reflectivity in this region depicts either no precipitation, or light precipitation, preventing downdrafts from being responsible for the cooling. Evaporation of sea spray is possible in this region and is likely responsible for the cooling in the offshore flow.

Plots of Bonnie's temperature against given wind speeds at 10 m and 50 m (Fig. 14a, b) display a considerable amount of scatter. Figure 14a (10 m) indicates low speeds and warm temperatures in the eye, then as speed increases, temperature increases. The temperature reaches a maximum at about 17 m s^{-1}, then falls. At 50 m (Fig. 14b) the maximum temperature is also reached at about 17 m s^{-1}, followed by a plateau before

temperatures fall. These results are similar to the work of Korolev et al. (1990) who gathered hourly observations in autumn 1988 for 18 days at a point (13 °N, 114 °E) in the South China Sea. During this time tropical storms Tess and Skip crossed the observation point. Korolev et al. found that the temperature gradient between the sea surface and the air increased once wind speeds surpassed about 17 m s^{-1}. They suggested that this large gradient was caused by decreasing air temperatures due to sea spray evaporation. My results differ from those of Korolev et al. since my observations (Figs. 14a, b) show that at higher speeds (>30 m s^{-1}) temperature levels off, and even slightly increases while Korolev et al. show an increasing temperature gradient at higher speeds. Overall, the cooling around the center of Bonnie's circulation is likely due to downdraft cooling while the cooling in Bonnie's offshore flow is likely due to sea spray evaporation.

The offshore flow (northwest of storm center) is 1 °C warmer than the onshore flow (southwest of storm center) at 1.5 degrees radius from storm center. This difference exists from 500 m and below. In this study, the dropwindsonde release period began at 8:20 am LST and ended at 7:00 pm LST. Evidently, radiative effects were not strong enough to enhance the temperature difference between the onshore and offshore flow.

3.2.2 Specific Humidity

Hurricane Bonnie's 10 m specific humidity (Fig.15) reveals a moist core with values equal to or greater than 21.5 g kg^{-1}. The air is noticeably drier to the southwest of the circulation center (<15 g kg^{-1}) than to the northeast. The 10 m total wind vectors on this plot indicate that as the air moves offshore (southwest of the circulation center) there is a moistening of the flow as the air moves toward the eye, from values of just over 18 g kg^{-1} to values exceeding 21 g kg^{-1}. There also appears to be some moistening of the onshore flow, noted by the 20 g kg^{-1} contour north of the circulation center. The 50 m plot of specific humidity (Appendix B.2.1.) is consistent with the 10 m plot.

By 500 m (Fig. 16) the values of specific humidity around the circulation center have decreased slightly (from 21.5 g kg^{-1} to 21 g kg^{-1}), yet overall the trend is similar to that at lower levels. Drier values are seen to the southwest than to the northeast of the storm center, with less asymmetry to the northwest or southeast of the circulation center. By 2 km (Fig. 17) the specific humidity difference to the southwest and northeast of the storm center fades although the storm still displays a moist core.

There is a considerable difference in specific humidity between the onshore and offshore flow, with the offshore flow approximately 4 g kg^{-1} drier at a radius of nearly 200 km from the storm center at 10 m. At this same level, at a radius of just over 100 km from storm center, the offshore flow is about 2 g kg^{-1} drier than the onshore flow. The offshore flow continues to be drier than the onshore flow until a height of 1 km, when this difference becomes less noticeable. By 1.5 km the specific humidity field is symmetric about the circulation center. Clearly, specific humidity has shown a greater onshore/offshore difference than the temperature field.

3.2.3 Potential Temperature

Potential temperature vertical profiles were used to establish approximate mixed layer heights relative to the storm center (Fig. 18). The highest mixed layer heights (ranging from 600 m to upward of 1 km) were located off the coast of South Carolina. Figure 19a displays the vertical profile of θ from a dropwindsonde 9 km off the South Carolina coast, in the offshore flow. The mixed layer height extends to 900 m. Shallow mixed layer heights (~100 m) were located around the eye, corresponding to convection. Similar mixed layer heights were found in the wake of the tropical cyclone. A vertical profile of θ from a dropwindsonde in Bonnie's wake is stable from the surface upward (Figure 19b). Similar to the θ profile in the wake of the storm, immediately off the coast in the onshore flow the mixed layer was shallow, or non-existent. Figure 19c displays the θ profile from a dropwindsonde 7 km off the coast in the onshore flow. The profile is stable from the surface upward. Farther away from the circulation center, to the far northeast or southwest mixed layer heights are closer to 300 m (Fig. 19d).

3.2.4 Equivalent Potential Temperature

Plots at 10 m (Fig. 20) and 50 m (Appendix B.4.1.) of Bonnie's equivalent potential temperature (θ_E) reveal a maximum surrounding the storm's core of 370 K. Values decrease with distance from storm center, but are not symmetric. At the eyewall the difference in θ_E is about 4 K between the flow to the southwest (~ 358 K) and that to the northeast (~ 362 K). Farther to the southwest of the storm center (just over 1.5 degrees latitude) θ_E decreases to below 346 K, while to the northeast of storm center values only decrease to below 358 K (50 m), or 354 K (10 m).

Maximum θ_E is again found around the core at 500 m (Fig. 21). Lower values continue to the southwest of the storm center, compared to northeast of storm center. By 2 km (Fig. 22) the highest values are still seen in the storm's core, to the east of the eye. The asymmetry seen in a southwest to northeast transect through the storm center is no longer apparent.

The highest values of θ_E were not found in the eyewall, but in the eye of the tropical cyclone. Previous work, such as that done by Jorgensen (1984) and Hawkins and Imbembo (1976) have also found that the highest values of θ_E exist in the eye of the storm. It is likely that as the air moves toward the storm center some of the high θ_E is mixed into the eye from the eyewall. Winds in Bonnie's eye are also sufficiently strong (>10 m s^{-1}) to allow for surface fluxes to continue supplying heat.

There is a distinction between the onshore and offshore values of θ_E. Onshore values tend to be higher, by up to 10 K, especially at lower levels. By 1.5 km the onshore/offshore difference diminishes. The vertical profiles of θ_E from two dropwindsondes in the onshore and offshore flow are displayed in Figures 23a and b. The greatest difference between the two profiles occurs at the surface, where the θ_E in the onshore flow is 10 K greater than the offshore flow. At 500 m the onshore flow continues to have higher θ_E, exceeding the offshore flow by 7 K. Near 1500 m the θ_E difference is roughly 2 K. At low levels the onshore flow displays higher values of θ_E, and thus moist static energy, than the offshore flow.

3.3 Atmospheric Stability

A modified Lifted Index (LI) was calculated to determine the stability of the low-level air in Hurricane Bonnie. This index was calculated at 800 hPa, versus the standard 500 hPa, since dropwindsondes were released from 700 hPa, or lower. Mean values of temperature and humidity in the lowest 500 m were used to calculate LI. This section examines meso-β asymmetries in LI.

A LI_{800} of -1.0 °C is typical for the Caribbean during hurricane season (July to October) based on the mean soundings presented by Jordan (1958). The storm-relative view of Bonnie's LI_{800} (Fig. 24) demonstrates that the low-level air is stable in the southern quadrants, with stability decreasing approaching the storm center. This region is coincident with the offshore flow, revealing that as the air approaches the circulation center it is destabilized. A LI_{800} maximum approximately 80 km northeast of the circulation center is collocated with the northeast eyewall as seen in the WSR-88D radar images (Fig. 8). The stability in this region may be attributed to convective downdrafts, transporting cooler air to lower levels. This region of the storm also features outflow at 800 hPa. Warm air is likely being drawn out over the cooler lower levels of the atmosphere, stabilizing the region. Farther to the north of the storm center, the index shows increasingly unstable air, where rainbands exist in the onshore flow. Recall that Bonnie's northern half featured a larger area of high reflectivity (> 38 dBZ) than her southern half (Figs. 8 and 9). The onshore flow is unstable save for regions where downdrafts are present.

The LI_{800} indicates that the offshore flow is more stable than the onshore flow. This supports the higher mixed layer heights in the offshore flow, relative to the lower

heights in the onshore flow (Fig. 18). Analysis of radar pictures also shows a void of higher reflectivities in the offshore flow collocated with these higher mixed layers.

Bonnie's LI_{800} is more stable than typical tropical LI_{800} during the hurricane season. This agrees with the prior work of Bogner et al. (2000) who found near neutral stability in six Atlantic hurricanes within 75 km from the eyewall. Further, Emanuel's (1986) modeling work has shown that tropical cyclones may be maintained without conditional instability of the surrounding air.

3.4 Kinematic Structure

3.4.1 Radial Winds

The storm-relative radial winds at 10 m, 50 m, 500 m, and 2 km (Figs. 25-28) reveal a sharp asymmetry. Maximum inflow exists to the southwest of storm center, in the offshore flow, while outflow is seen on the storm's east-northeast side.

At 10 m (Fig. 25) the strongest inflow is to the southwest of the storm center, with values in excess of 20 m s^{-1}. This strong inflow coincides with the location of the eyewall as identified by reflectivity features. At 50 m (Fig. 26) and 500 m (Fig. 27) this inflow region shows an anticyclonic rotation with height. Kepert (2002) also found an anticyclonic rotation of Hurricane Mitch's (1998) maximum inflow. At both 50 m and 500 m in Hurricane Bonnie the maximum inflow has increased to over 25 m s^{-1}. Simultaneously, an outflow region persists from the 10 m level upward, expanding with height. Both inflow and outflow exist at these low levels, suggesting the storm's eye is well ventilated. Air does not remain trapped in the eye for long periods.

By 2 km (Fig. 28) outflow dominates most of the storm with the highest values to the east of the storm center. The only remaining inflow is weak (~ 5 m s^{-1}) and south of the storm center.

Bonnie's strong radial asymmetry may have many different causes. Shapiro's modeling work (1983) examined the effect of storm speed on radial flow and found that the greatest inflow in slow moving hurricanes (translation speed $\leq$ 5 m s^{-1}) was located in the right front quadrant. Once the translation speed increased ($\geq$ 10 m s^{-1}) the inflow maximum remains in the right front quadrant, but expands to the north and east of the storm center. The observational study by Shea and Gray (1973) agrees with Shapiro's work. Their 900 hPa radial wind composite from 533 radial flight legs also reveals maximum inflow in the right front quadrant. While Bonnie's speed (~ 4 m s^{-1}) is similar to Shapiro's slow-moving storm, the maximum inflow is found to the left rear of the storm, not the right front. The organization of convection can also explain radial wind asymmetries. Powell's (1982) analysis of Hurricanes Frederic (1979) at landfall revealed maximum inflow angles (actual radial winds were not calculated) in the right front quadrant of the storm which agreed with the radar reflectivity that showed most of the convection on the leading edge of the storm. Overall, Hurricane Bonnie's northern half displayed more reflectivity than her southern half, and maximum inflow was found to her left rear quadrant. Examination of the reflectivity solely around Bonnie's eyewall reveals that initially the highest reflectivities are seen in the left quadrants, then shift to the storm's right rear quadrant with time (Figs. 8a-g). While Bonnie's highest radar reflectivities in the eyewall are not perfectly collocated with the maximum inflow, the

two pictures are on different time scales; a single snapshot (radar) versus a composite (radial wind figure).

The orientation of the environmental flow as well as the nearness to land may also create radial wind asymmetries. Hurricane Alicia's (1983) inflow maximum in the offshore flow (left front quadrant) is explained by the southwesterly environmental flow (~ 4 m s^{-1}) which paralleled the orientation of the coastline. Hurricane Bonnie's low-level environmental flow, as identified by NCEP/NCAR reanalysis data, was negligible in magnitude and likely not responsible for the strong radial inflow in the offshore flow. The storm's proximity to land can also create asymmetries in the radial flow. Kepert (2002) analyzed Hurricane Mitch (1998) and found the strongest inflow in the eyewall region to the left rear of the storm, similar to Hurricane Bonnie. Kepert concluded that even though Mitch was 85 km offshore at the time of the study, the maximum inflow was due to the nearness of land. Mitch tracked south, making landfall nearly perpendicular to the coast. While land remains a possibility for contributing to Bonnie's maximum inflow in the left rear quadrant, my study cannot make this declaration. Hurricanes Bonnie (MSLP ~ 964 hPa) and Mitch (MSLP ~ 930 hPa) were dissimilar in that Bonnie's intensity was constant during the study, while Mitch had begun to fill. Further, Mitch was about to encounter the mountainous terrain of Honduras, while Bonnie's landfall occurred on the flatter grounds of the Carolina coastal region.

3.4.2 Tangential Winds

Bonnie's tangential wind speed at 10 m, 50 m, 500 m, and 2 km can be seen in Figures 29-32, respectively. At 10 m (Fig. 29) the strongest winds only exceed 30 m s^{-1}

in an annulus around the eyewall. The weakest tangential winds at this level are found to the south of storm center as well as to the southwest of storm center, in the offshore flow.

By 50 m (Fig. 30) wind speeds have increased to just over 40 m s^{-1} in a small area to the northeast of the circulation center, on the outskirts of the eyewall. Winds continue to be weak (~ 15 m s^{-1}) to the southwest of storm center, in the offshore flow. At 500 m (Fig. 31) there are two areas of maximum winds (> 45 m s^{-1}) found to the northeast and southwest of the storm center. Minimum winds speeds (< 20 m s^{-1}) are found surrounding the core and to the far south and far northeast of storm center. In the offshore flow, to the southwest of storm center, winds are also light (~ 25 m s^{-1}). At 2 km (Fig. 32) the region of strong winds (≥ 40 m s^{-1}) to the southwest of the circulation center expands and coincides with the location of the reflectivity features labelled the eyewall. Examination of southwest to northeast, and southeast to northwest transects through the storm center reveals that the winds are weakest in the southern legs of the transects at the lower levels (10 m, 50 m, 500 m), yet by 2 km the strongest winds are found in these regions. At these lower levels the offshore flow is slightly weaker (~ 5 m s^{-1}) than the onshore flow at a radius of 1.5 degrees latitude from storm center.

None of the horizontal maps of tangential wind exhibit any contours lower than 15 m s^{-1}. According to the relative vorticity equation,

$$\zeta_r = (V_\theta / r) + (\partial V_\theta / \partial r)$$

the absence of a zero tangential wind speed contour implies that infinite vorticity exists across the circulation center. Rarely does an aircraft flying through a hurricane reach the dynamic center of the storm. Shea and Gray (1973) also provided horizontal maps of tangential winds at various levels. The lowest tangential wind speed offered on their

maps is 30 knots (~ 15 m s^{-1}). None of the dropwindsondes in this study sampled the dynamic center of the storm. Had this observation been available, these lower tangential wind contours would have had to be omitted, as they would have been too tightly packed in the composite to distinguish.

3.4.3 Hodographs

Figures 33a-d show hodographs in each quadrant of the hurricane, at approximately the same distance from storm center (~ 115 km). Figure 33a is a typical hodograph in the northeast storm-relative quadrant, with modest inflow (~ 10 m s^{-1}) changing to outflow at 720 m and an arc shape. This inflow depth is the lowest of all the quadrants. Figure 33b shows a horseshoe-shaped hodograph from the northwest storm-relative quadrant which exhibits a much stronger and deeper inflow layer, up until 3 km (the top of the hodograph). To the southwest storm-relative quadrant the hodograph (Fig. 33c) shows a flat arc shape with strong inflow (> 20 m s^{-1}). The transition to outflow occurs at 1.5 km. To the southeast storm-relative quadrant the hodograph (Fig. 33d) reveals an inflow layer 1273 m deep, with moderate inflow of ~ 15 m s^{-1}.

The hodographs emphasize the plan views of radial wind at different levels. The strongest inflow is seen in the western quadrants of the hurricane, while outflow establishes itself first in the northeast quadrant, at low levels, and then expands to other quadrants with height. A map of Bonnie's inflow depth (Fig. 34) indicates greatest depths to the north, west and south of storm center. Lowest inflow depth (or no inflow) is found to the east of storm center.

3.5 Surface Analysis over Land

The 1200 Z surface analysis on August 26th, 1998 (Fig. 35) indicates that Hurricane Bonnie was not interacting with any significant weather features as she neared the coastline. At this time a weak high of 1018 hPa is centered near Chicago. Farther east, stretching from the northeast to Arkansas is a very weak cold front. The cold front is located on the far side of the Appalachian Mountains, relative to the approaching hurricane, and does not impact the storm. At the surface there is no synoptic-scale feature that is moderating the oncoming hurricane. The 0000 Z surface analysis on the following day is similar to the 1200 Z analysis, only the weak cold front has edged closer to the coast, but does not impinge on Hurricane Bonnie.

The NCEP/NCAR reanalysis total wind speeds at upper levels (850 hPa, 500 hPa, and 200 hPa) were also examined to search for any upper level features that might have affected the storm. A trough north of the storm, identified at 42 °N on the 200 hPa total wind speed plot (Fig. 36), was the only noticeable feature. This is approximately 9 ° latitude north of the storm at the 1730 Z composite time. Hanley et al. (2001) composited 121 Atlantic TCs between 1985 and 1996 and found that for distant trough interactions (upper potential vorticity maximum between 400 and 1000 km from the TC center) the TC may intensify or weaken. Bonnie's MSLP remained fairly constant during the study, suggesting the trough likely did not affect the storm's intensity.

The surface temperature at 1800 Z on August 26th (Fig. 37) reveals that the air imported from land is approximately 2 to 3 °C warmer than the air coming off the ocean along a SW-NE transect through the circulation center (33.26 °N, 77.90 °W). This time (1800 Z) is chosen since it is near the composite time (1730 Z). The onshore air has

temperatures near 27-28 °C while the offshore air is warmer at 29-30 °C. At 10 m the composite gathered from the dropwindsonde data (Fig. 11) displays onshore temperatures of 27 °C, with offshore flow warming to over 28 °C farther to the southwest of the storm center. Specific humidity at 1800 Z (Fig. 38) is 2 to 3 g kg^{-1} drier in the offshore flow than the onshore flow. The 10 m dropwindsonde composite (Fig. 15) also shows offshore flow at least 3 g kg^{-1} drier than the onshore flow. Both the surface temperature and specific humidity data were obtained from the NCEP/NCAR reanalysis data (2.5° resolution), and are independent of the 10 m temperature and specific humidity values obtained by the dropwindsondes. The NCEP/NCAR and GPS dropwindsonde analyses generally agree, considering the large differences in resolution and that the dropwindsonde composites cover 11 hours.

At 850 hPa, temperature and specific humidity from the NCEP/NCAR reanalysis data (Figs. 39 and 40, respectively) reveal a more homogeneous atmosphere surrounding the storm center. Temperature differs by only 1 °C in either the onshore or offshore flow (between 19 and 20 °C). Specific humidity also shows little difference in the onshore or offshore flow, with the field becoming more symmetric about the circulation center. This agrees with the dropwindsonde analyses, where asymmetries dissipate with height.

Hurricane Bonnie was not impacted by any synoptic scale weather features as she neared landfall that would have introduced strong asymmetries into her structure. The thermodynamic asymmetries that do exist were likely created by the low-level differences in the flow that was coming from over land or from over water. This explains why these differences are most evident at lower levels in the storm and fade with height.

CHAPTER 4:
SUMMARY

4.1 Conclusions

On August 26th, 1998 two NOAA WP-3D research aircraft deployed 85 dropwindsondes in Hurricane Bonnie, as the storm made landfall on the Carolina coast. Radar images were also captured by two WSR-88Ds and the aircraft's lower fuselage radar. The dropwindsondes are used to identify Bonnie's horizontal and vertical structure from 10 m to 2 km. GPS dropwindsondes allow us to map both thermodynamic and kinematic fields near the sea surface. This study marks one of the first times that radar data from the WSR-88Ds are coupled with the dropwindsondes.

The temperature and pressure sensors on the dropwindsondes perform well, based on the ability to produce coherent fields in the vertical and horizontal. The quality of the relative humidity sensor is more problematic. Corrections are needed for this sensor when it fails to dry out upon exiting cloud base. In this experiment the relative humidity sensor quality did not cause a major setback as the majority of the relative humidity observations were reasonable.

NCEP/NCAR reanalysis data of air temperature, specific humidity and wind fields at various levels over land supports the analysis gathered by the dropwindsondes. As Bonnie makes landfall only a weak cold front on the far side of the Appalachian Mountains and an upper level trough well to the north of the storm (~ 42 °N) are present. Both are too distant to affect the storm.

Radar pictures reveal the asymmetric nature of Bonnie, with a greater number of rainbands to her north (onshore) than her south (offshore). The lower fuselage and WSR-

88D images provide no evidence for a change in band structure or orientation in the onshore flow, while suppressed convection exists in the offshore flow beyond the eyewall. Bonnie also displays deep convective cells within the eye that extend to 16 km altitude. These cells originate from the eyewall, break off, and enter the eye. All through the experiment the eyewall radius shrinks, from 92 km at 1115 Z to 64 km at 2037 Z. The storm's behavior does not seem to fit Willoughby et al.'s (1982) concentric ring model. I do not have any evidence to suggest that this behavior is caused by the storm's proximity to land.

Storm-relative composite maps of Bonnie's thermodynamics and kinematics provided a detailed meso-β analysis of the storm's structure. Bonnie's low-level temperature fields agree with the work of Cione et al. (2000) and Barnes and Bogner (2001) as the storm's inflow is not isothermal. At 10 m altitude the offshore flow is 1.0 °C warmer than the onshore flow. Cooler temperatures are located to the right rear of the storm, over the SST wake. A cool region is also found surrounding the circulation center, collocated with the eyewall and rainbands as identified on the radar images. This suggests that downdrafts likely play a role in this cooling. Air moving in the offshore flow, to the southwest of storm center, is also cooled as it moves closer to the eye. This region of the storm features little or no radar reflectivity, but does exhibit low relative humidity and high wind speeds that would favor the evaporation of sea spray. The strongest temperature differences around the storm center are found at low levels and weaken with height.

Examination of moisture fields shows the strongest asymmetry at low-levels, with air in the offshore flow as much as 4 g kg^{-1} drier at a radius of ~1.5 degrees latitude from

storm center than air in the onshore flow. Similar to the temperature plots, by the time this air moves closer to the circulation center it has increased its moisture and the field becomes more symmetric about the circulation center.

Mixed layer heights in Hurricane Bonnie at a radius of 1.5 degrees latitude from storm center surpass 750 m in the offshore flow, yet are zero (stable) in the onshore flow. The warmer, drier, and more stable air in the offshore flow is collocated with a precipitation-free region as seen by the WSR-88Ds and the aircraft lower fuselage radar.

Energy content (as measured by θ_E) reveals that the air to the southwest of storm center has lower energy than that to the northeast. At the eyewall, the difference in θ_E at 10 m is only ~ 4 K between the flow to the southwest and northeast of the circulation center.

Bonnie's radial winds show strongest inflow to the southwest, in the eyewall, with outflow to the north and east of the storm center. Inflow depth around the eyewall ranges from 1.0 to 1.5 km except for the northeast eyewall where it decreases to 500 m, then zero. The asymmetry in Bonnie's radial winds may be due to storm motion, the organization of convection in the eyewall and the nearness to land. Like Hurricane Bonnie, Hurricane Mitch (1998) displayed maximum inflow in the left rear quadrant, which was attributed to Mitch's proximity to Honduras (Kepert 2002).

The tangential wind fields display Bonnie's large RMW, averaging just under 80 km at the time of the storm-relative composite (1730 Z). The onshore/offshore difference is only about 5 m s^{-1} well away from storm center. Closer to the storm center the field is more symmetric. Tangential flow also does not decrease to very low magnitudes in the

storm's eye due to the presence of convective cells that have broken off the eyewall and spiraled into the storm's center.

4.2 Discussion

This study has revealed that Bonnie's proximity to land resulted in warmer, drier and more stable air being entrained into the outer portions of the storm. As the air in the offshore flow travels toward the circulation center it cools slightly, moistens more, and thus increases its energy content (θ_E). Thus, closer to the storm center the thermodynamics reveal a more symmetric storm structure. While the proximity of the coast likely resulted in the slightly weaker low-level offshore tangential flow, Bonnie's strongest inflow in the left rear quadrant of the storm is also likely due to the nearness of land, similar to Kepert's (2002) analysis of Mitch (1998).

Despite any changes in Bonnie's structure at landfall, the storm's intensity (MSLP) remained nearly constant. This is likely because the modifications to storm structure were occurring at a great distance (~ 1.5 degrees latitude radius) from storm center. Closer to the storm center the structure was more homogeneous. By the time air from the outer regions of the storm arrived at the storm center it had likely been modified by the high surface fluxes which nearly eliminated any continental characteristics.

4.3 Future Work

The relationship between energy (equivalent to θ_E) and the reduction of sea level pressure is well known; $-\partial p = 2.5\, \partial \theta_E$ (Riehl, 1963). Energy budgets around Bonnie's eyewall could be calculated to reveal where most of the energy is entering the storm. As Bonnie makes landfall the storm's thermodynamics become more homogeneous around

the eyewall. Still, a closer inspection of the eyewall's energy budget to the southwest (offshore) and to the northeast (onshore) may explain why the intensity did not change.

Examining offshore trajectories to assess how long the air retains its continental characteristics could also be used to study intensity. If the flow regained oceanic characteristics by the time it reached the eyewall, proximity to land would not matter, and the storm's intensity would not be modified by this flow.

Further analysis of onshore and offshore flows should be examined in other storms, with various synoptic conditions, making landfall on different types of terrain. This necessitates extending the analysis beyond the U.S. east coast, which does not have substantial terrain. A data set of the onshore and offshore flows in multiple tropical cyclones would help forecasters predict changes in storm structure and intensity at landfall.

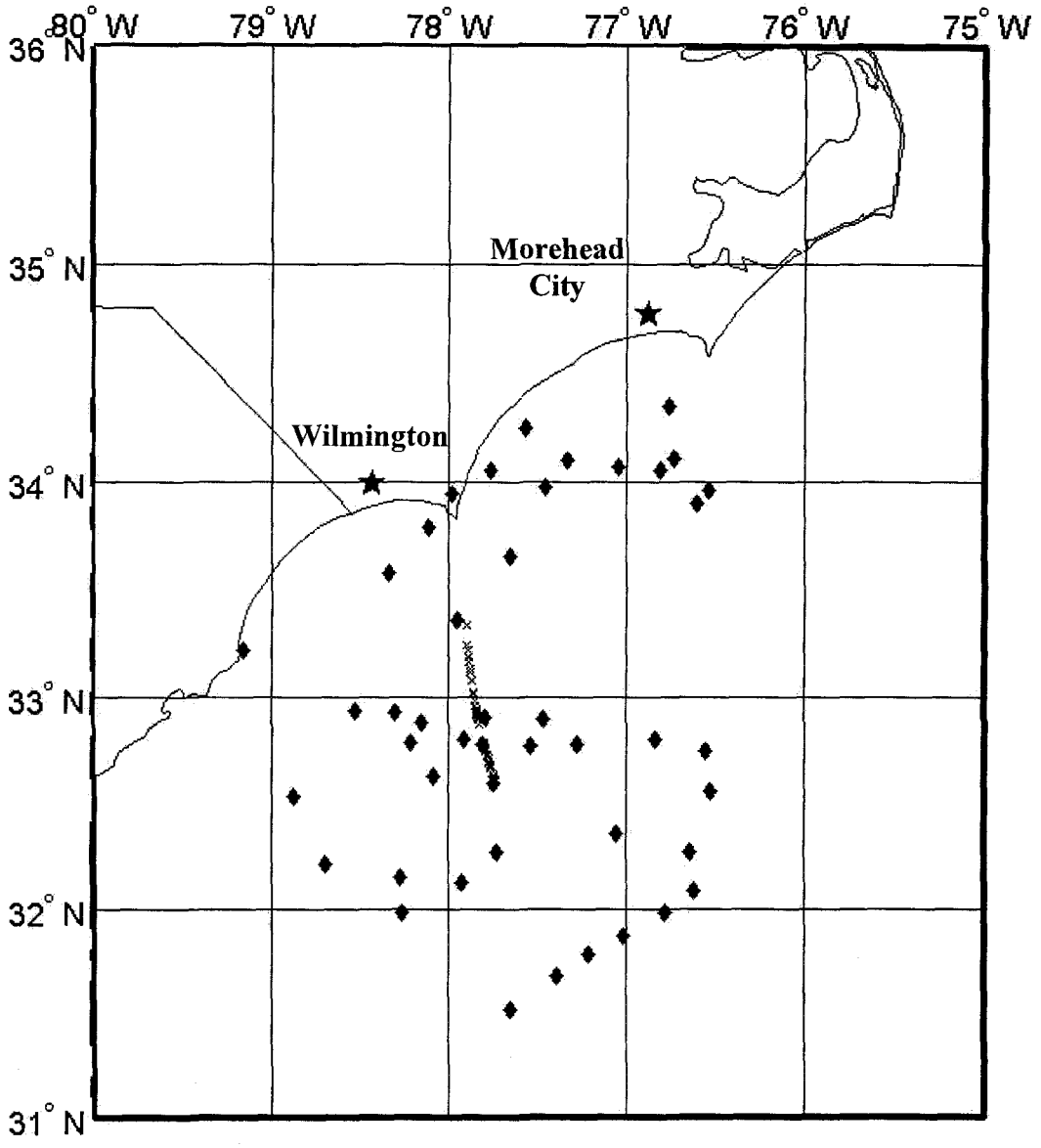

Figure 1. Location of the dropwindsondes (diamonds) and storm centers (x's) of the 42RF aircraft. From 1220 Z to 1800 Z on August 26th, 1998, 45 successful dropwindsondes were released. Radar stations are located at Wilmington and Morehead City, North Carolina, as indicated by the black stars.

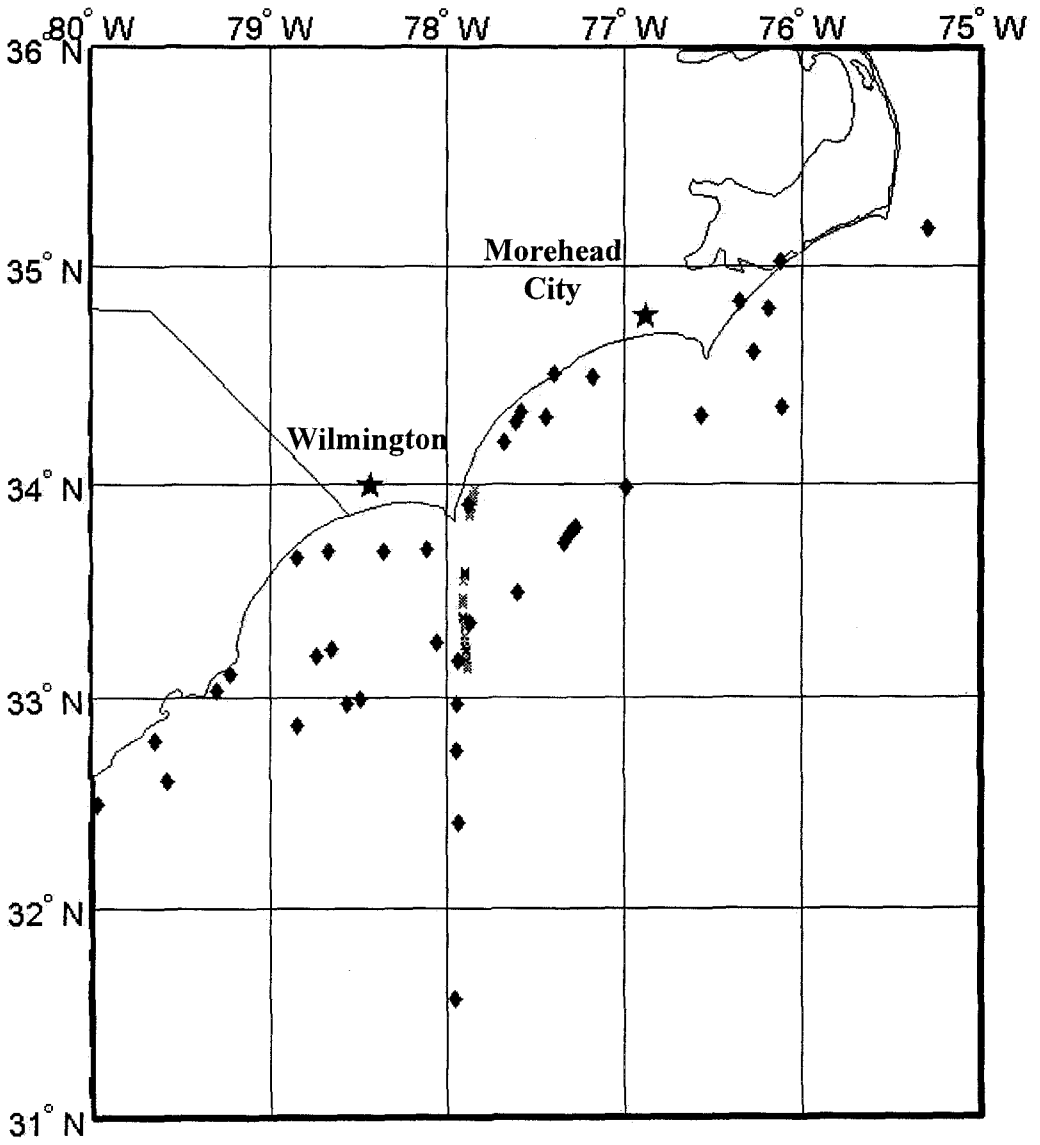

Figure 2. Similar to Figure 1, but for the dropwindsondes (diamonds) and storm centers (x's) of the 43RF aircraft. From 1630 Z to 2300 Z on August 26th, 1998, 40 successful dropwindsondes were released.

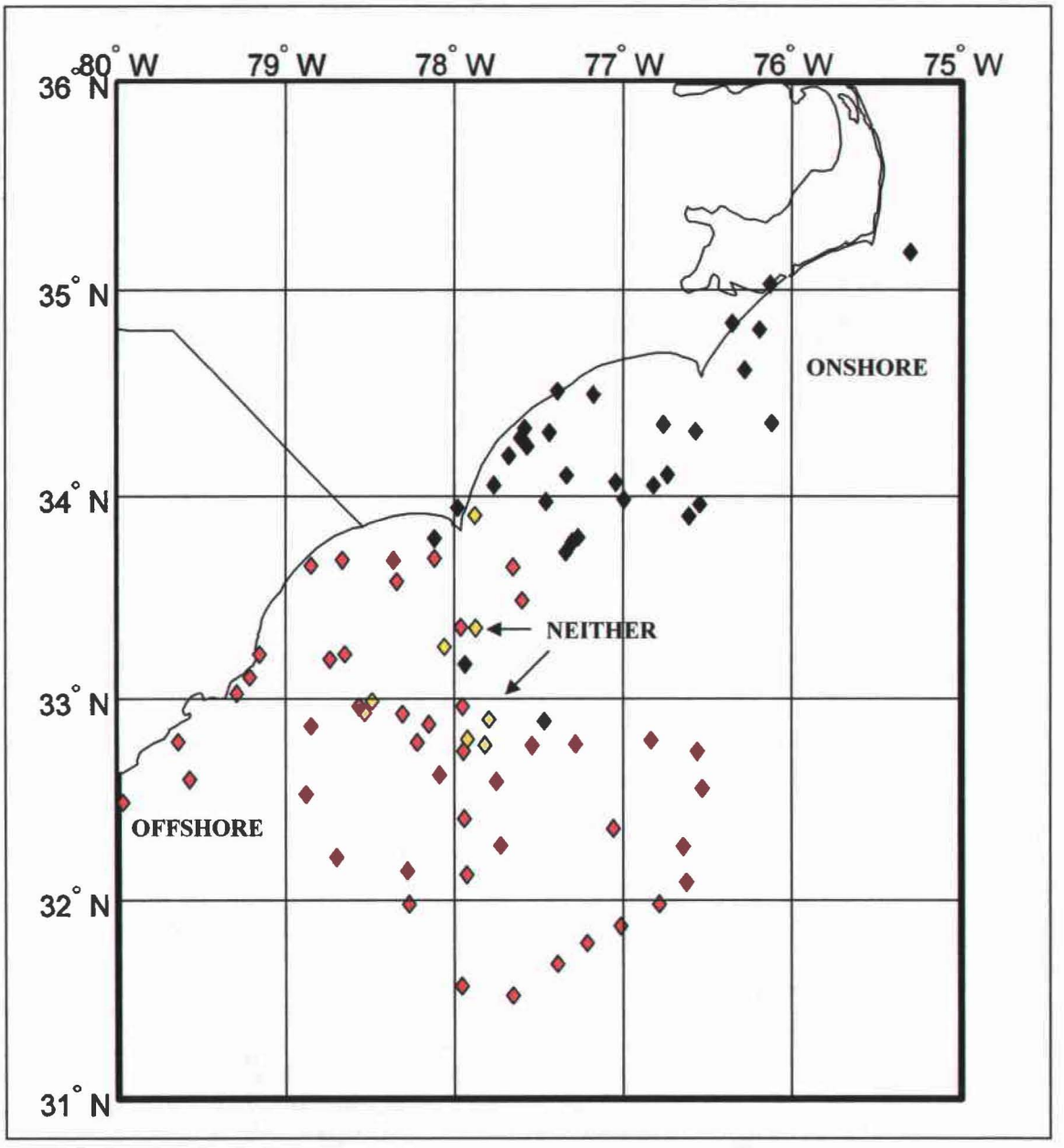

Figure 3. Earth-relative position of the dropwindsondes and whether the flow sampled is onshore (black: 31), offshore (red: 46), or neither (yellow: 8). "Neither" includes dropwindsondes that are sampling air parcels that have only resided over the ocean. The number in parentheses is the number of dropwindsondes in each category.

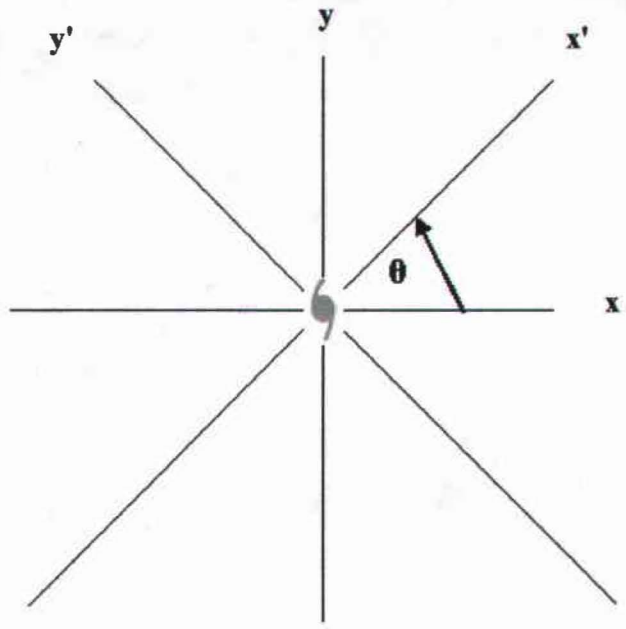

Figure 4. The original coordinate system where the (x, y) axes point east and north, and the rotated coordinate system where the (x') axis is aligned with the dropwindsonde.

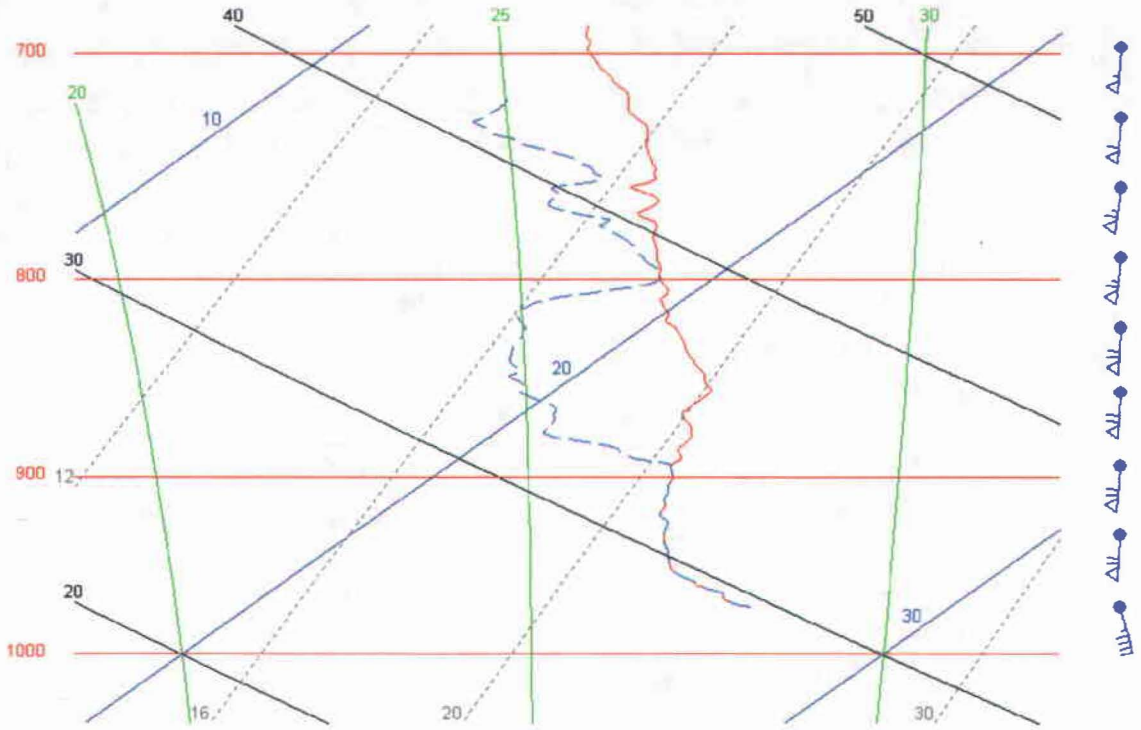

Figure 5. Example of a questionable sounding. The air is saturated from approximately 950 hPa down to 973 hPa, yet the lapse rate is dry adiabatic.

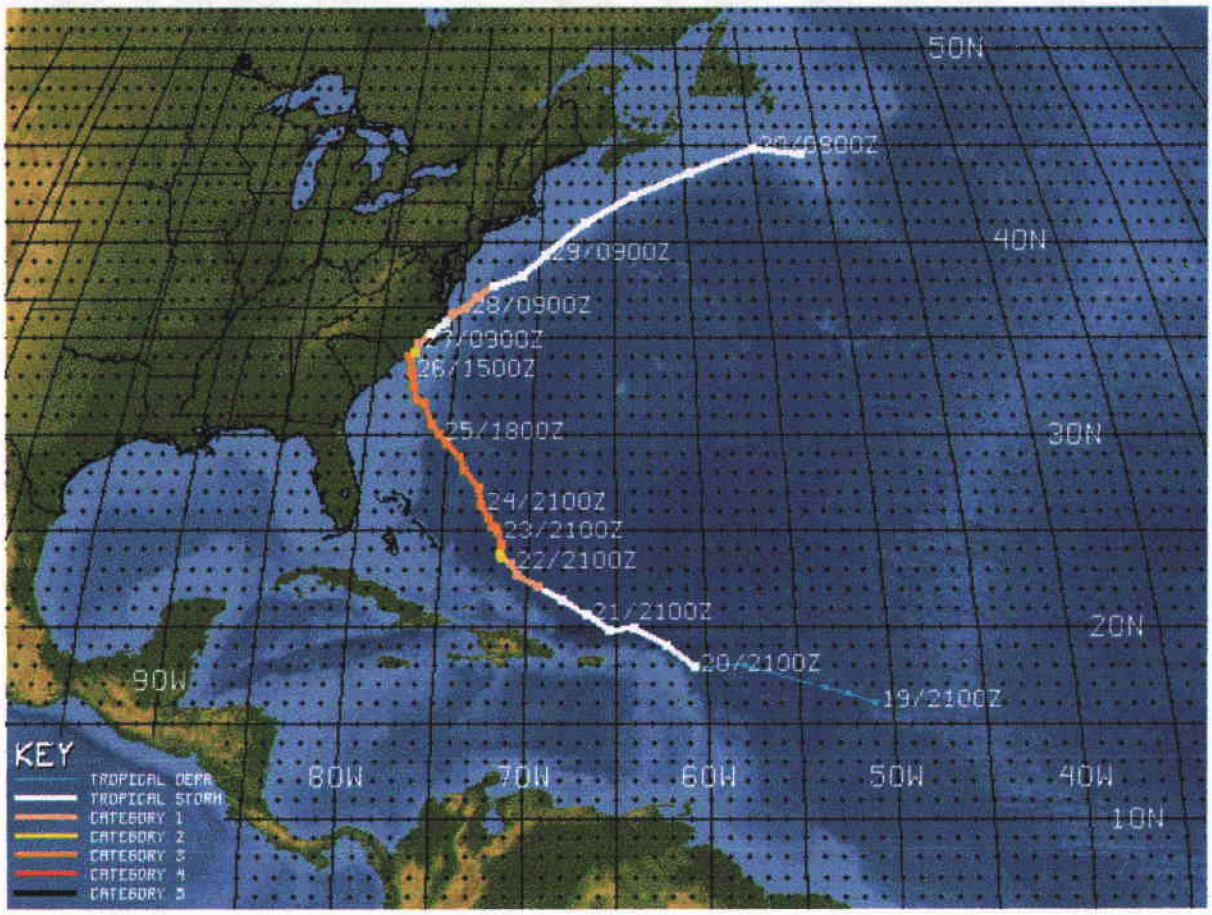

Figure 6. Hurricane Bonnie's path according to Best Track.
Obtained from http://cimss.ssec.wisc.edu/tropic/archive/1998/storms/bonnie/bonnie.html.

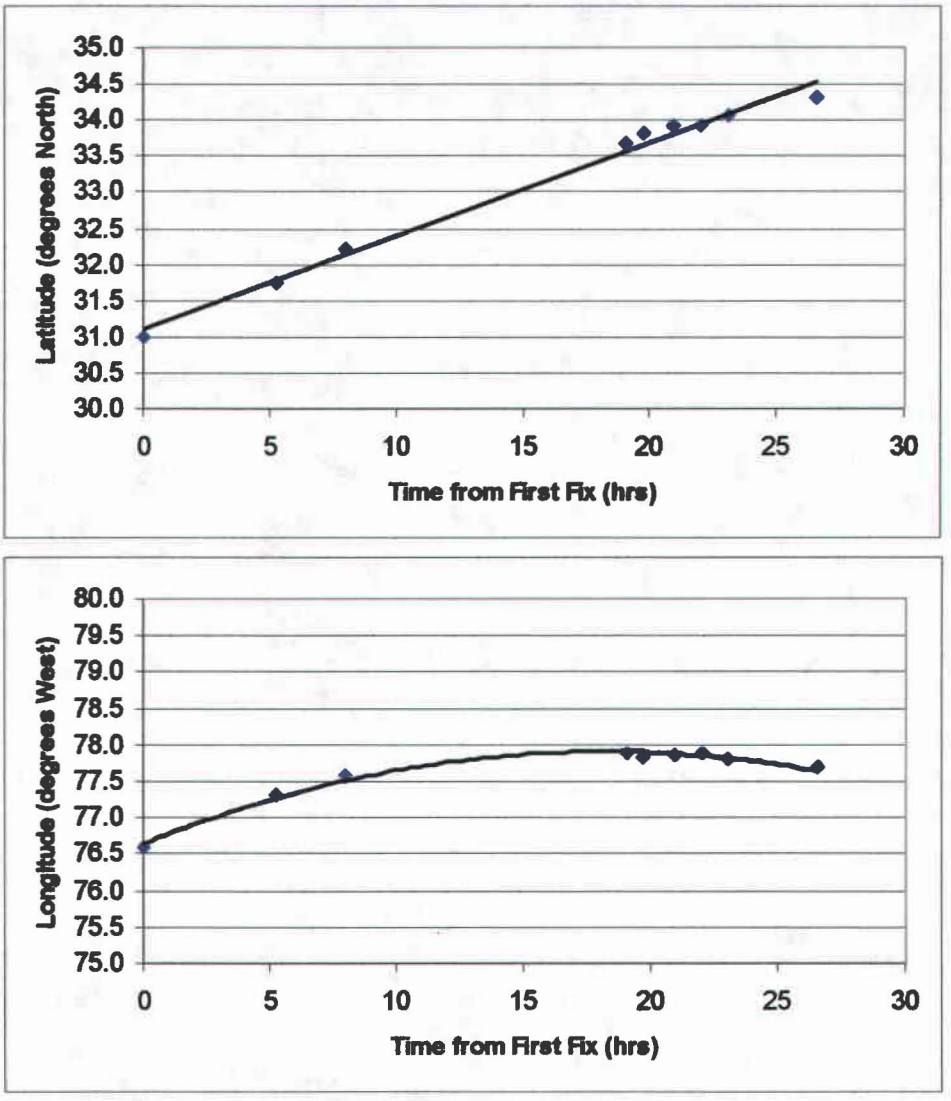

Figure 7. Hurricane Bonnie's position in time for latitude (top panel) and longitude (bottom panel). Curves indicate the best fit track according to a linear regression (top panel) and a second order polynomial regression (bottom panel). Time from first fix means the hours from 0050 Z on August 26th, 1998, the time of the first center position used in the storm track.

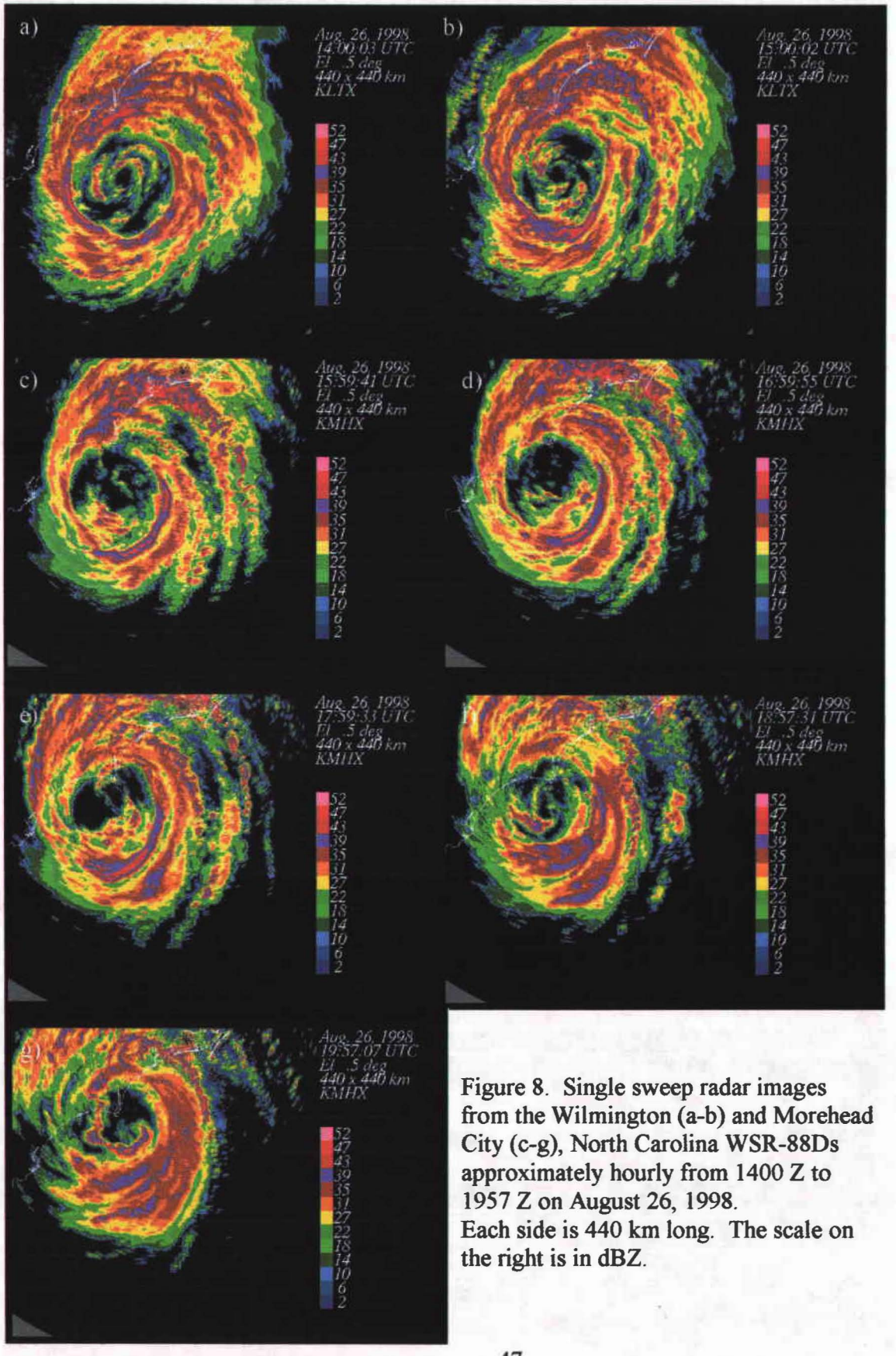

Figure 8. Single sweep radar images from the Wilmington (a-b) and Morehead City (c-g), North Carolina WSR-88Ds approximately hourly from 1400 Z to 1957 Z on August 26, 1998.
Each side is 440 km long. The scale on the right is in dBZ.

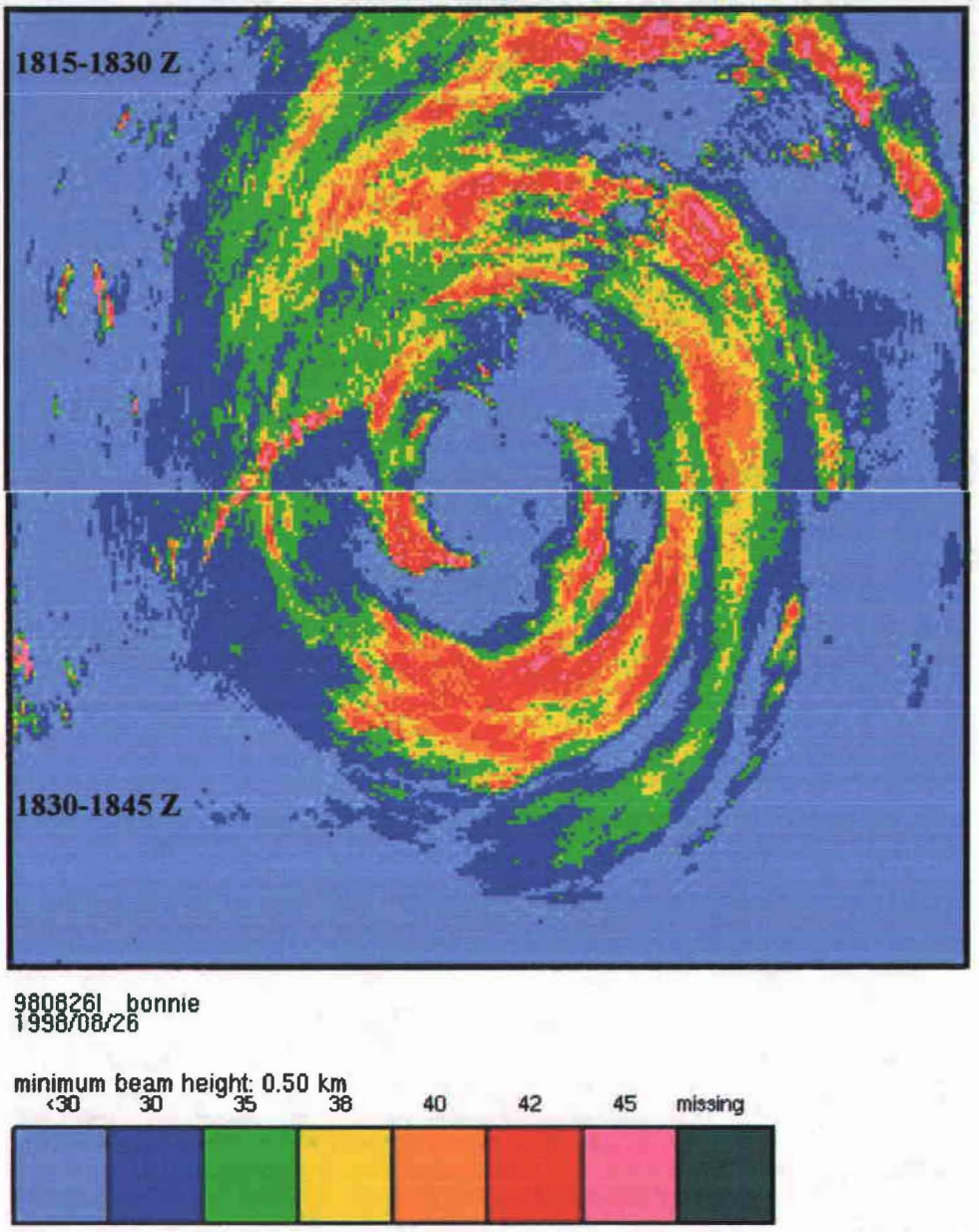

Figure 9. Two 15-minute composites; the top half is from 1815 to 1830 Z, the bottom half is from 1830 to 1845 Z. Dimensions are 360 km by 360 km.

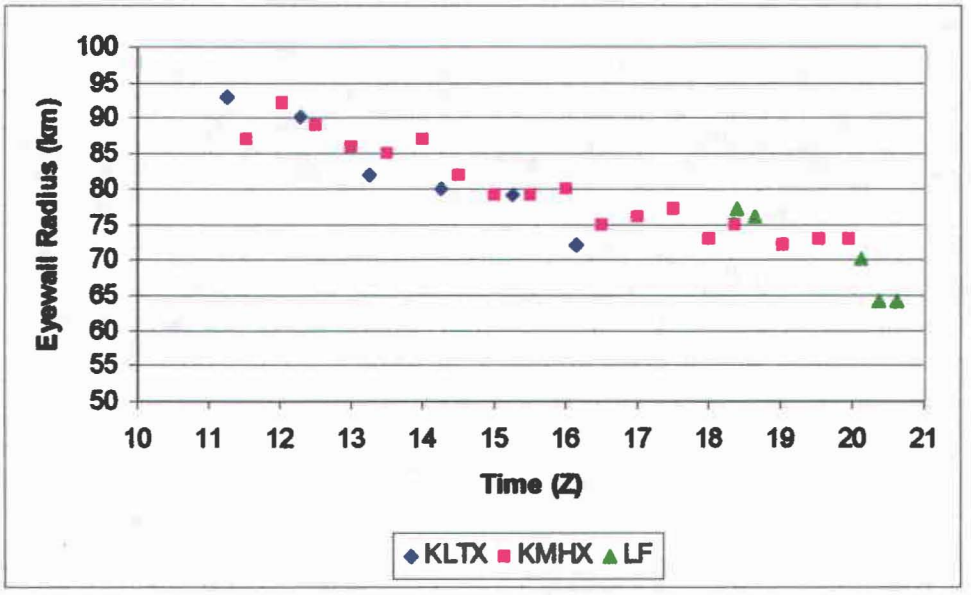

Figure 10. Bonnie's eyewall radius (km), as indicated by highest reflectivity features from 1000 Z to 2100 Z on August 26, 1998. Measurements come from KLTX (Wilmington WSR-88D), KMHX (Morehead City WSR-88D), and LF (lower fuselage radar).

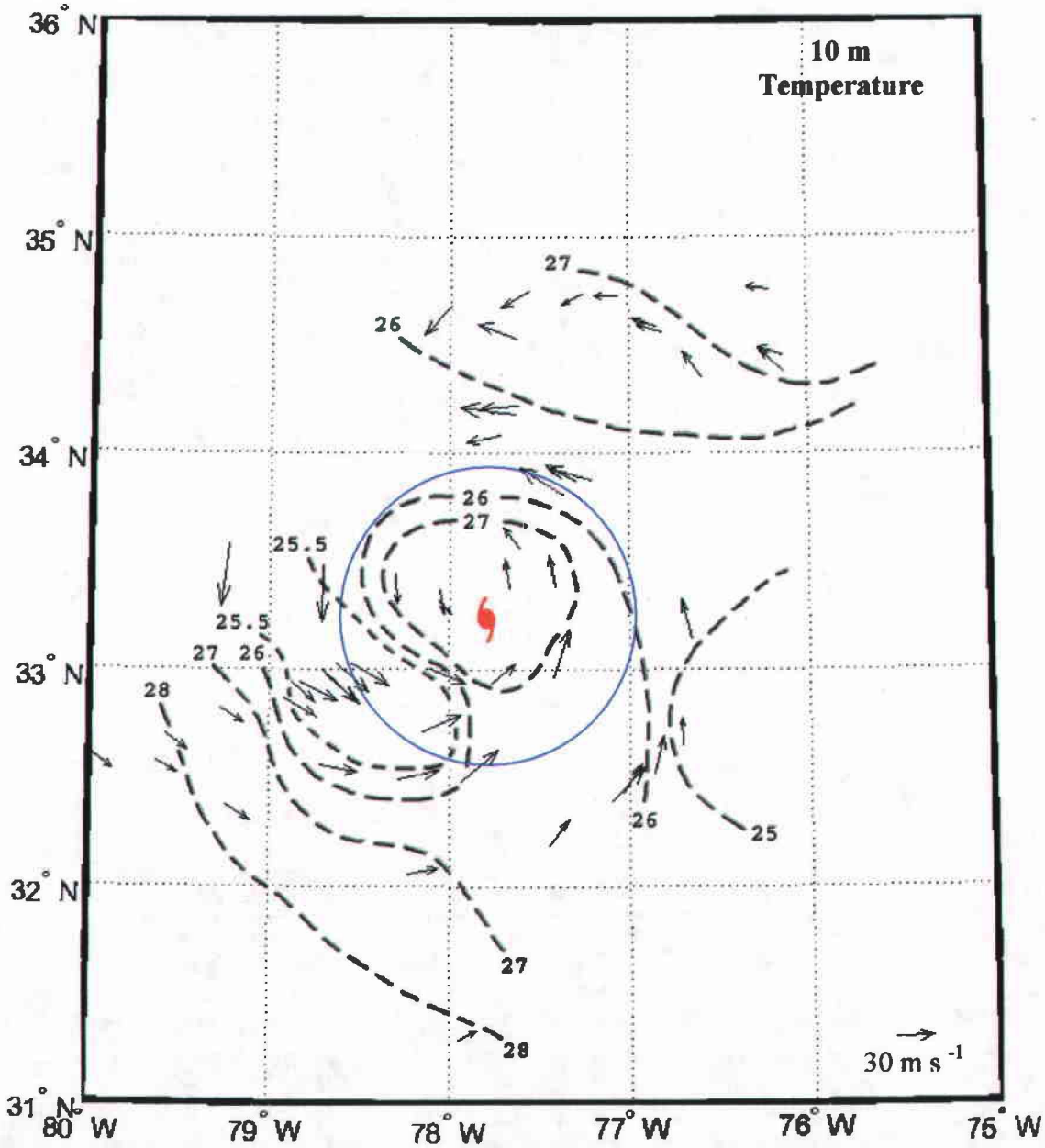

Figure 11. Storm-relative composite of Bonnie's temperature (°C) at 10 m. The red symbol denotes the storm center and the blue ring is Bonnie's approximate eyewall location at 1730 Z, the time of this composite. The black arrows represent the wind speed and direction at 10 m. The scale is indicated to the lower right side of the image.

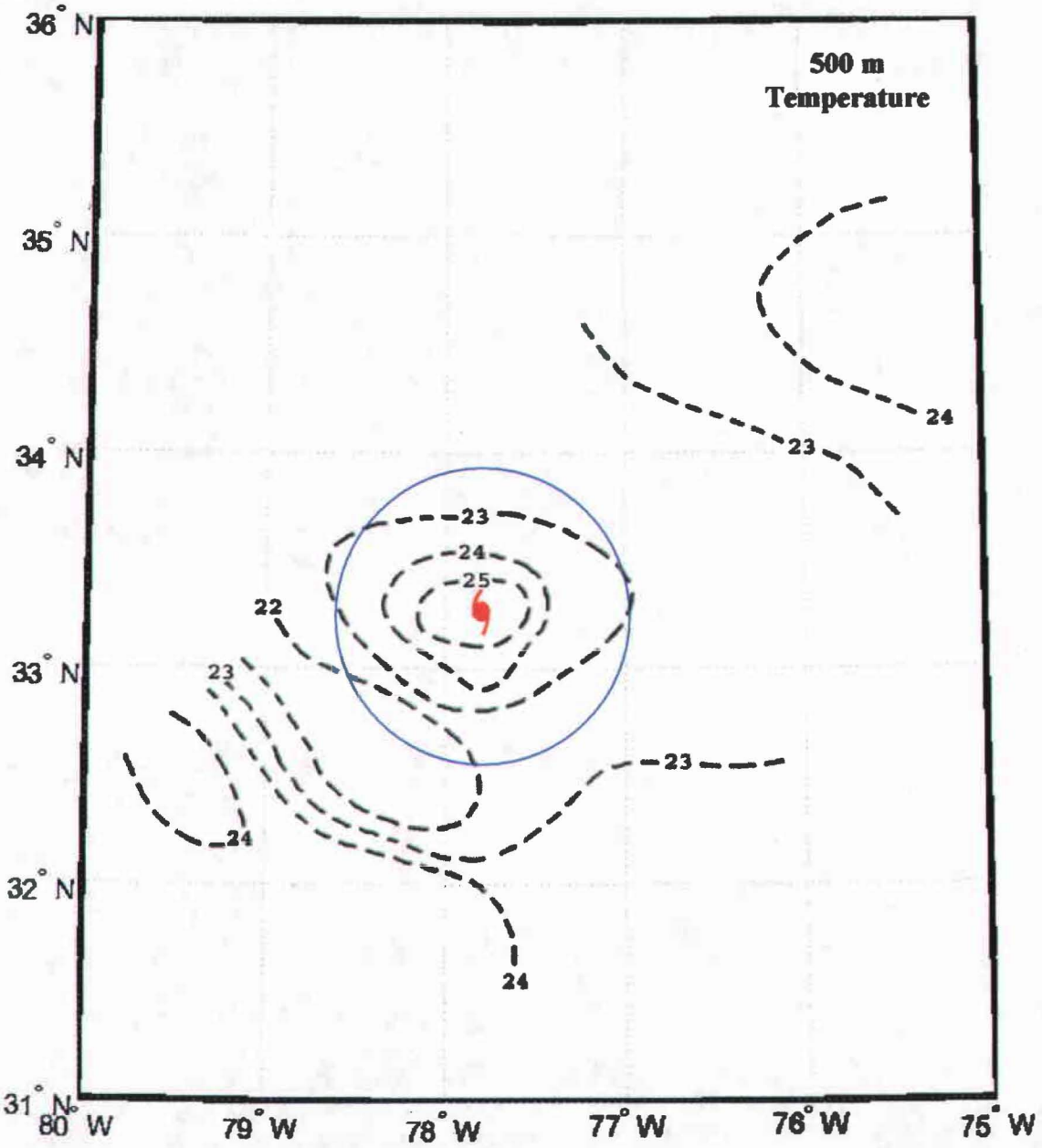

Figure 12. Similar to Figure 11, but at 500 m.

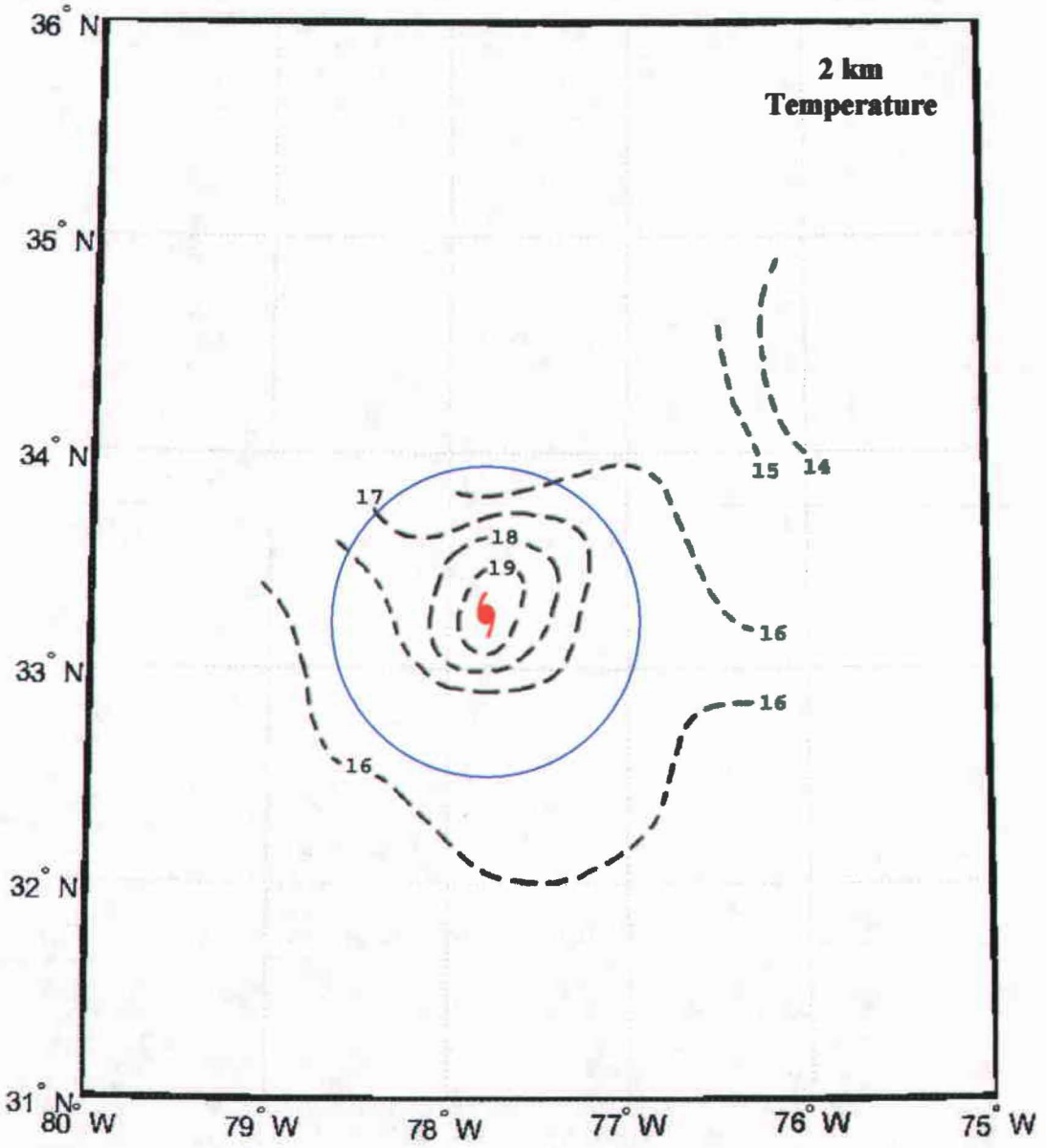

Figure 13. Similar to Figure 11, but at 2 km.

a)

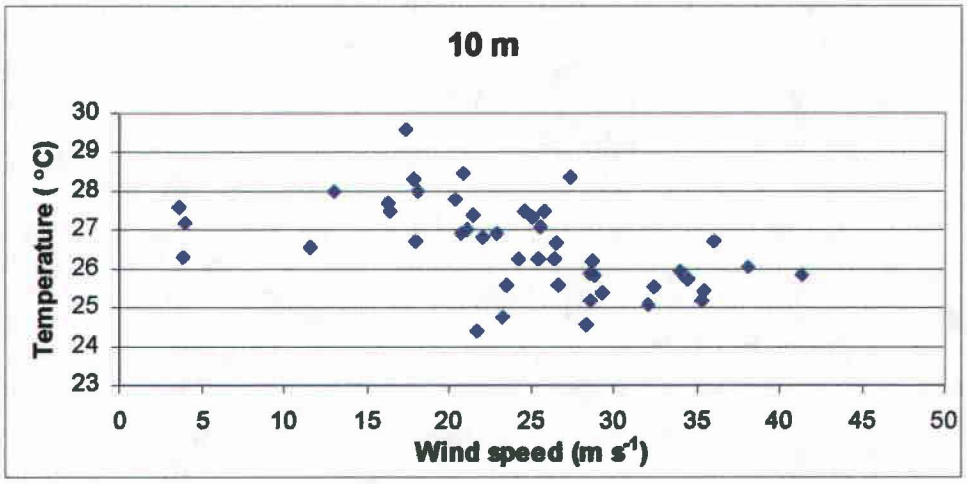

b)

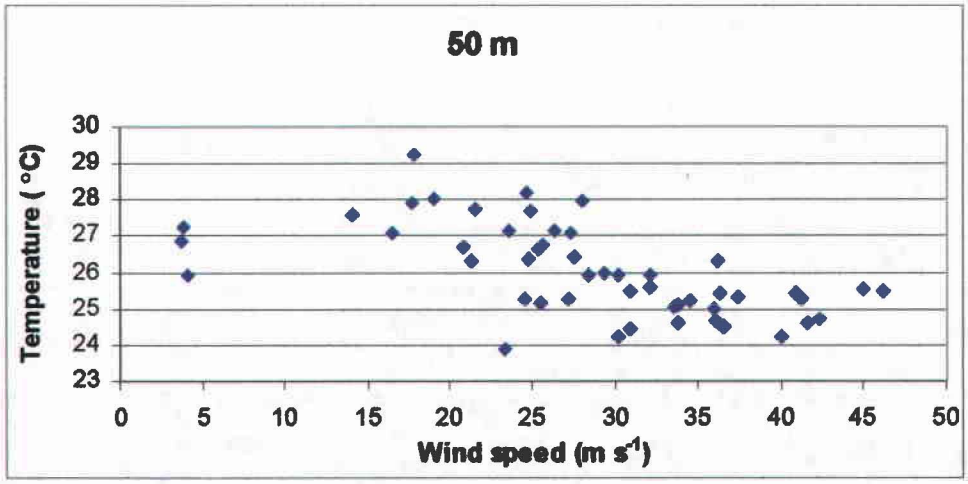

Figure 14. Temperature (°C) recorded by the dropwindsondes for a given wind speed. a) At 10 m. b) At 50 m.

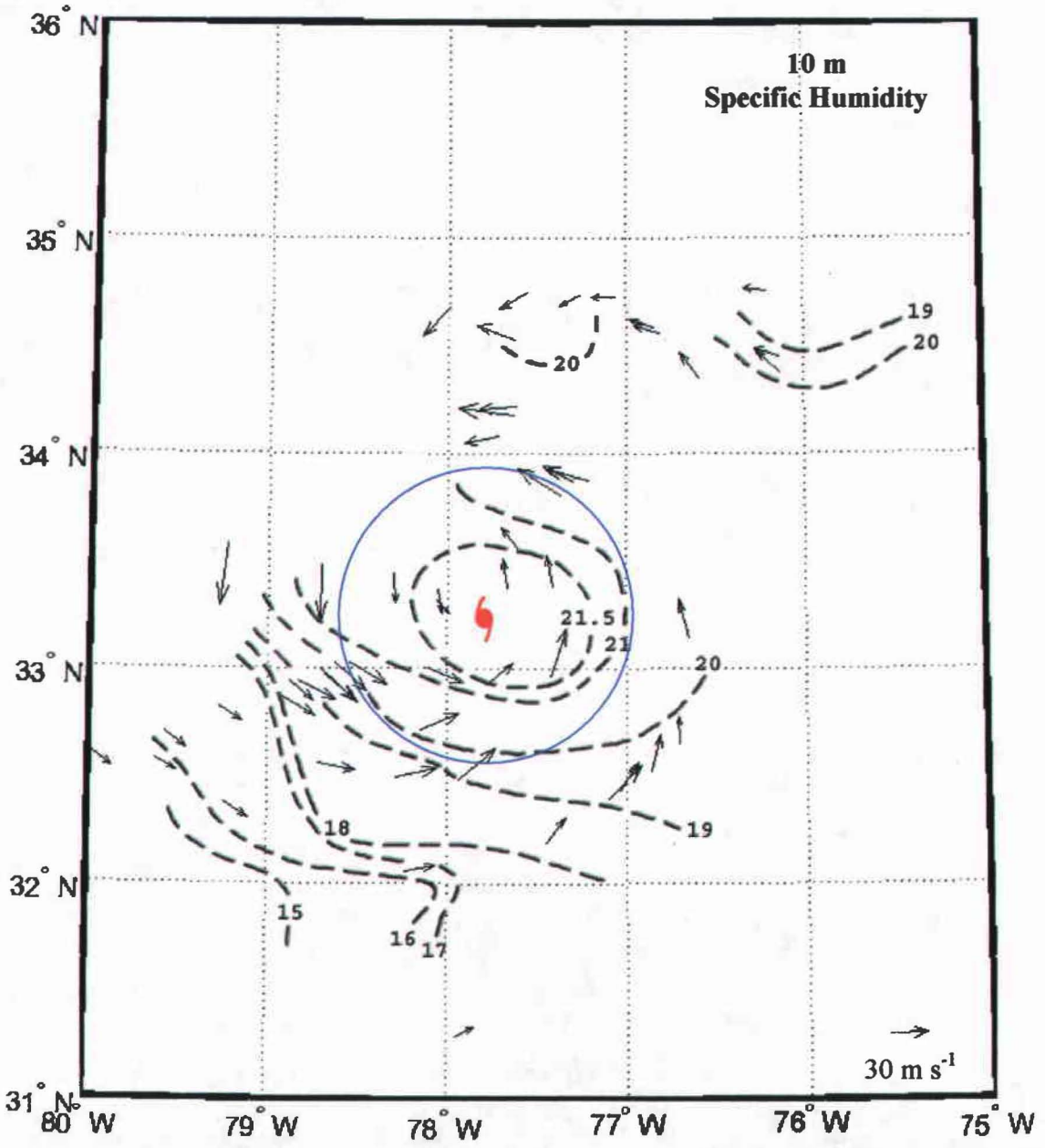

Figure 15. Storm-relative composite of Bonnie's specific humidity (g kg^{-1}) at 10 m. The red symbol denotes the storm center and the blue ring is Bonnie's approximate eyewall location at 1730 Z, the time of this composite. The black arrows represent the wind speed and direction at 10 m. The scale is indicated to the lower right side of the image.

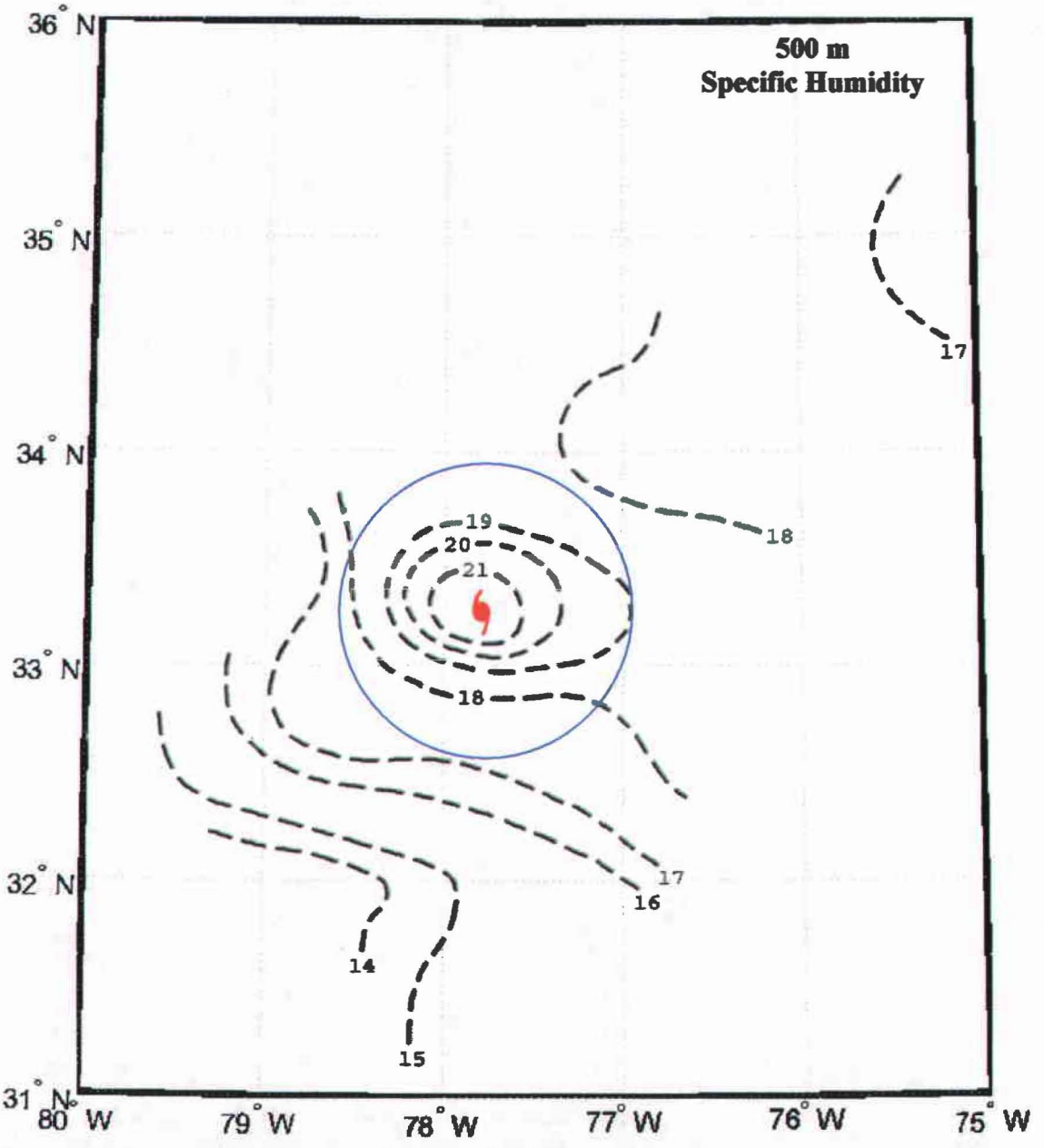

Figure 16. Similar to Figure 15, but at 500 m.

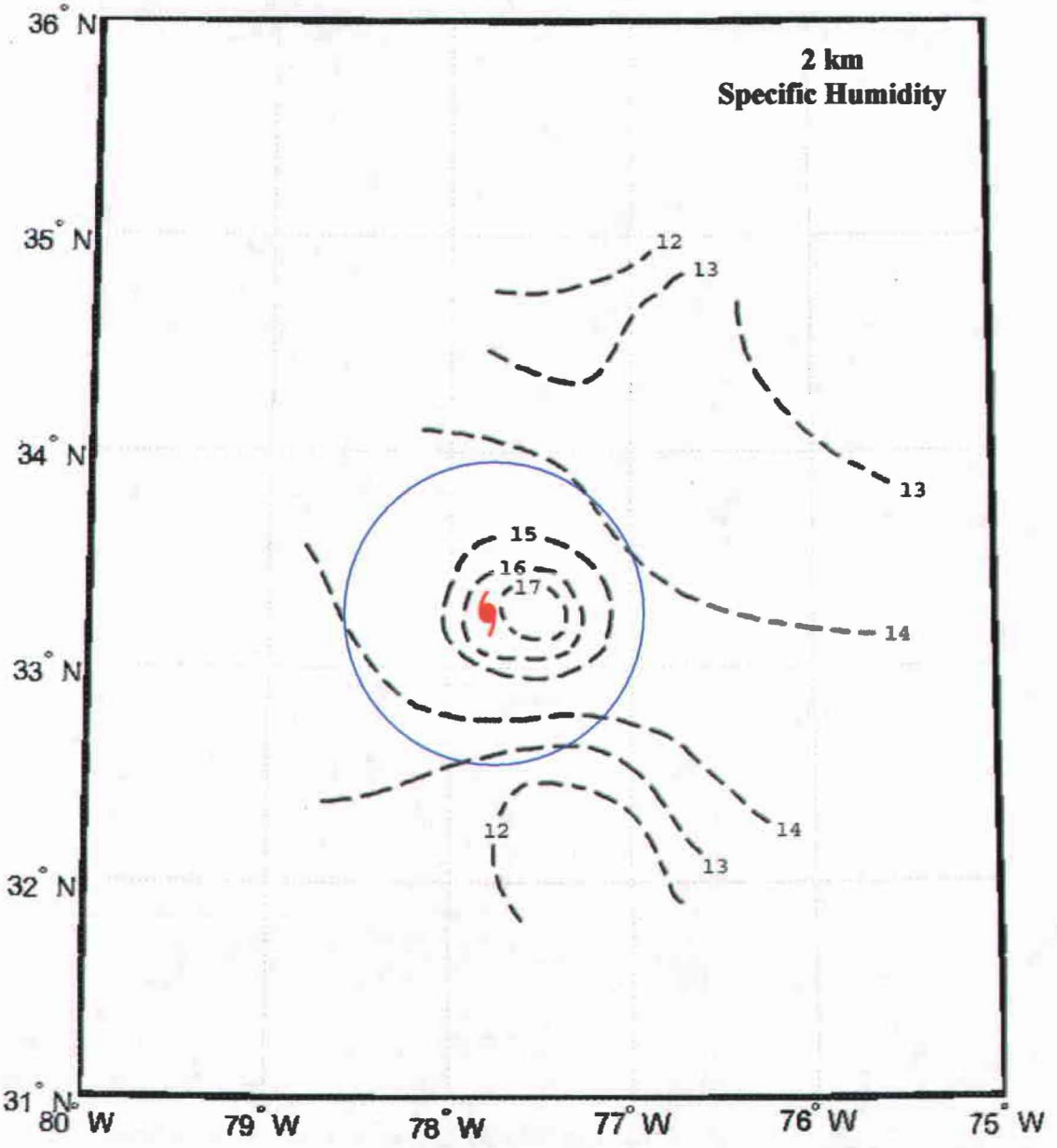

Figure 17. Similar to Figure 15, but at 2 km.

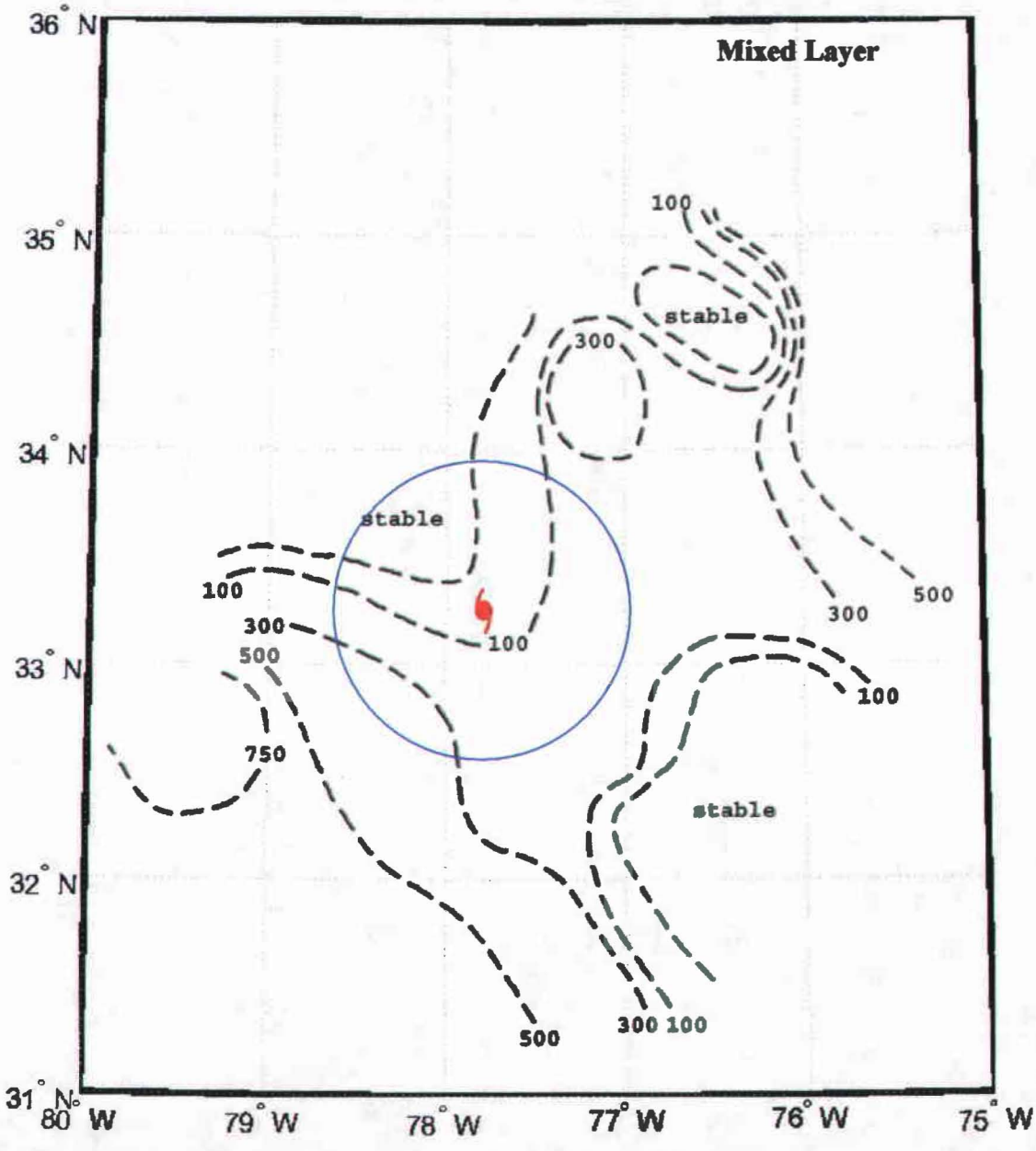

Figure 18. Storm-relative composite of Bonnie's mixed layer (m).
The red symbol denotes the storm center and the blue ring is Bonnie's approximate eyewall location at 1730 Z, the time of this composite.

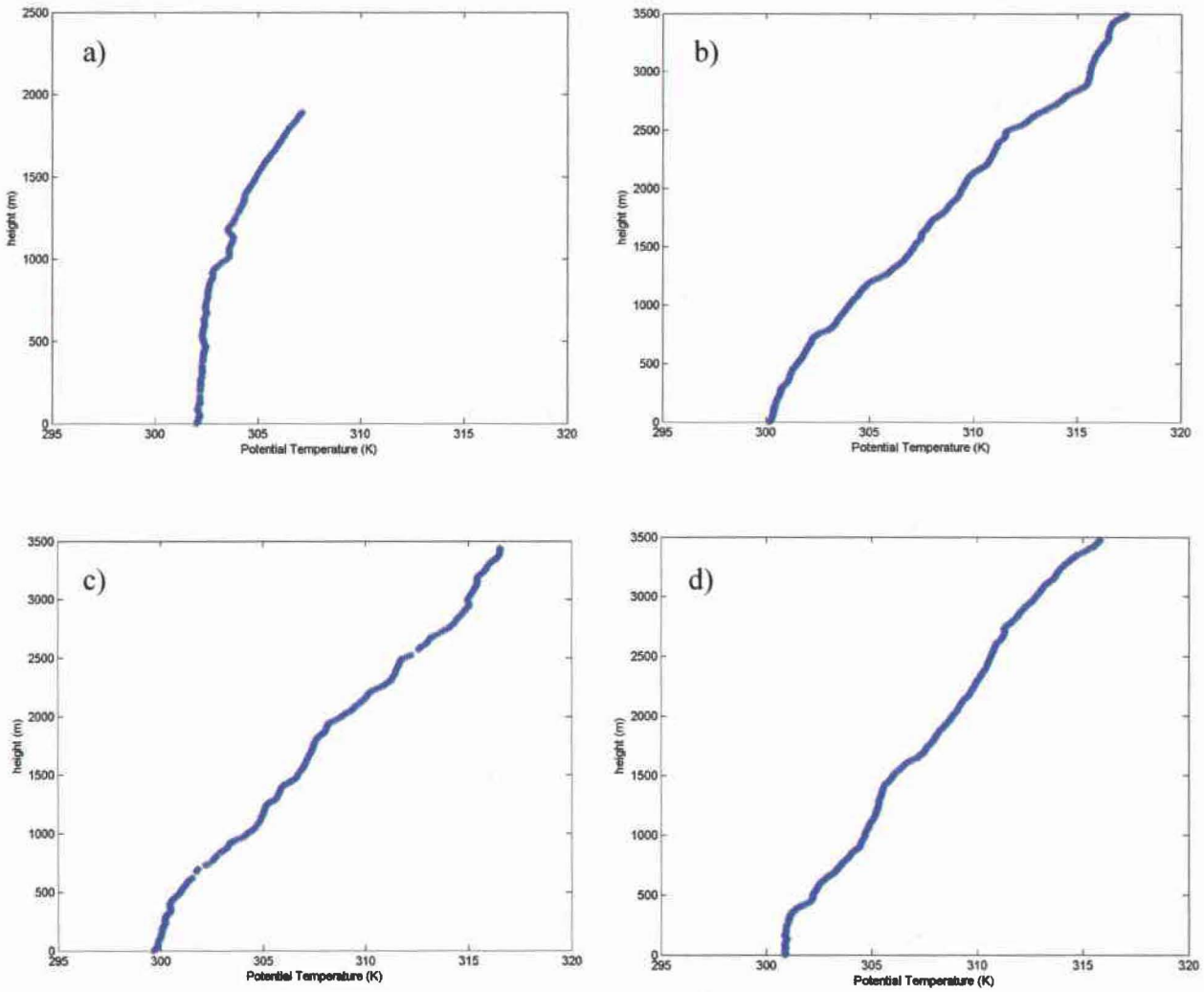

Figure 19. Vertical profiles of potential temperature (K) for various dropwindsondes. Bracketed value is the radial distance from storm center. a) In the offshore flow 9 km off the coast of South Carolina (r ~ 137 km). b) In Bonnie's wake (r ~ 124 km). c) In the onshore flow, 7 km off the coast of North Carolina (r ~ 158 km). d) South of the circulation center (r ~ 139 km).

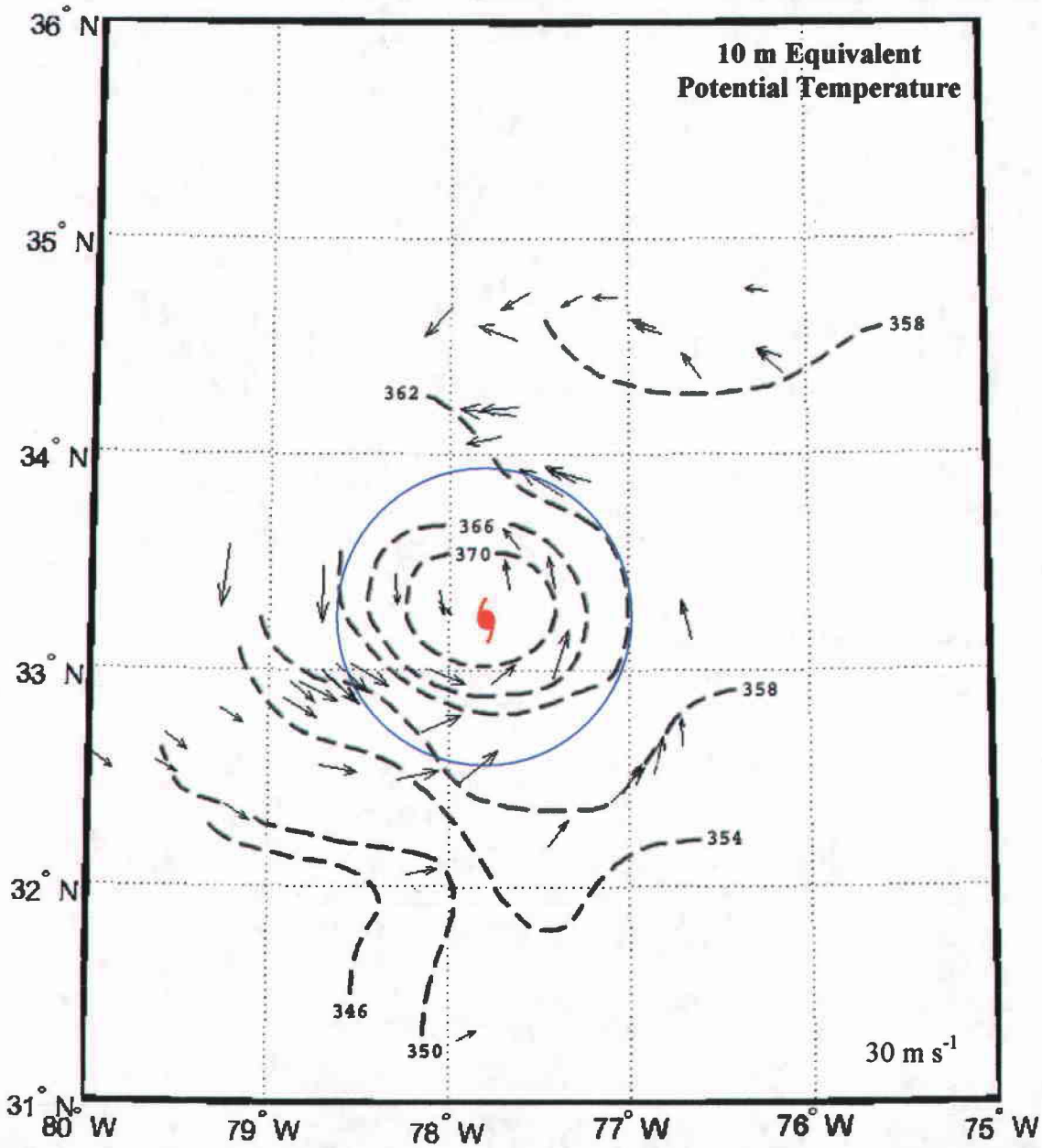

Figure 20. Storm-relative composite of Bonnie's equivalent potential temperature (K). The red symbol denotes the storm center and the blue ring is Bonnie's approximate eyewall location at 1730 Z, the time of this composite. The black arrows represent the wind speed and direction at 10 m. The scale is indicated to the lower right side of the image.

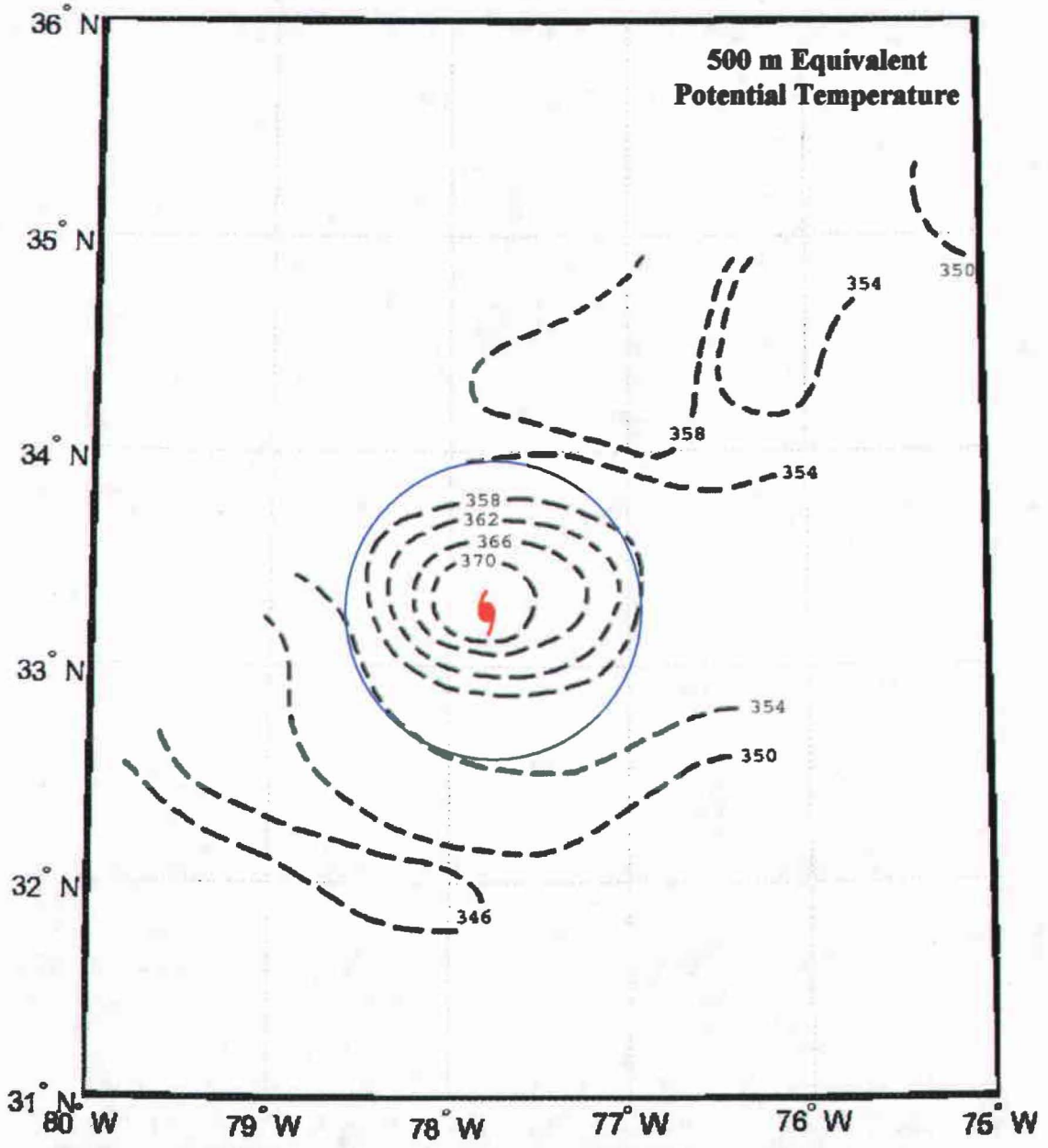

Figure 21. Similar to Figure 20, but at 500 m.

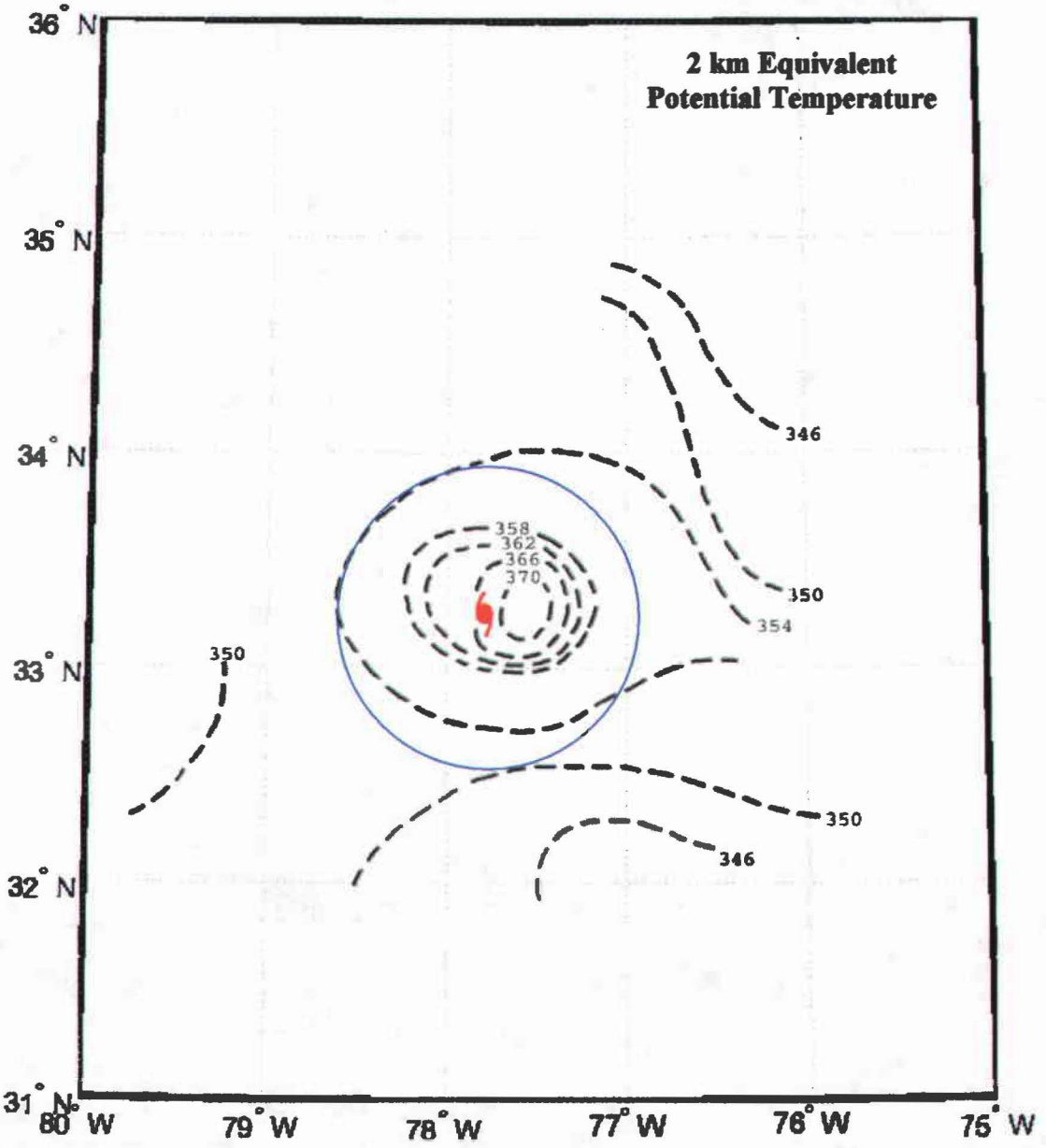

Figure 22. Similar to Figure 20, but at 2 km.

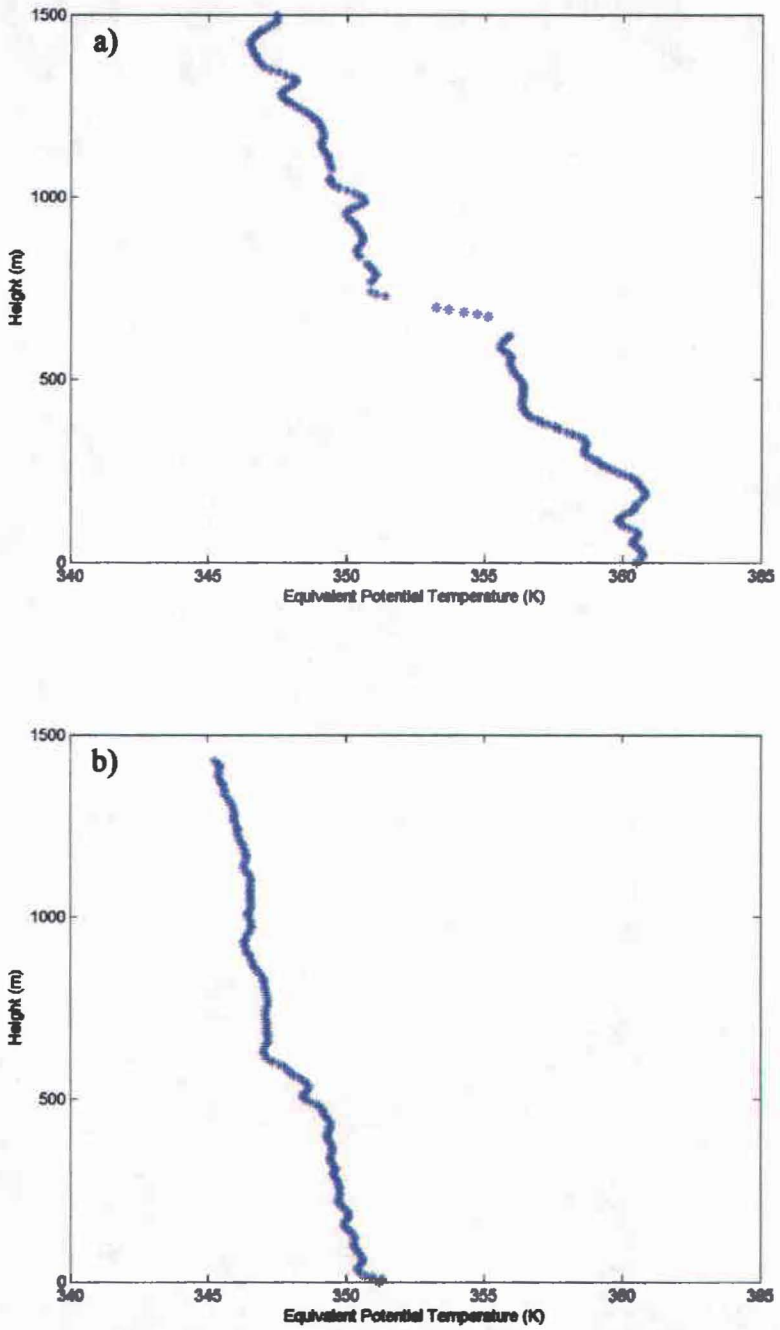

Figure 23. Vertical profiles of θ_E from the surface to 1500 m. Bracketed value is the radial distance from storm center. a) In the onshore flow, 7 km off the coast of North Carolina (r ~ 158 km). b) In the offshore flow, 13 km off the coast of South Carolina (r ~ 178 km).

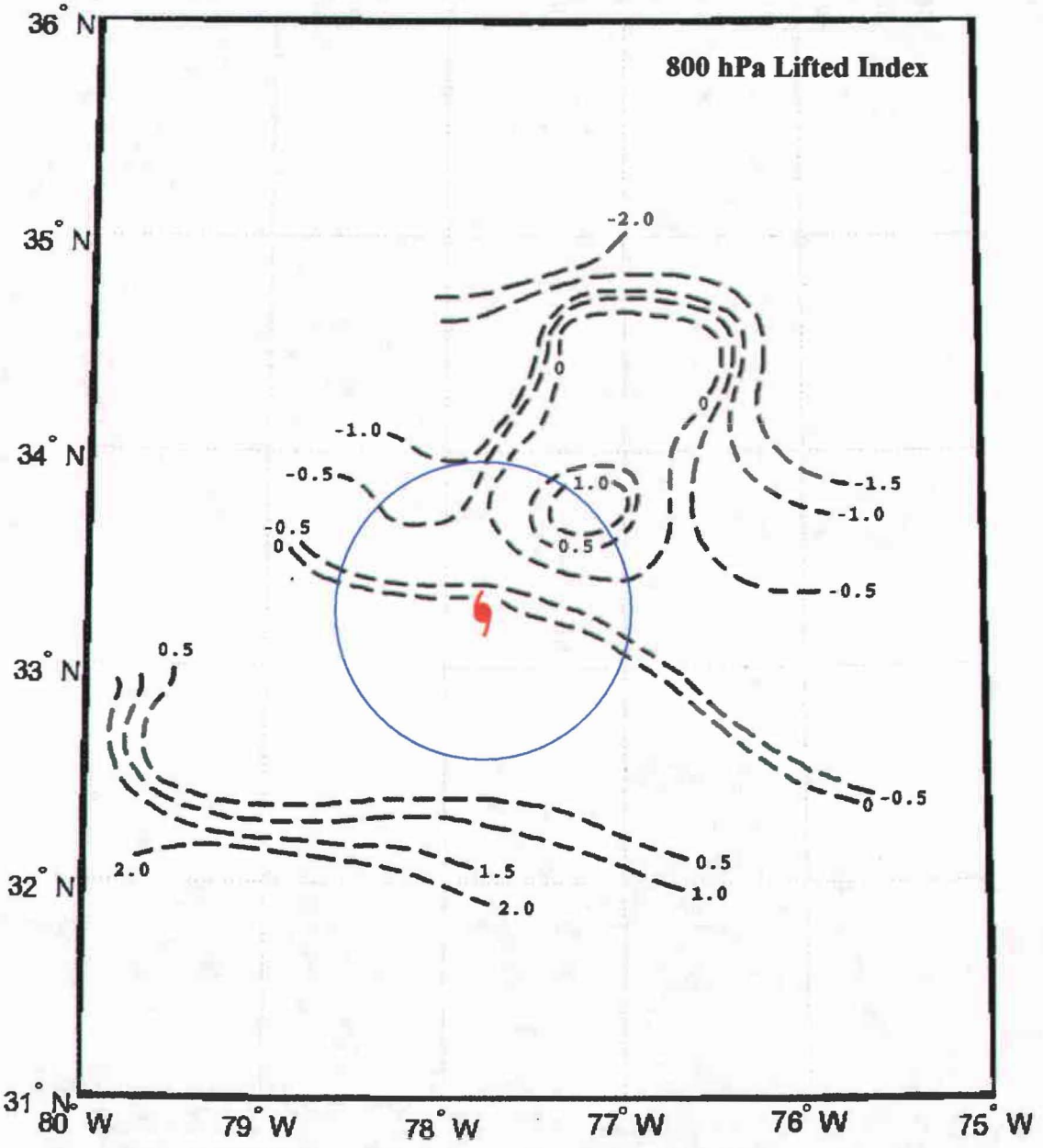

Figure 24. Storm-relative composite of Bonnie's lifted index at 800 hPa (°C). The red symbol denotes the storm center and the blue ring is Bonnie's approximate eyewall location at 1730 Z, the time of this composite.

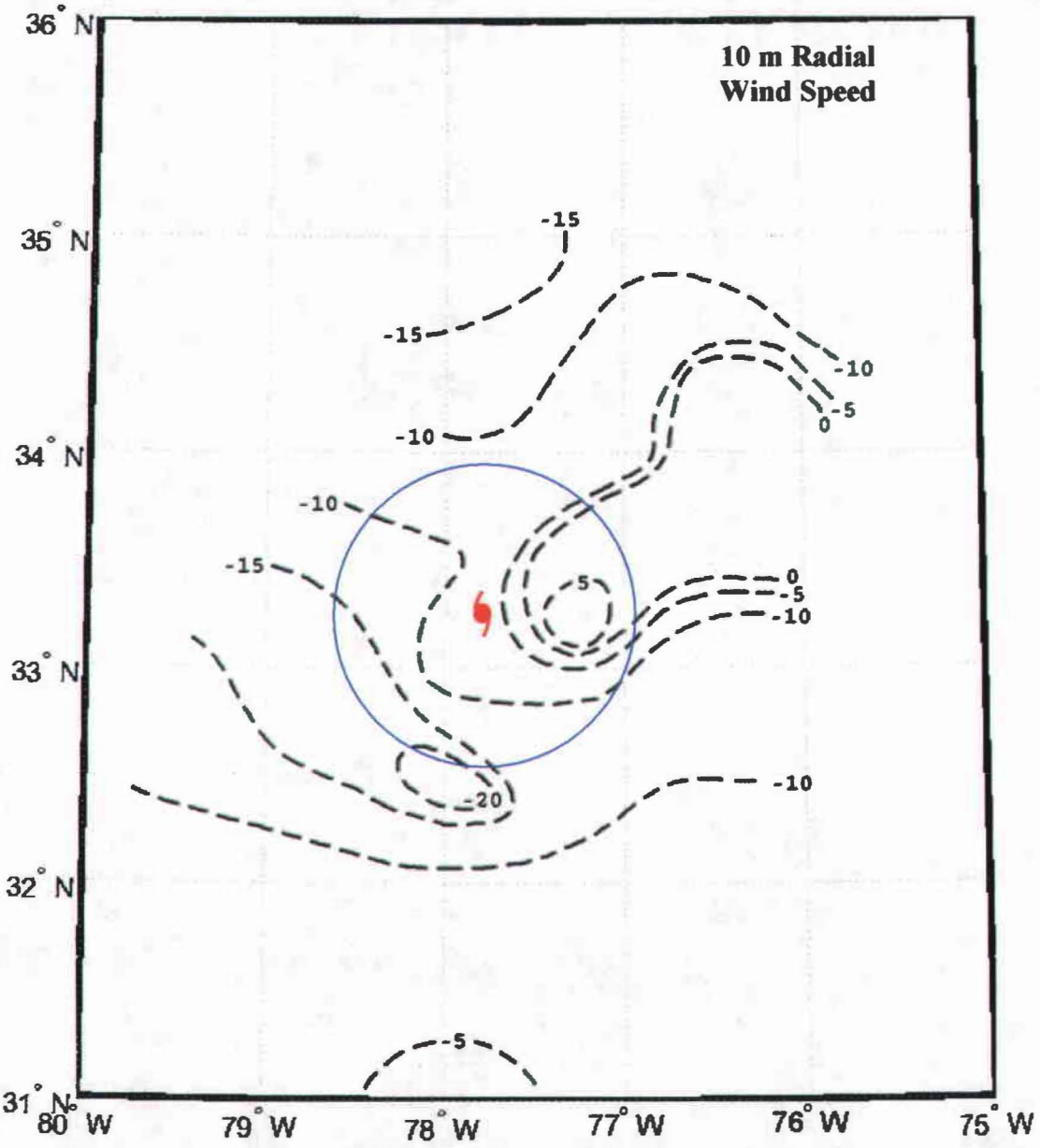

Figure 25. Storm-relative composite of Bonnie's radial winds (m s^{-1}) at 10 m. The red symbol denotes the storm center and the blue ring is Bonnie's approximate eyewall location at 1730 Z, the time of this composite. Negative values imply inflow.

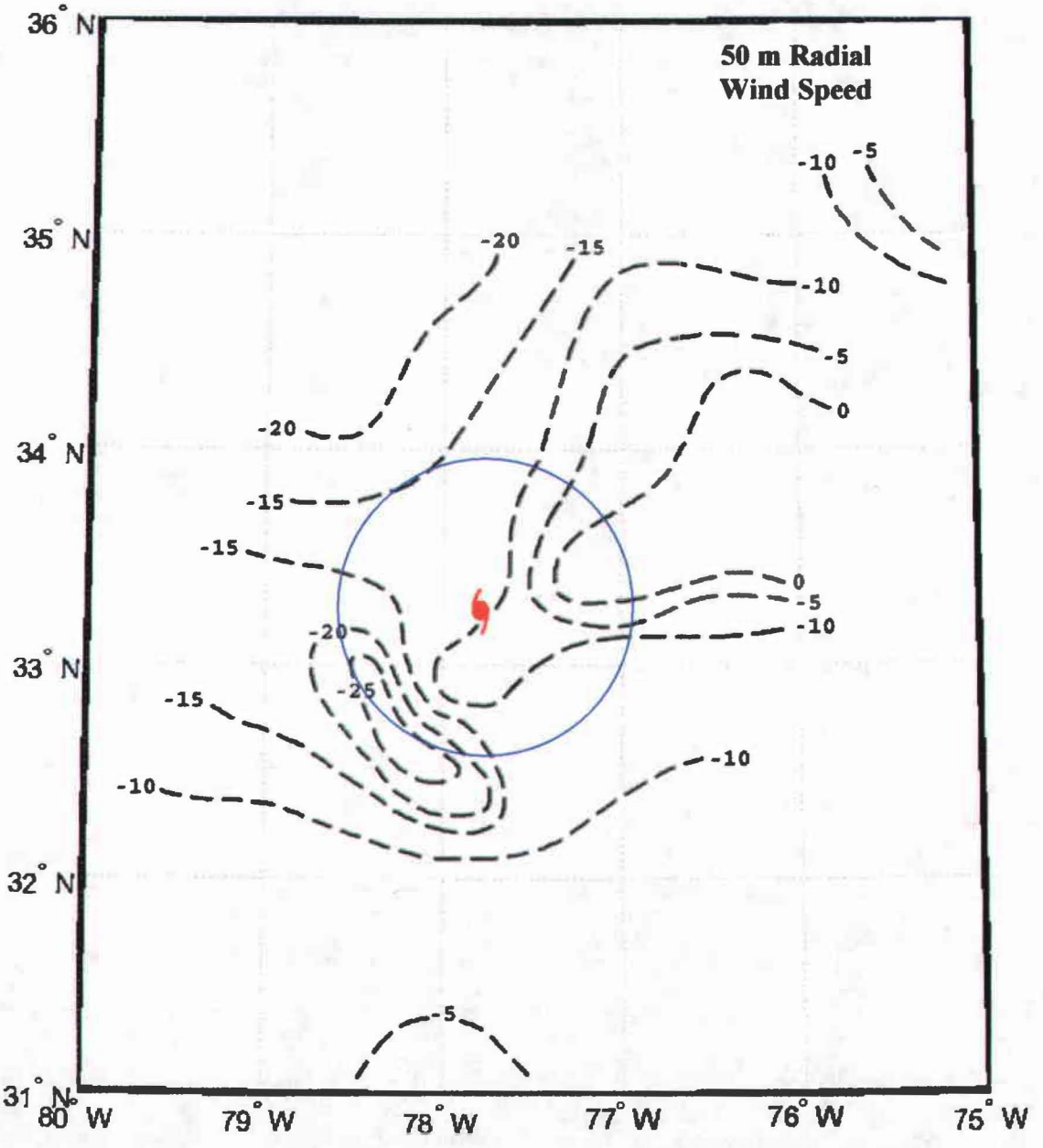

Figure 26. Similar to Figure 25, but at 50 m.

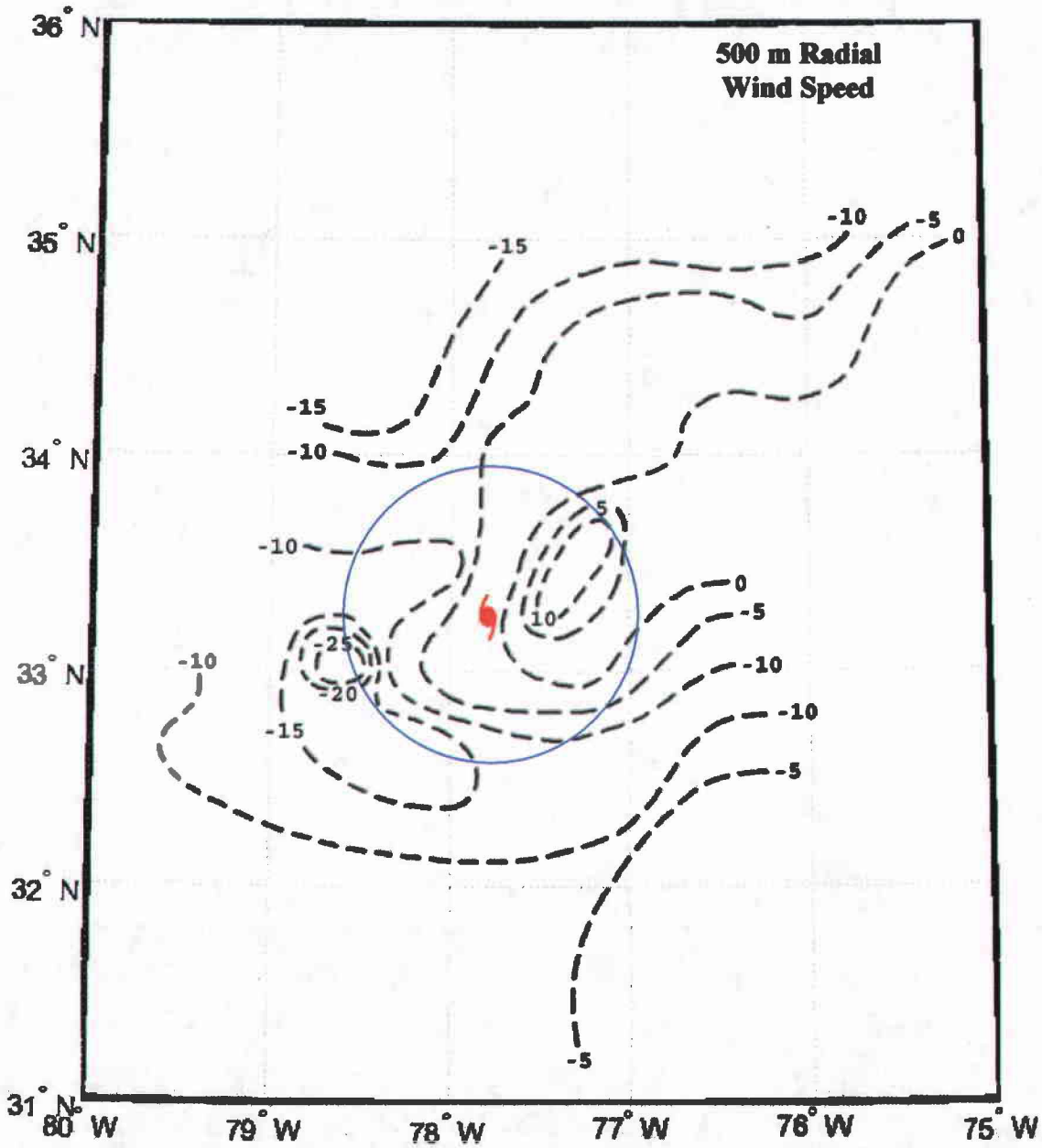

Figure 27. Similar to Figure 25, but at 500 m.

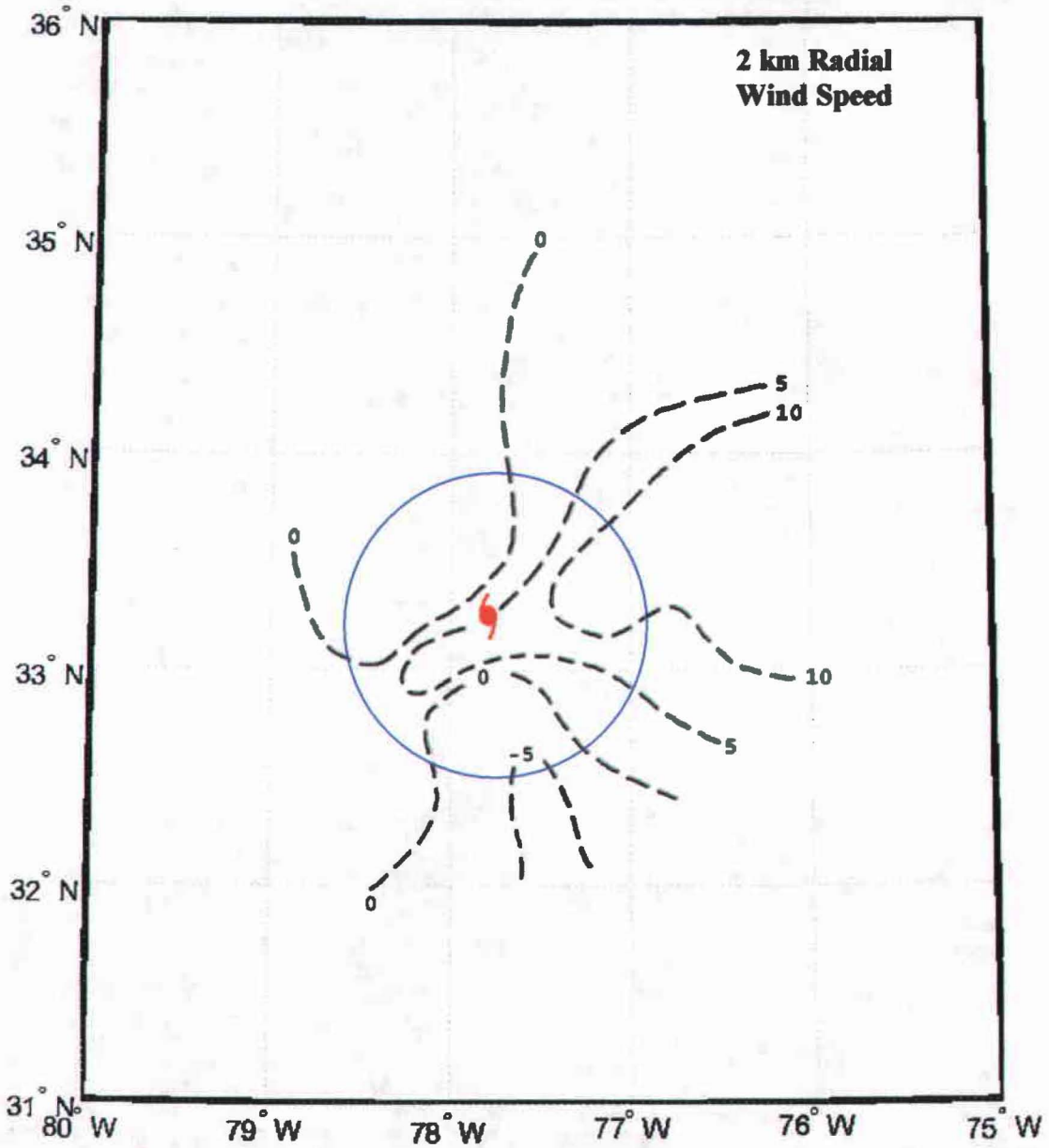

Figure 28. Similar to Figure 25, but at 2 km.

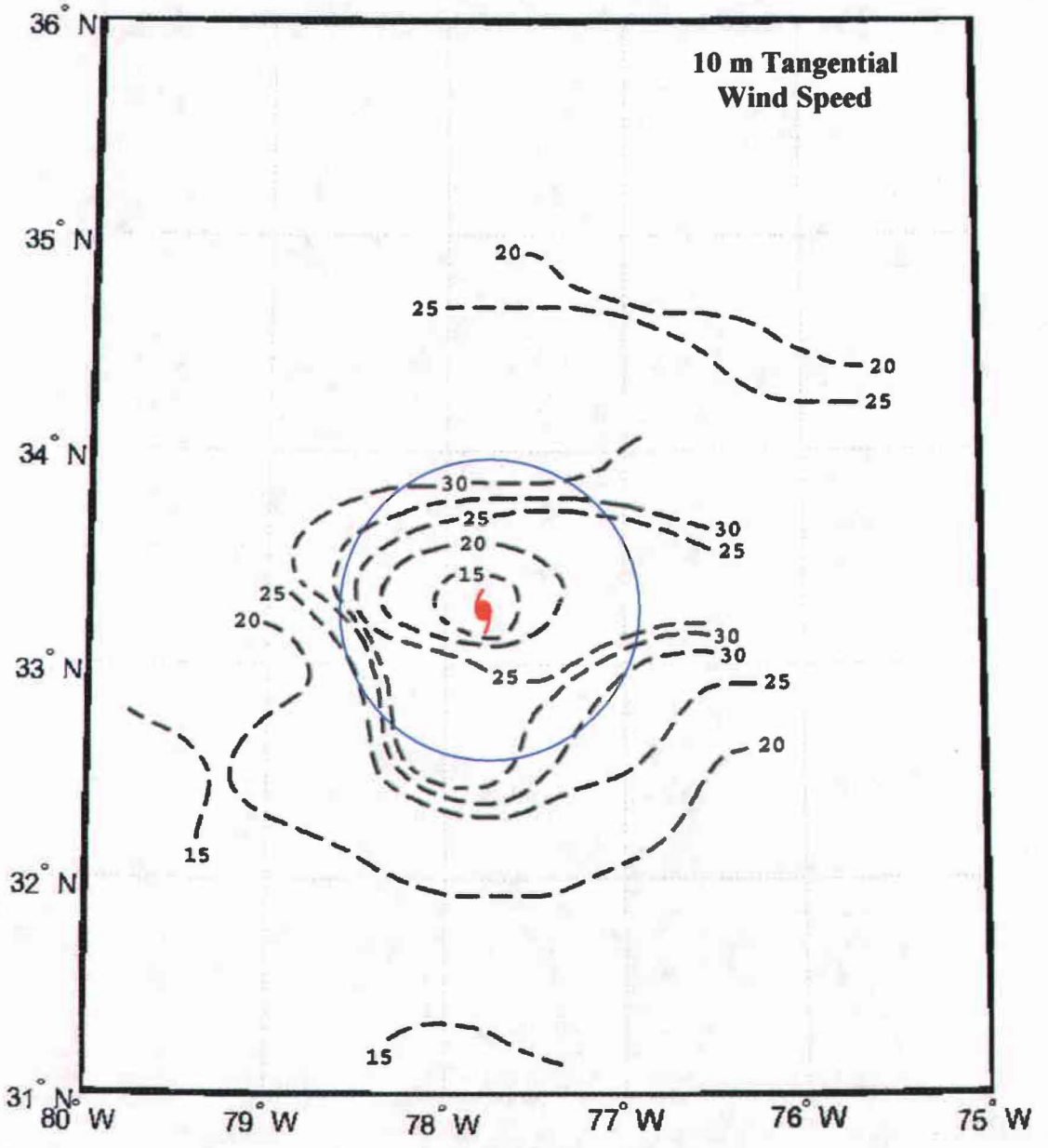

Figure 29. Storm-relative composite of Bonnie's tangential winds (m s^{-1}) at 10 m. The red symbol denotes the storm center and the blue ring is Bonnie's approximate eyewall location at 1730 Z, the time of this composite.

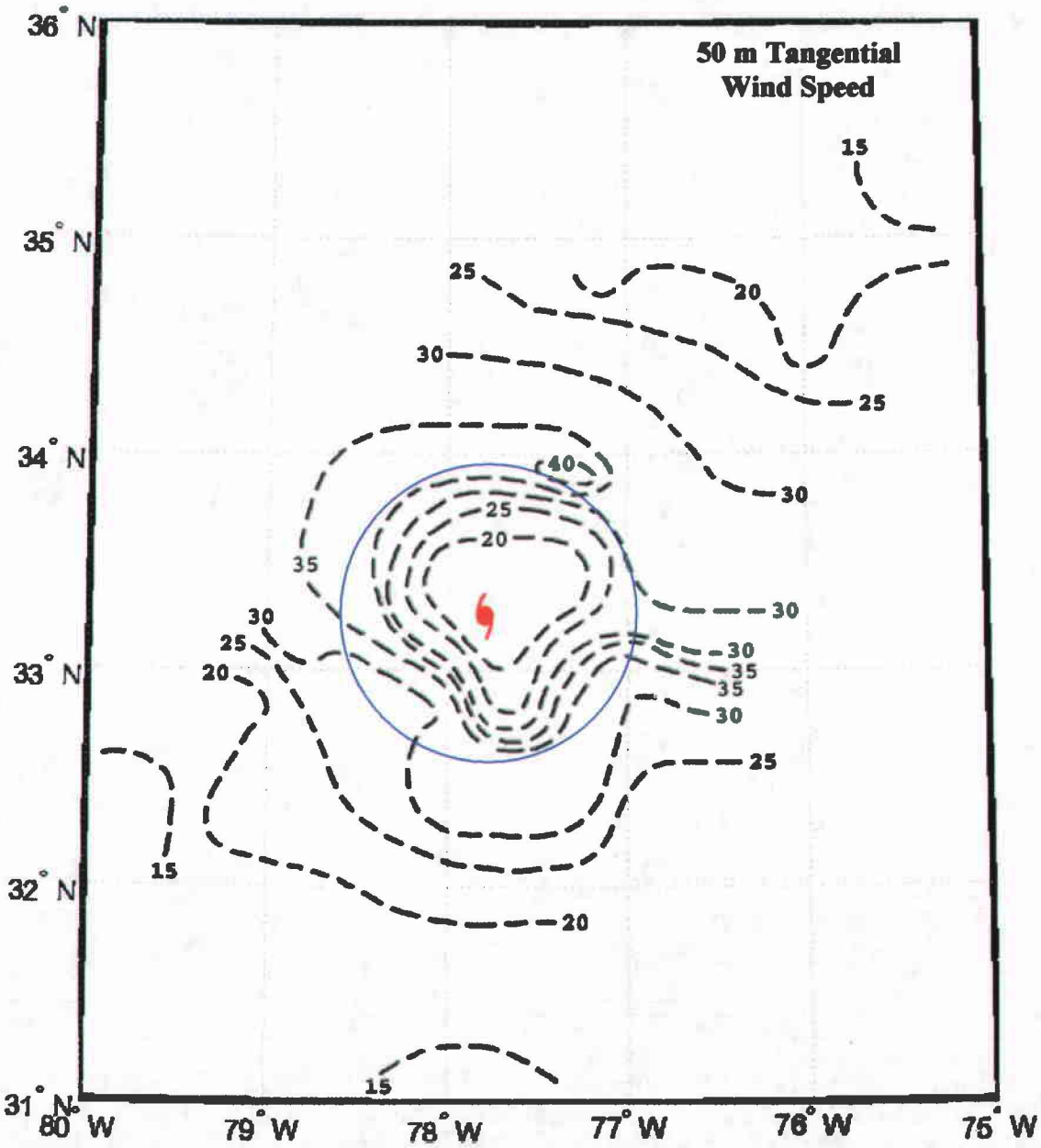

Figure 30. Similar to Figure 29, but at 50 m.

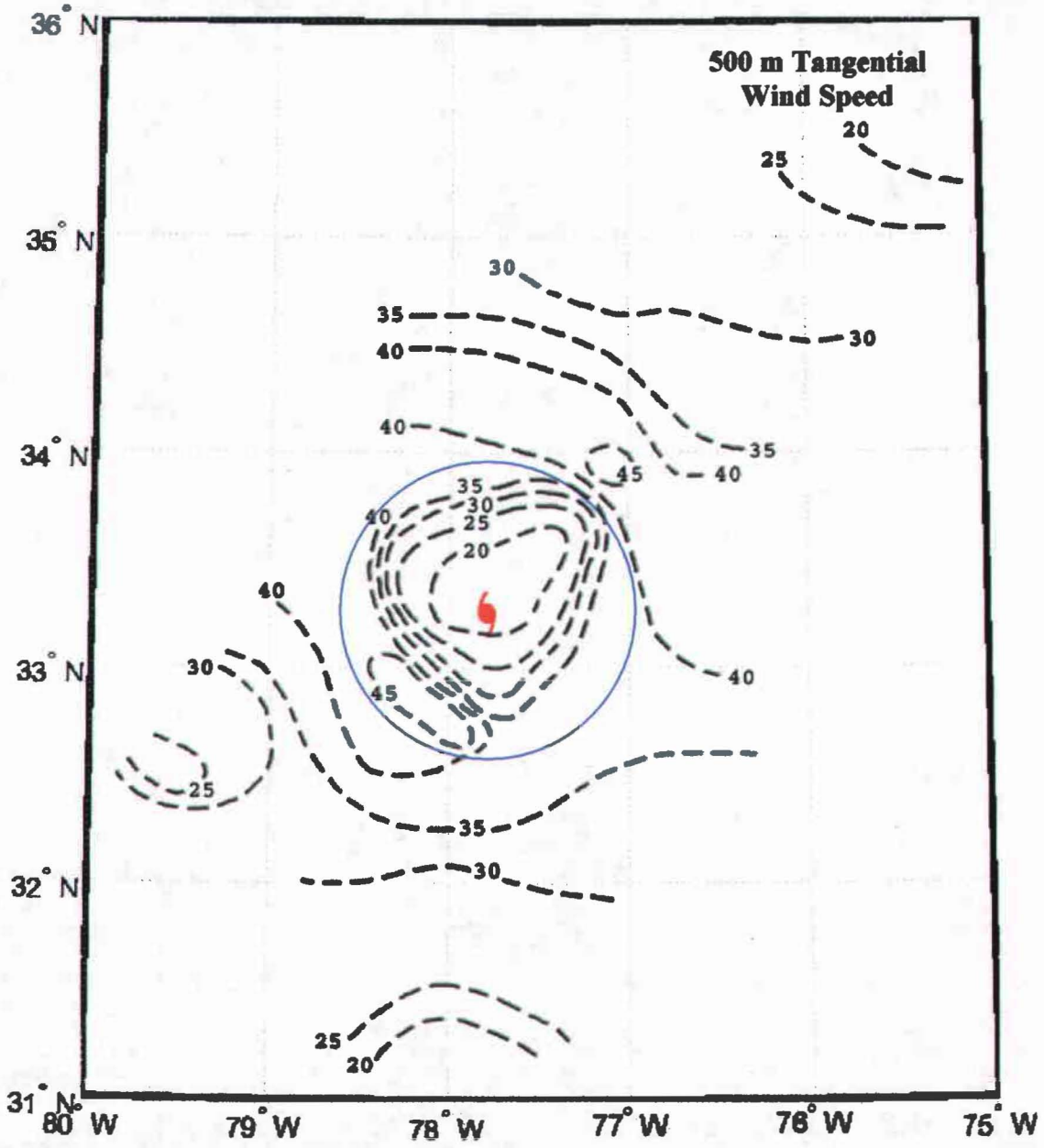

Figure 31. Similar to Figure 29, but at 500 m.

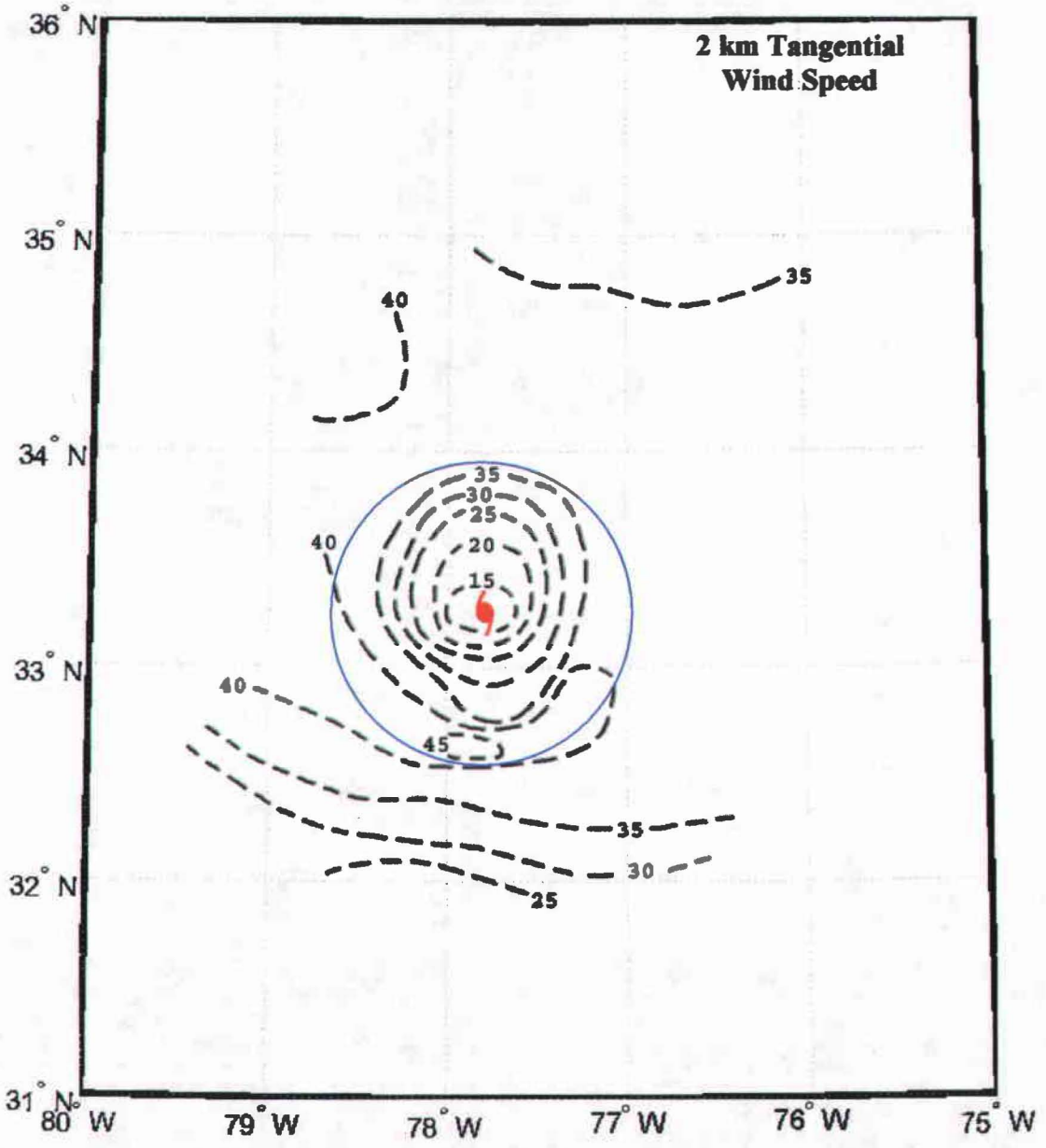

Figure 32. Similar to Figure 29, but at 2 km.

a)

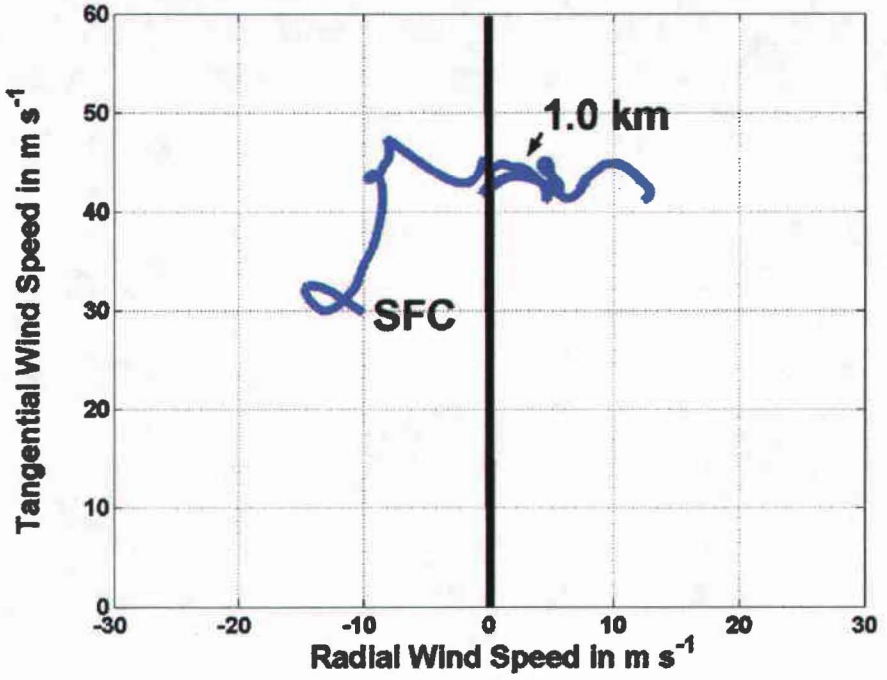

b)

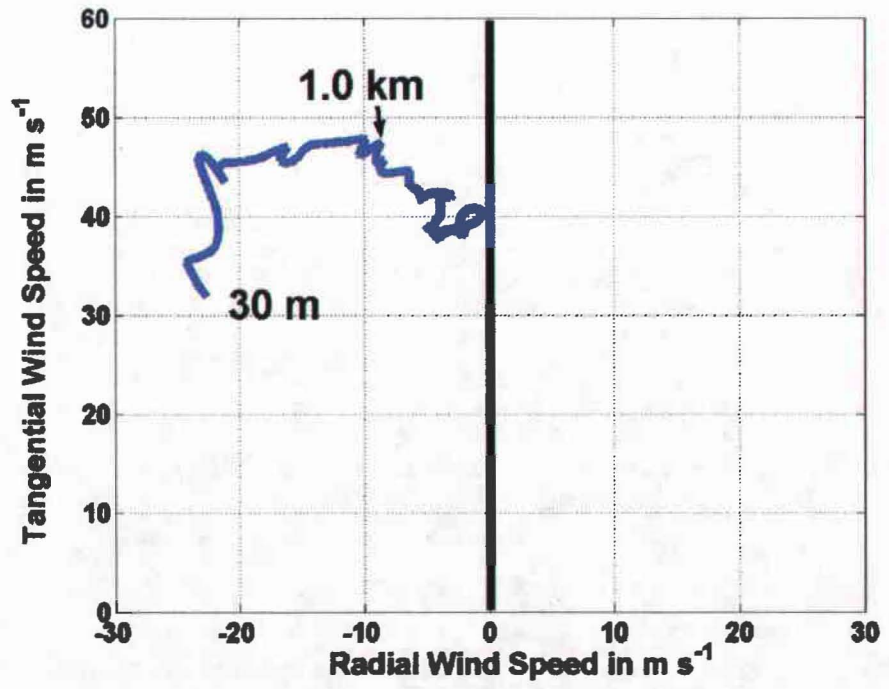

Figure 33. Hodographs from each storm relative quadrant a radial distance of ~115 km from storm center. a) NE quadrant, b) NW quadrant, c) SW quadrant, d) SE quadrant.

c)

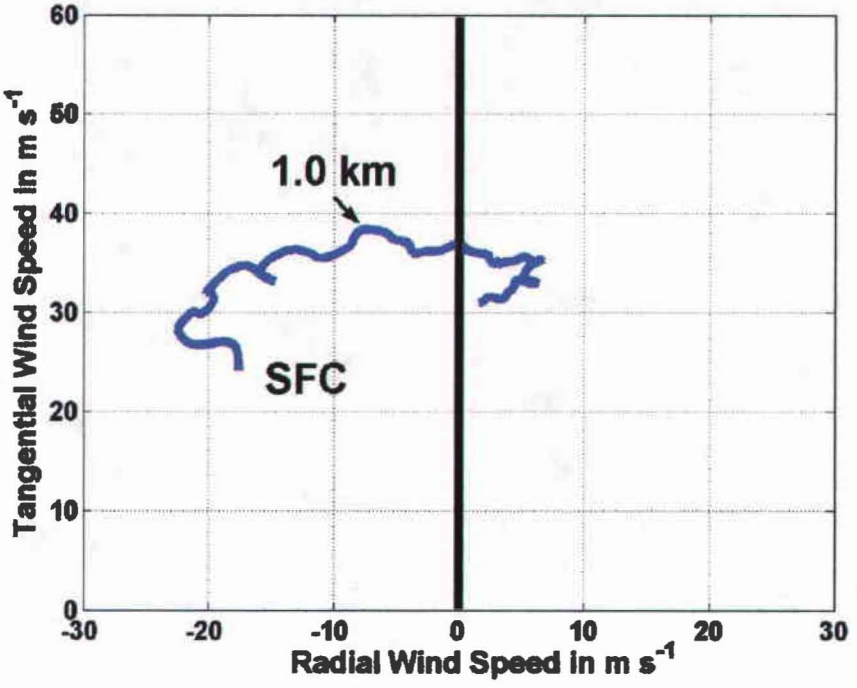
1.0 km
SFC
Tangential Wind Speed in m s-1
Radial Wind Speed in m s-1
60
50
40
30
20
10
0
-30
-20
-10
0
10
20
30

d)

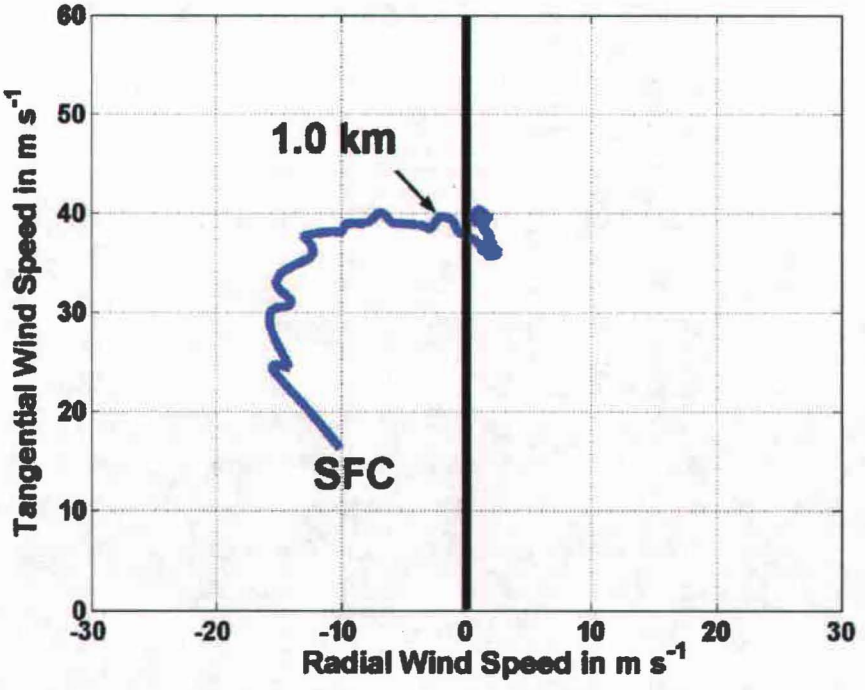
1.0 km
SFC
Tangential Wind Speed in m s-1
Radial Wind Speed in m s-1
60
50
40
30
20
10
0
-30
-20
-10
0
10
20
30

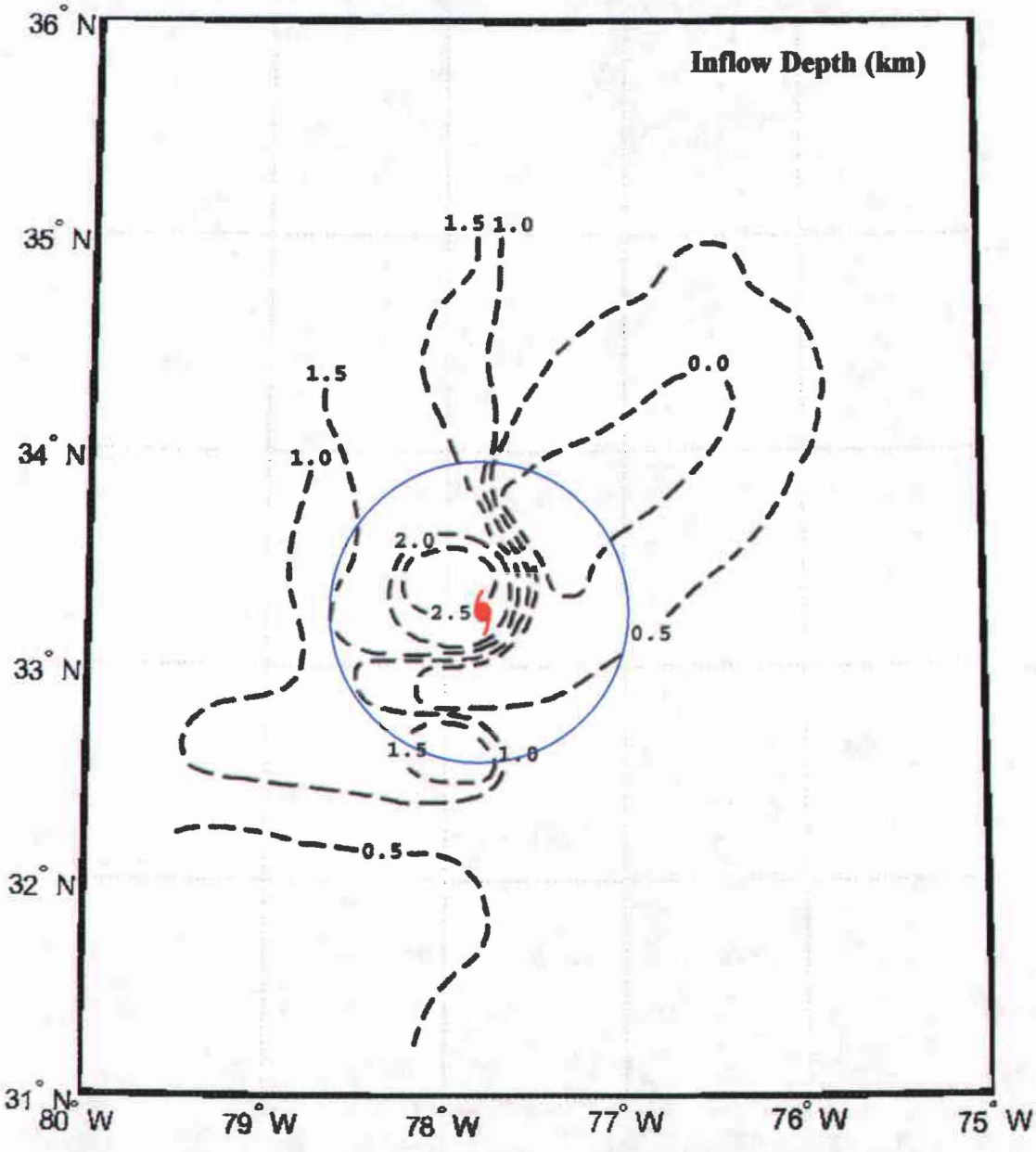

Figure 34. Storm-relative inflow depth (km) of Hurricane Bonnie.

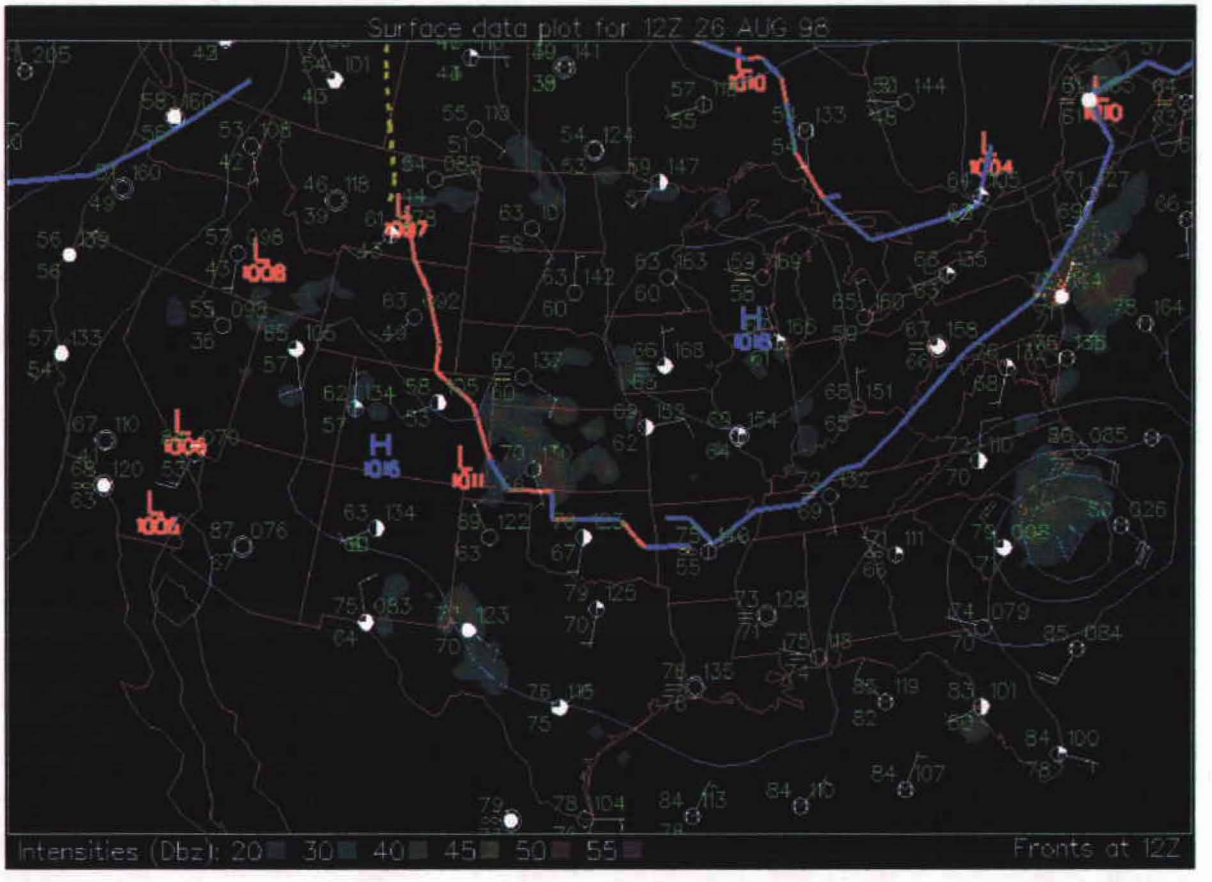

Figure 35. Surface analysis for 1200 Z August 26, 1998. Taken from http://weather.unisys.com.

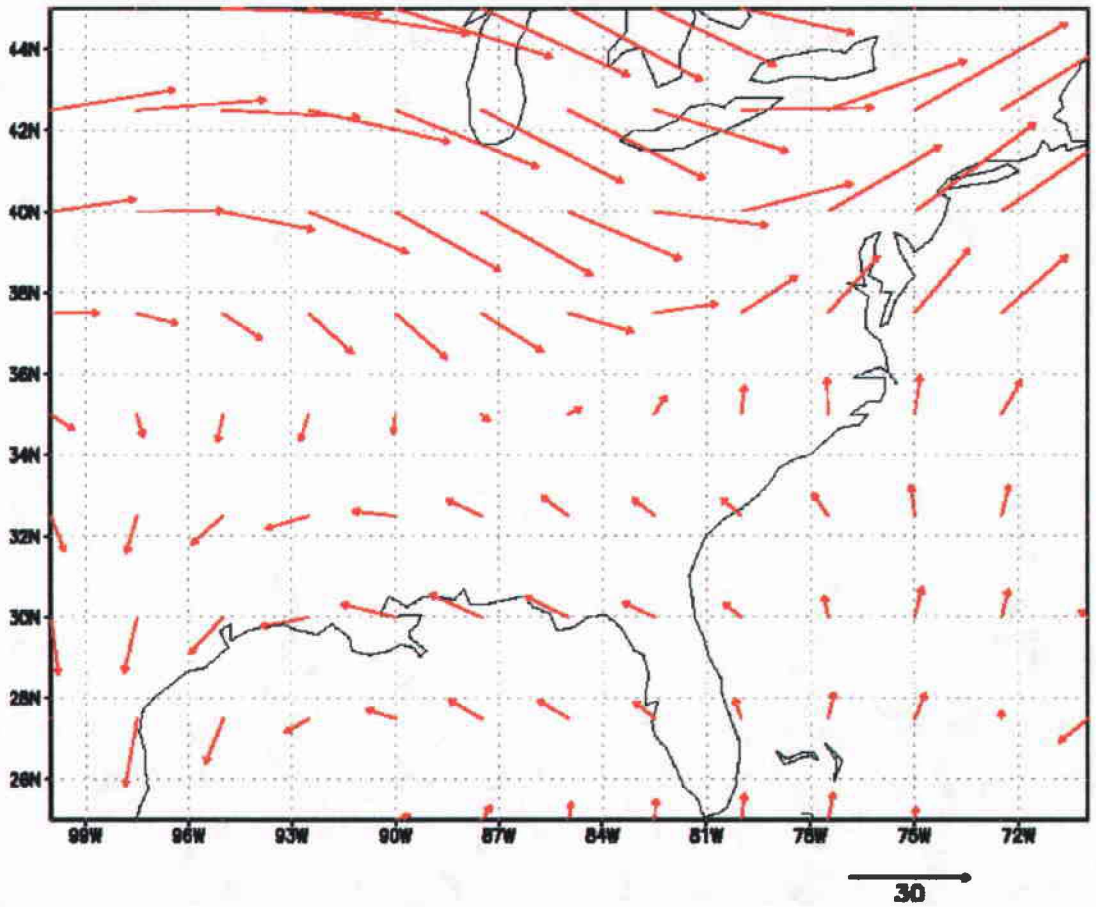

Figure 36. Winds at 200 hPa (m s^{-1}) at 1800 Z on August 26, 1998.

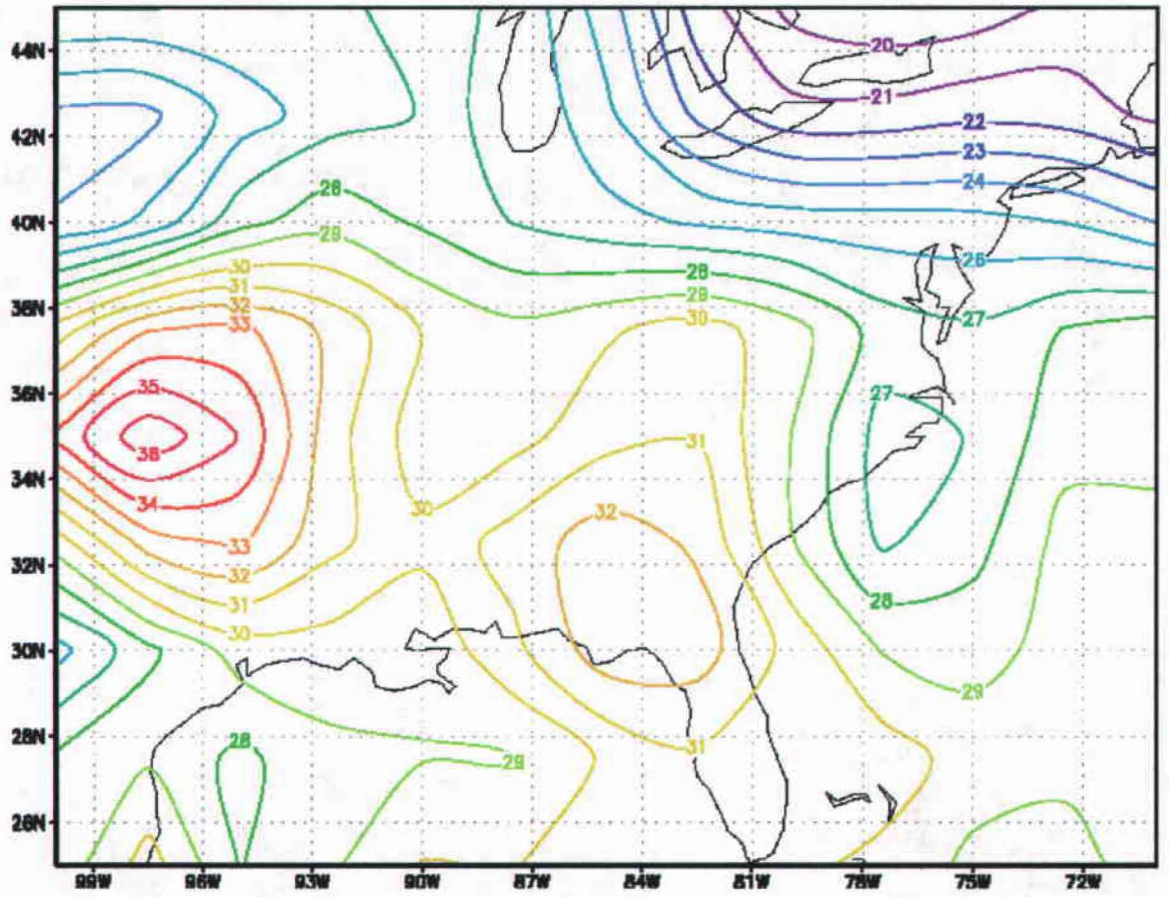

Figure 37. Surface temperature (°C) at 1800 Z on August 26, 1998.

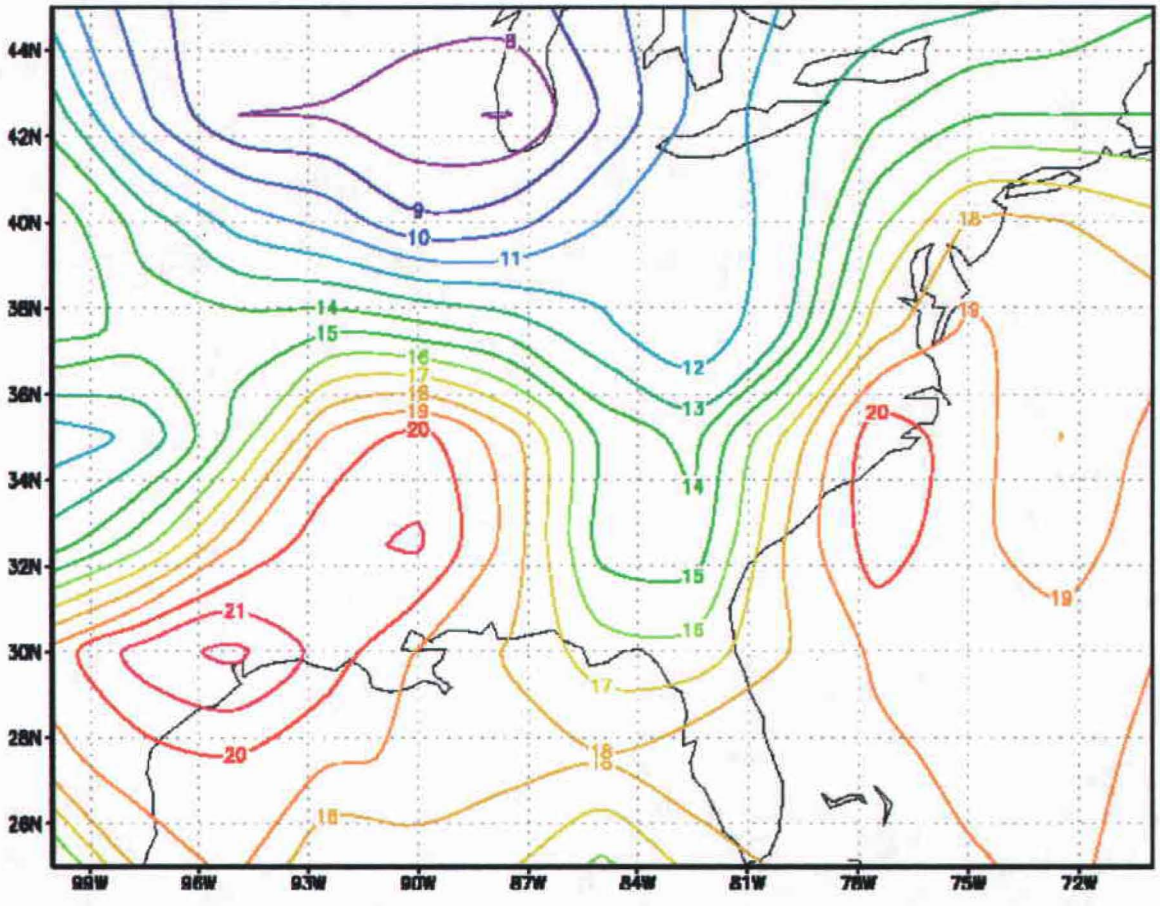

Figure 38. Surface specific humidity (g kg^{-1}) at 1800 Z on August 26, 1998.

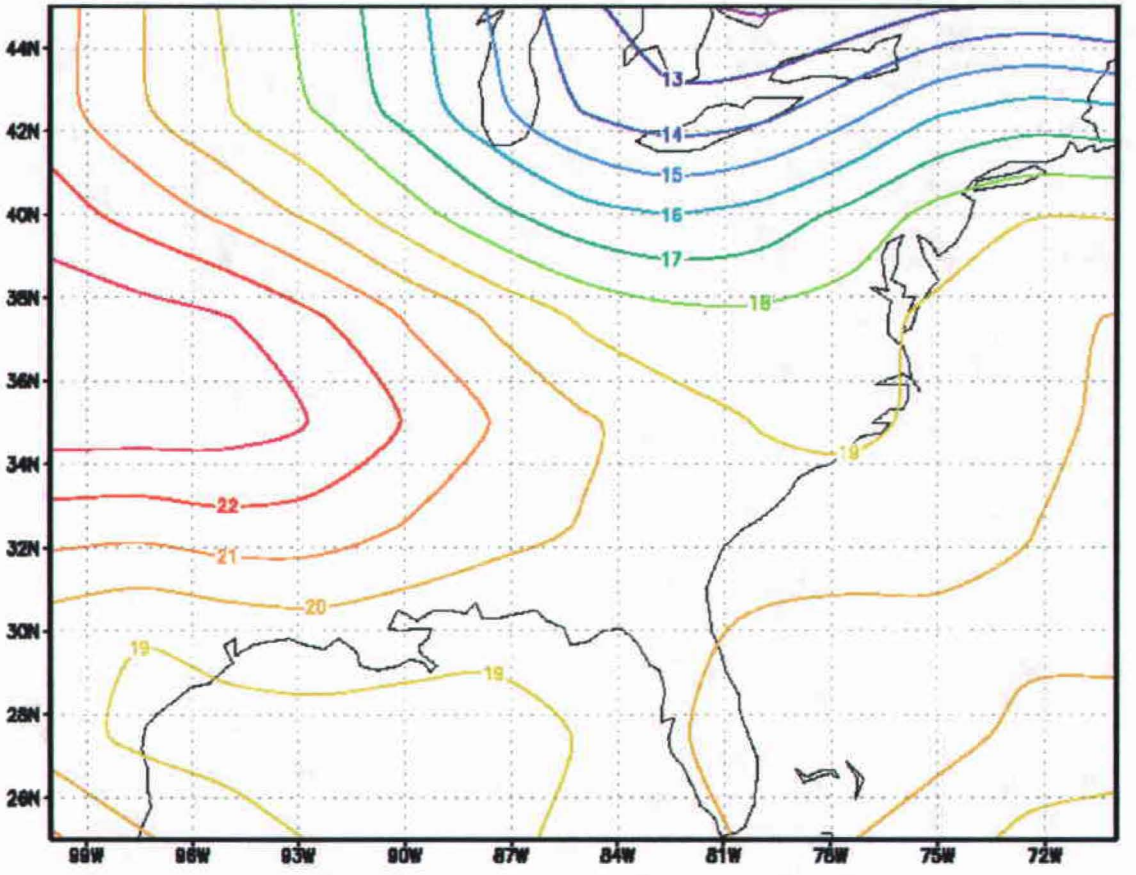

Figure 39. Temperature (°C) at 850 hPa, 1800 Z on August 26, 1998.

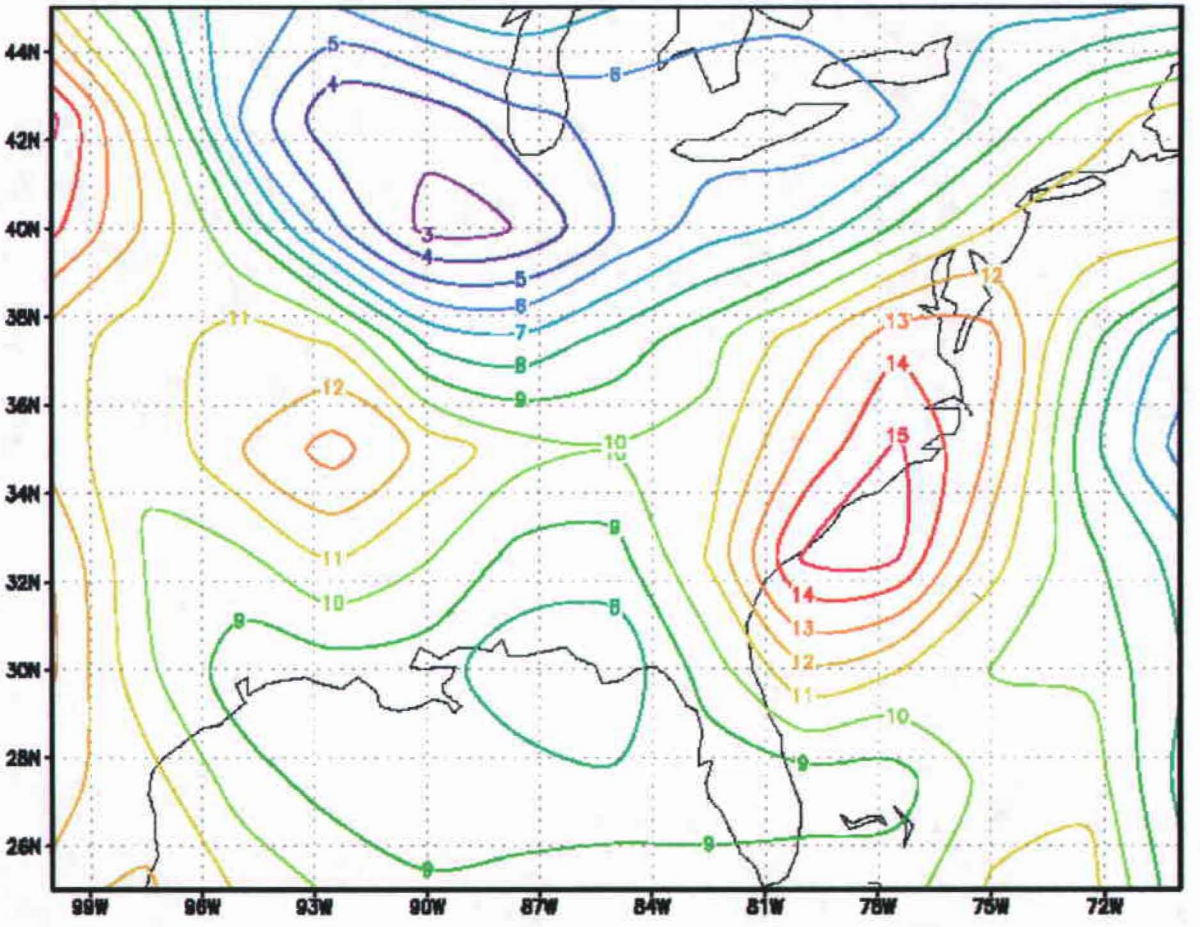

Figure 40. Specific humidity (g kg^{-1}) at 850 hPa, 1800 Z on August 26, 1998.

APPENDIX

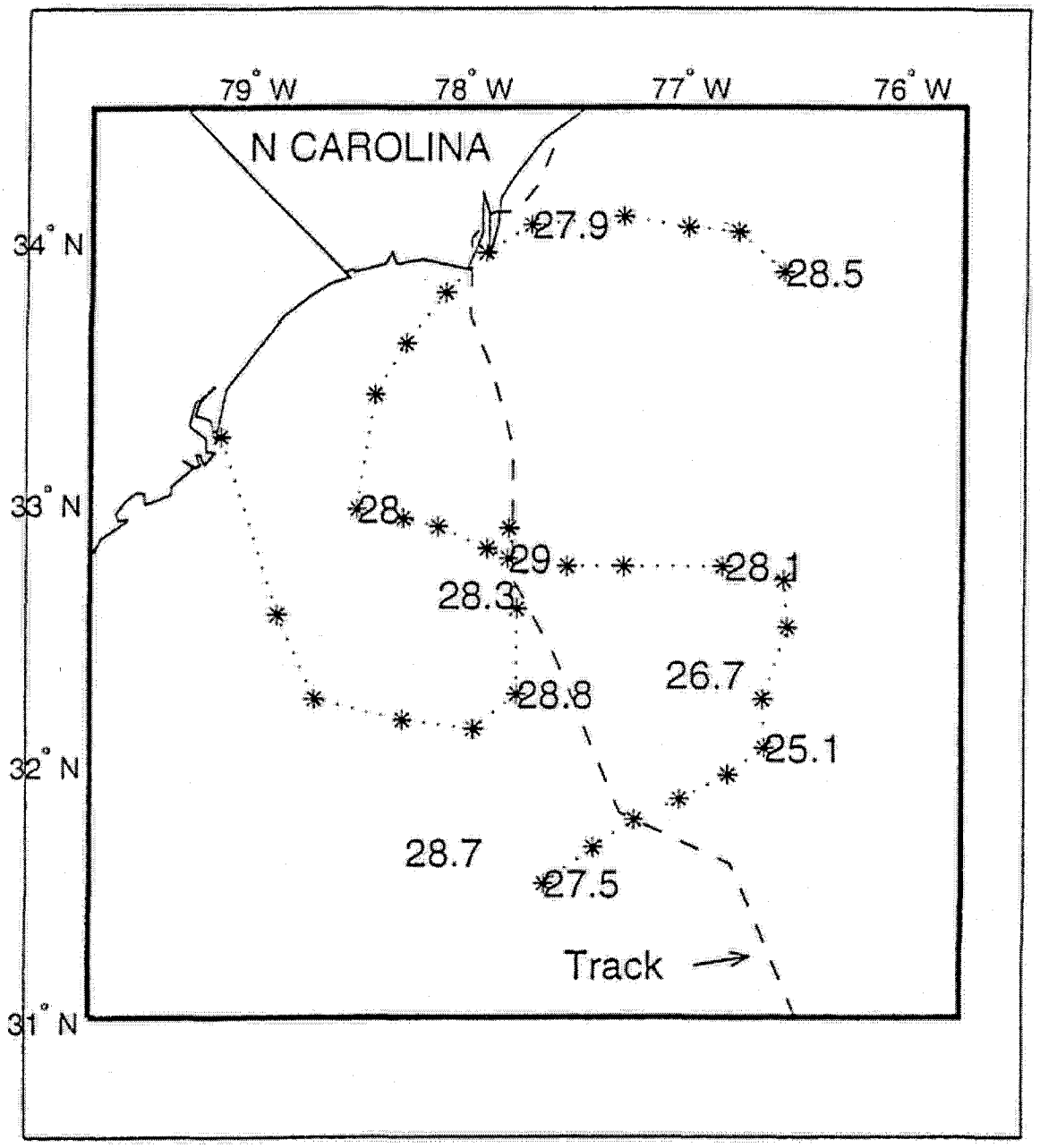

A. Sea surface temperature for Hurricane Bonnie as measured by AXBTs (Airborne Expendable Bathythermographs) deployed from 1220-1716 Z August 26th, 1998. The dropwindsondes are noted by the stars and the dotted lines mark the trajectories. The storm's track is noted by a dashed line. (Wroe and Barnes 2003.)

B. Storm-Relative Composites of Various Fields

B.1. Temperature (°C)

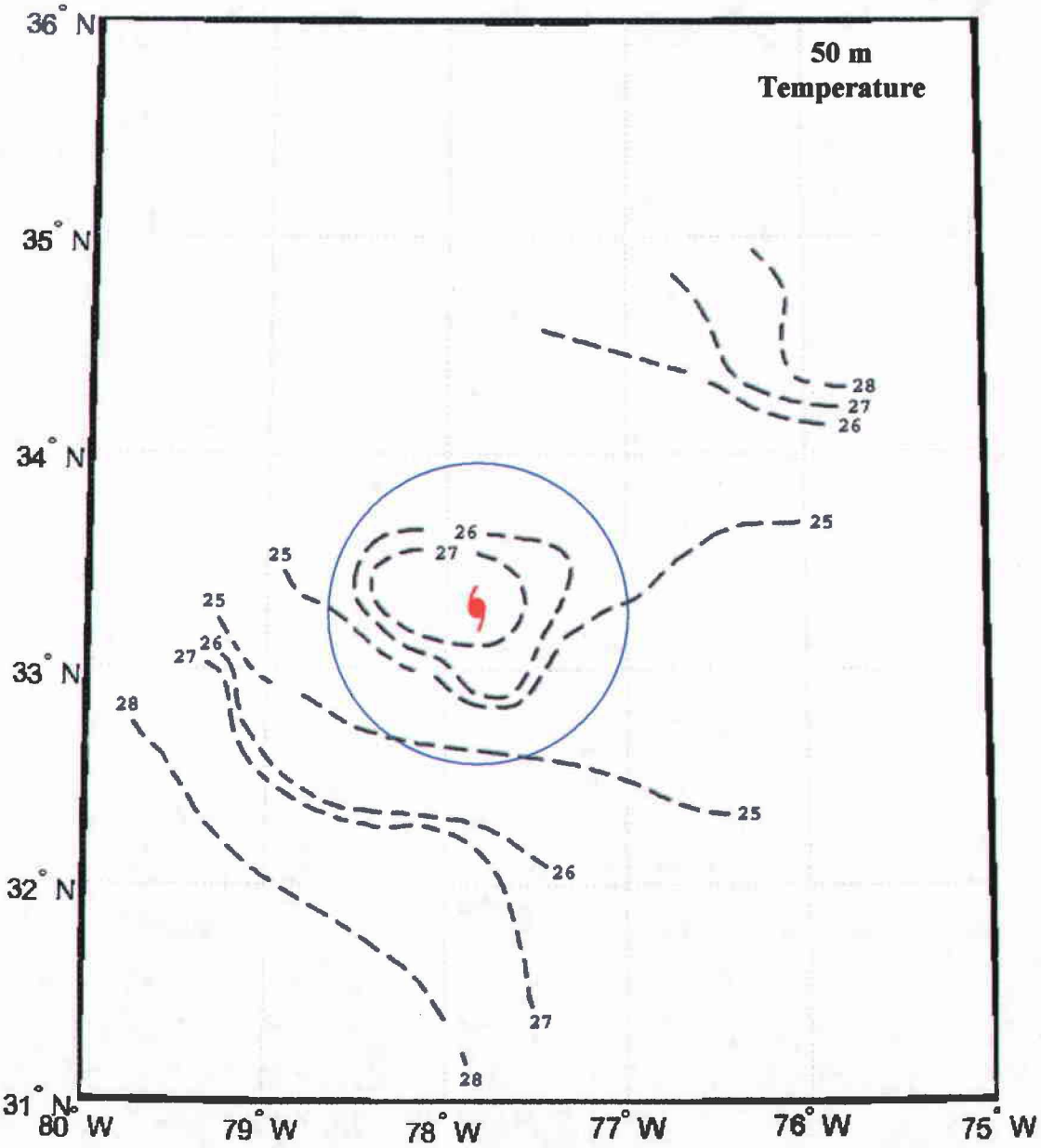

B.1.1. Storm-relative composite of Bonnie's temperature (°C) at 50 m. The red symbol denotes the storm center and the blue ring is Bonnie's approximate eyewall location at 1730 Z, the time of this composite.

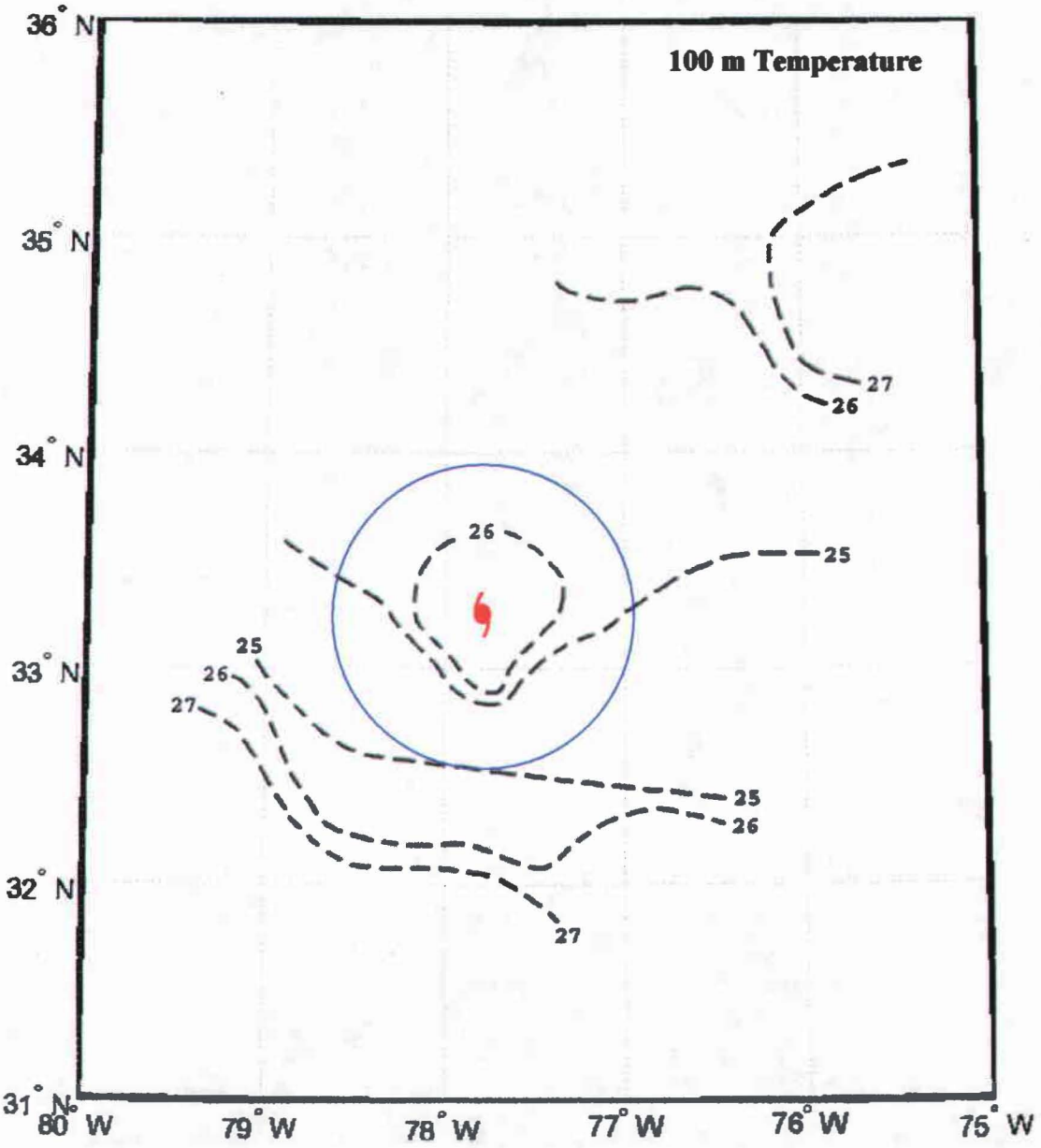

B.1.2. Similar to B.1.1., but at 100 m.

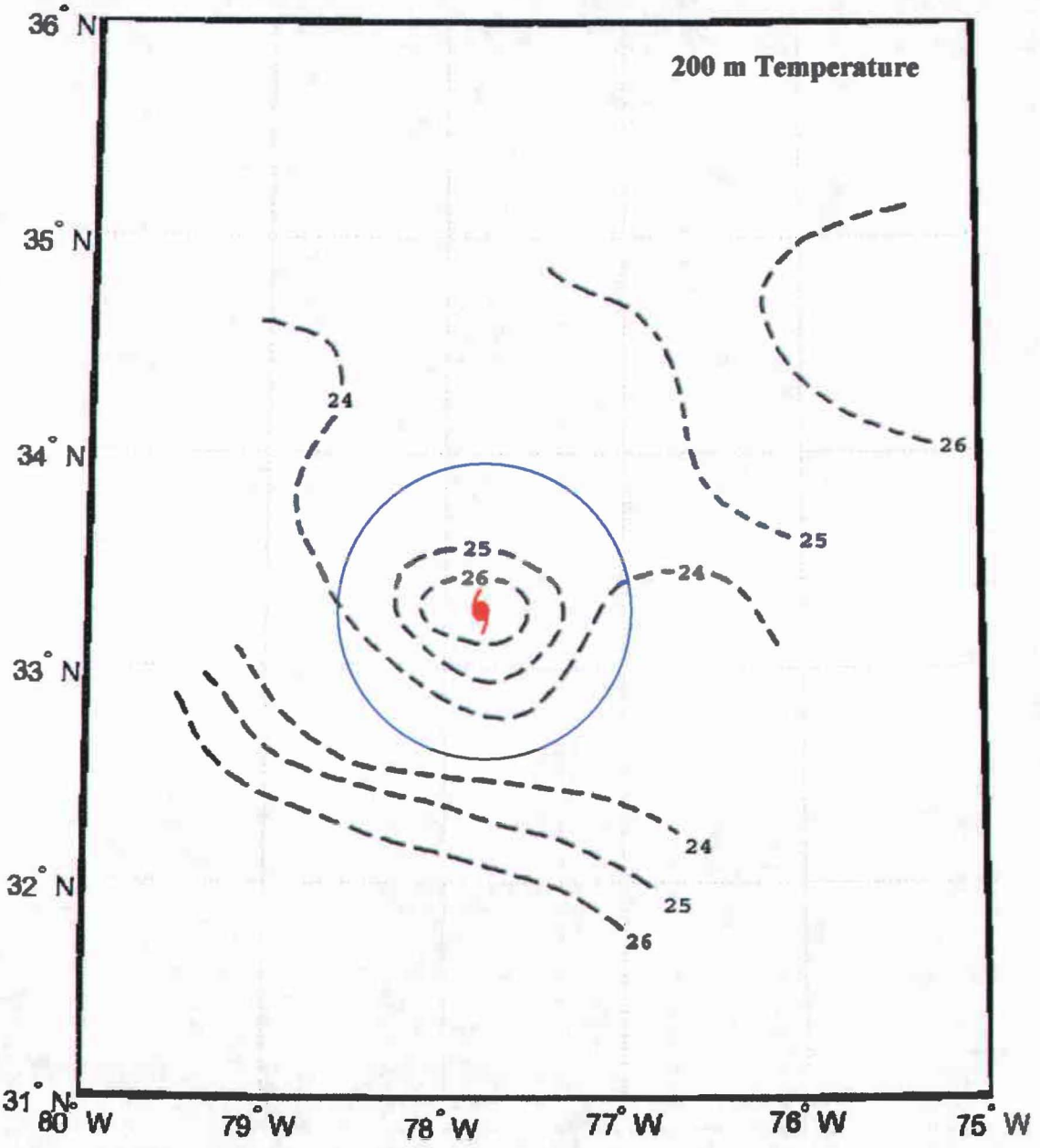

B.1.3. Similar to B.1.1., but at 200 m.

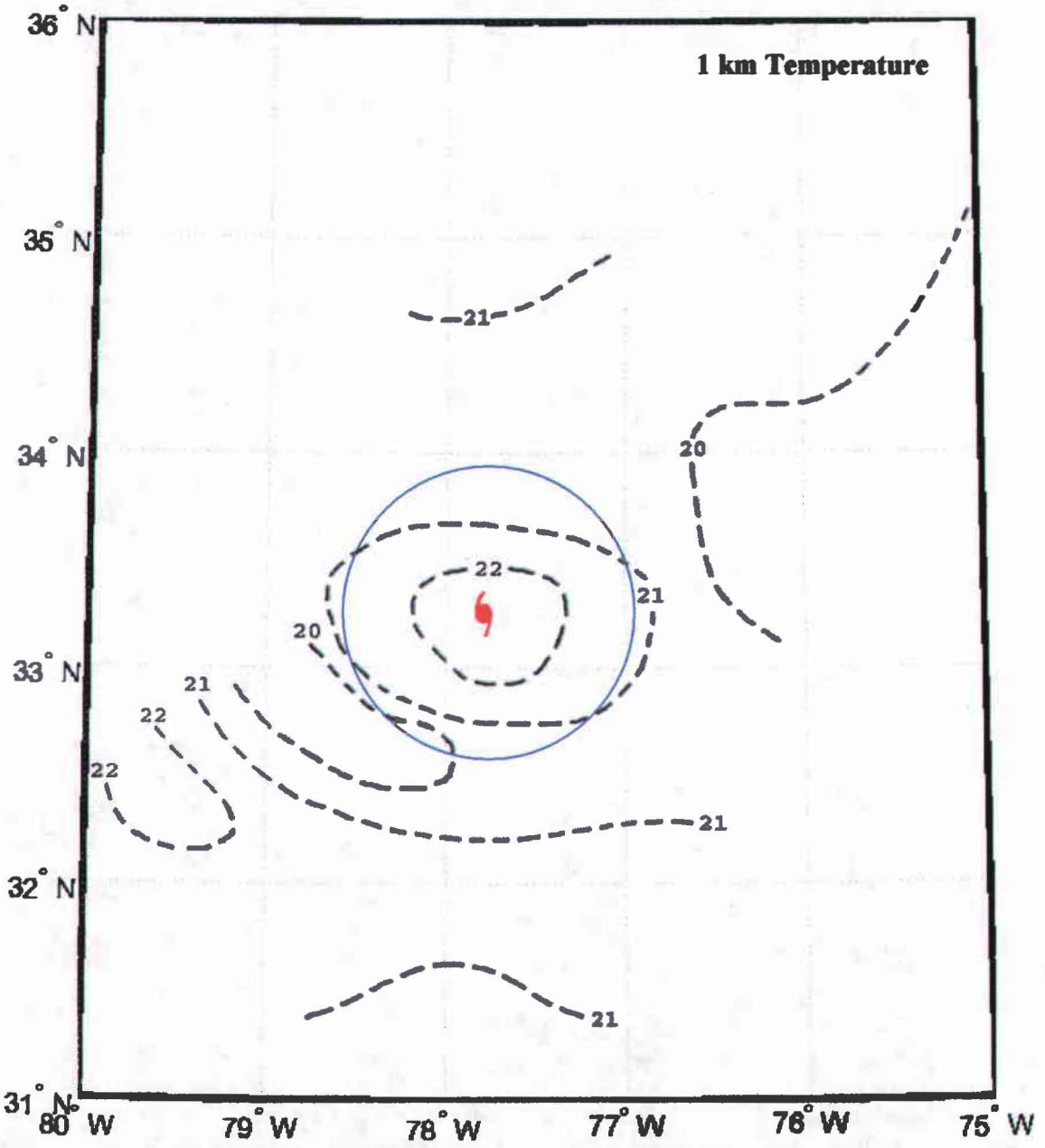

B.1.4. Similar to B.1.1., but at 1 km.

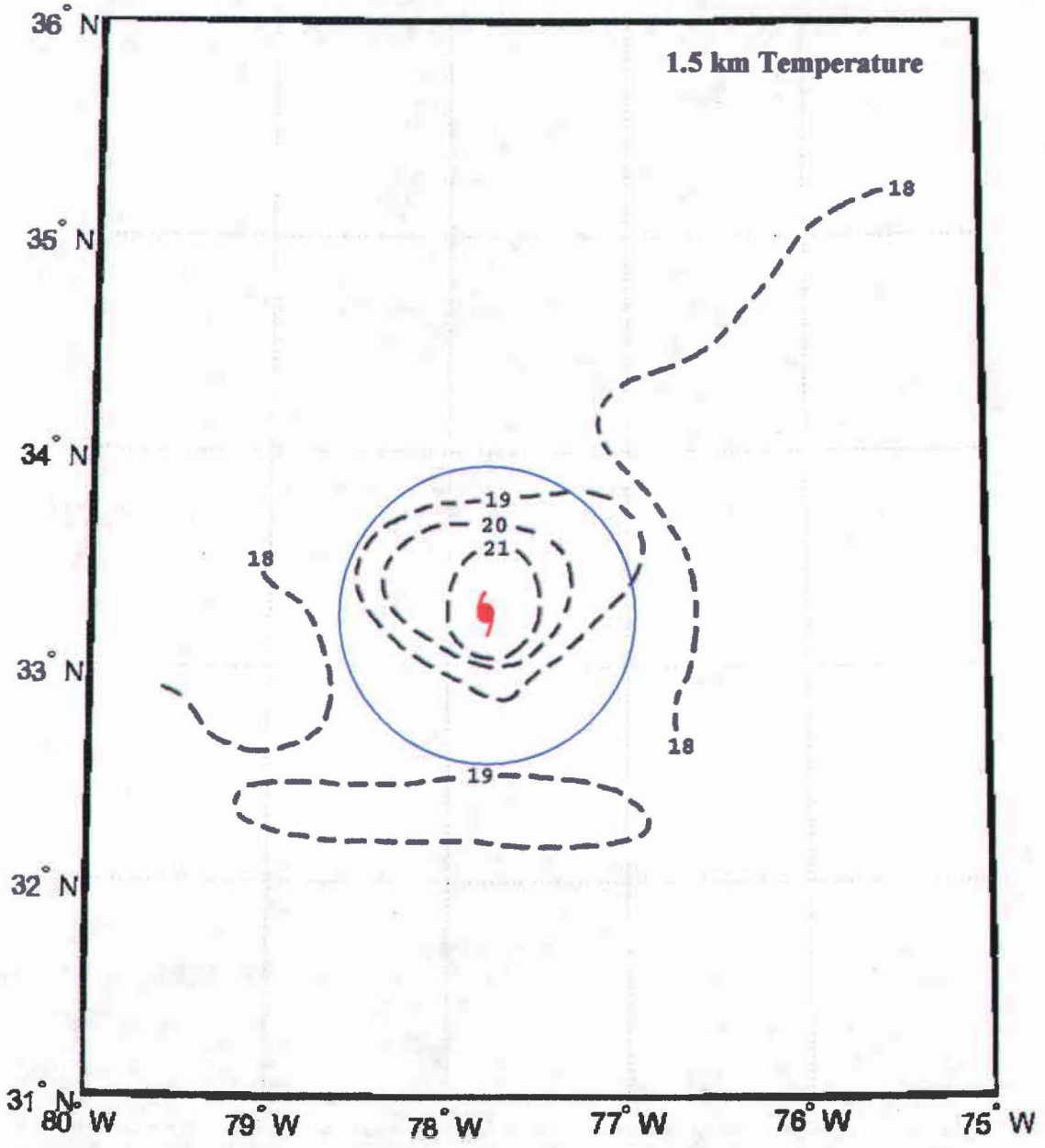

B.1.5. Similar to B.1.1., but at 1.5 km.

B.2. Specific Humidity (g kg^{-1})

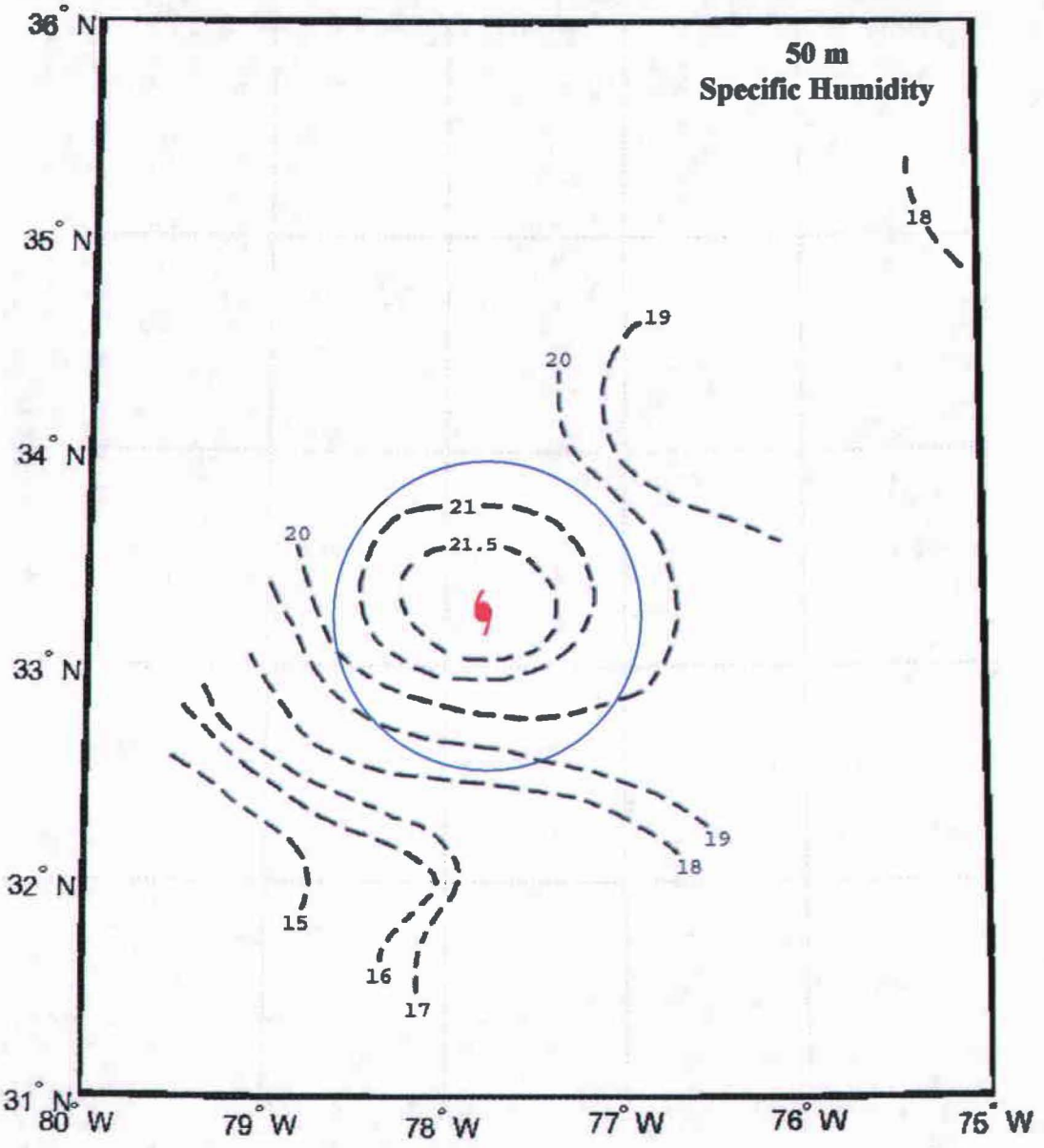

B.2.1. Storm-relative composite of Bonnie's specific humidity (g kg^{-1}) at 50 m. The red symbol denotes the storm center and the blue ring is Bonnie's approximate eyewall location at 1730 Z, the time of this composite.

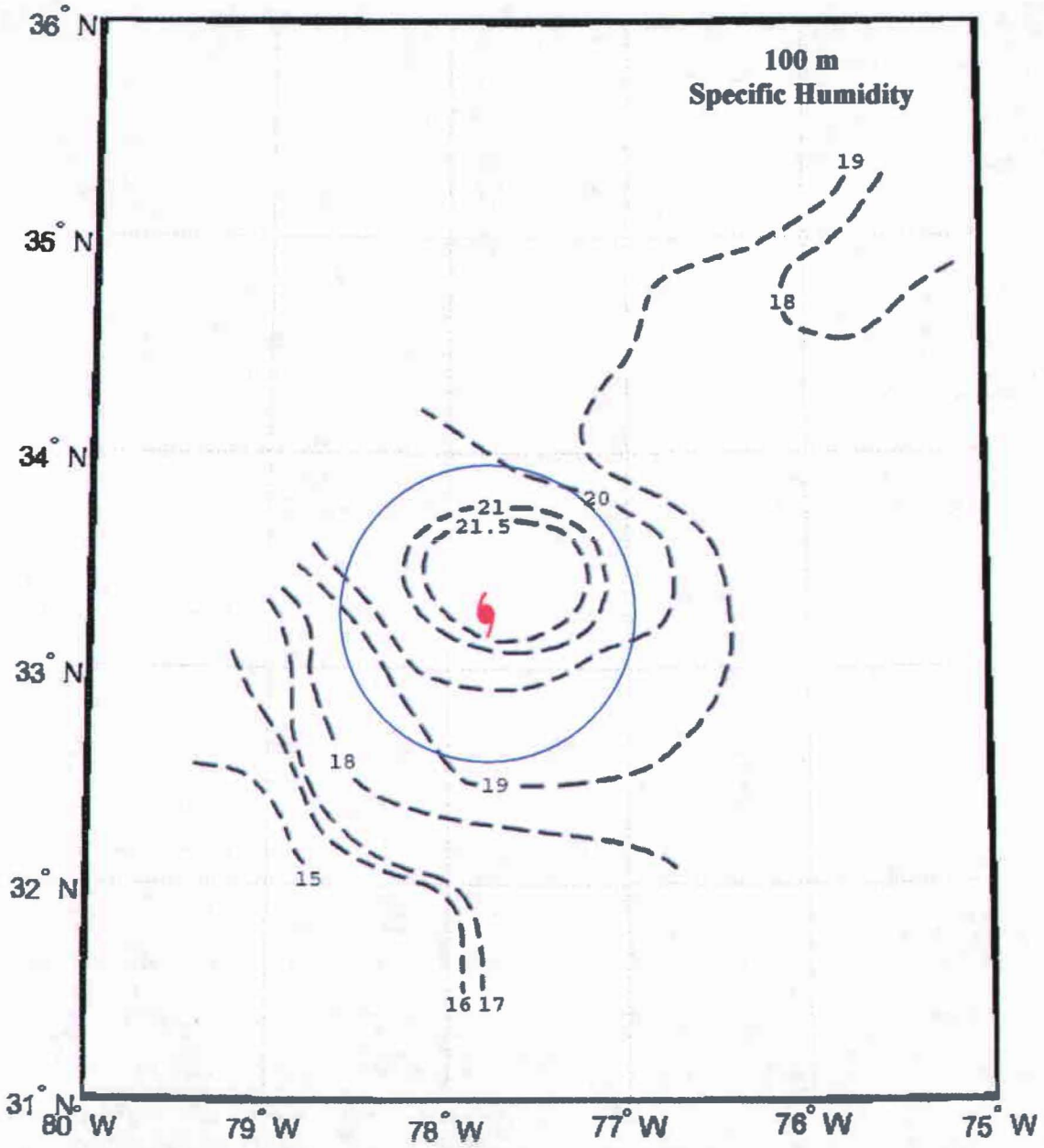

B.2.2. Similar to B.2.1., but at 100 m.

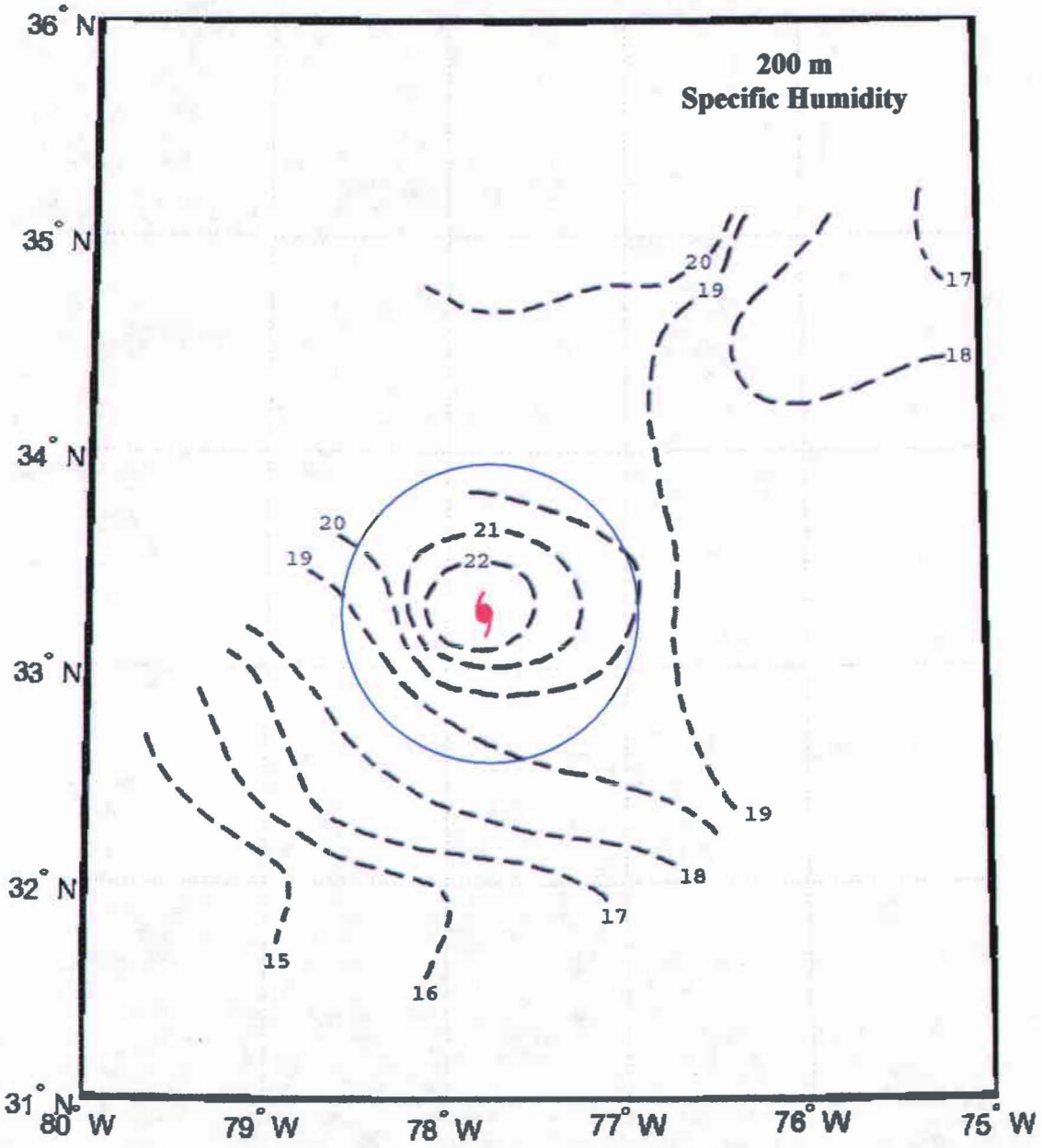

B.2.3. Similar to B.2.1., but at 200 m.

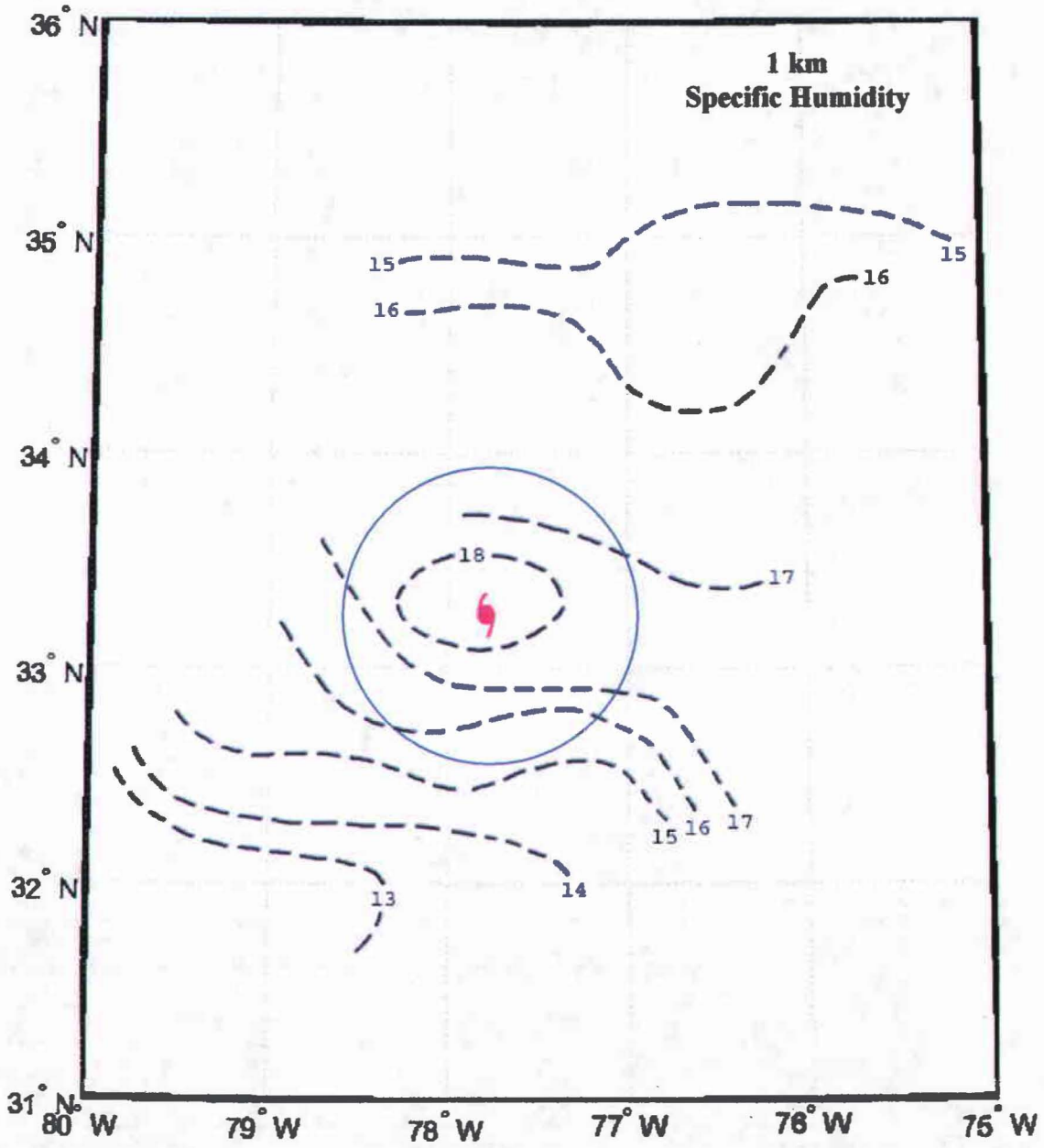

B.2.4. Similar to B.2.1., but at 1 km.

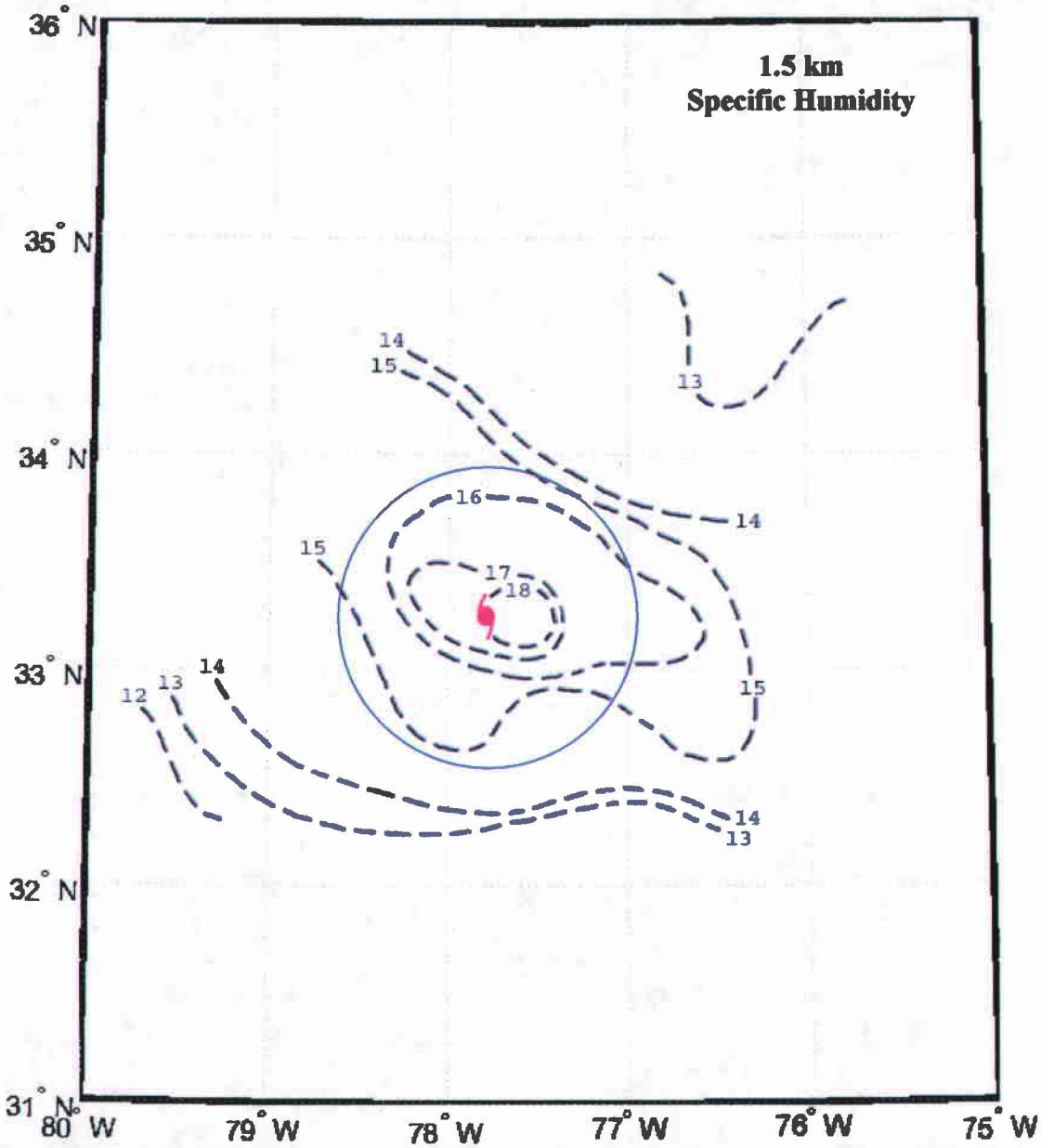

B.2.5. Similar to B.2.1., but at 1.5 km.

B.3. Potential Temperature (K)

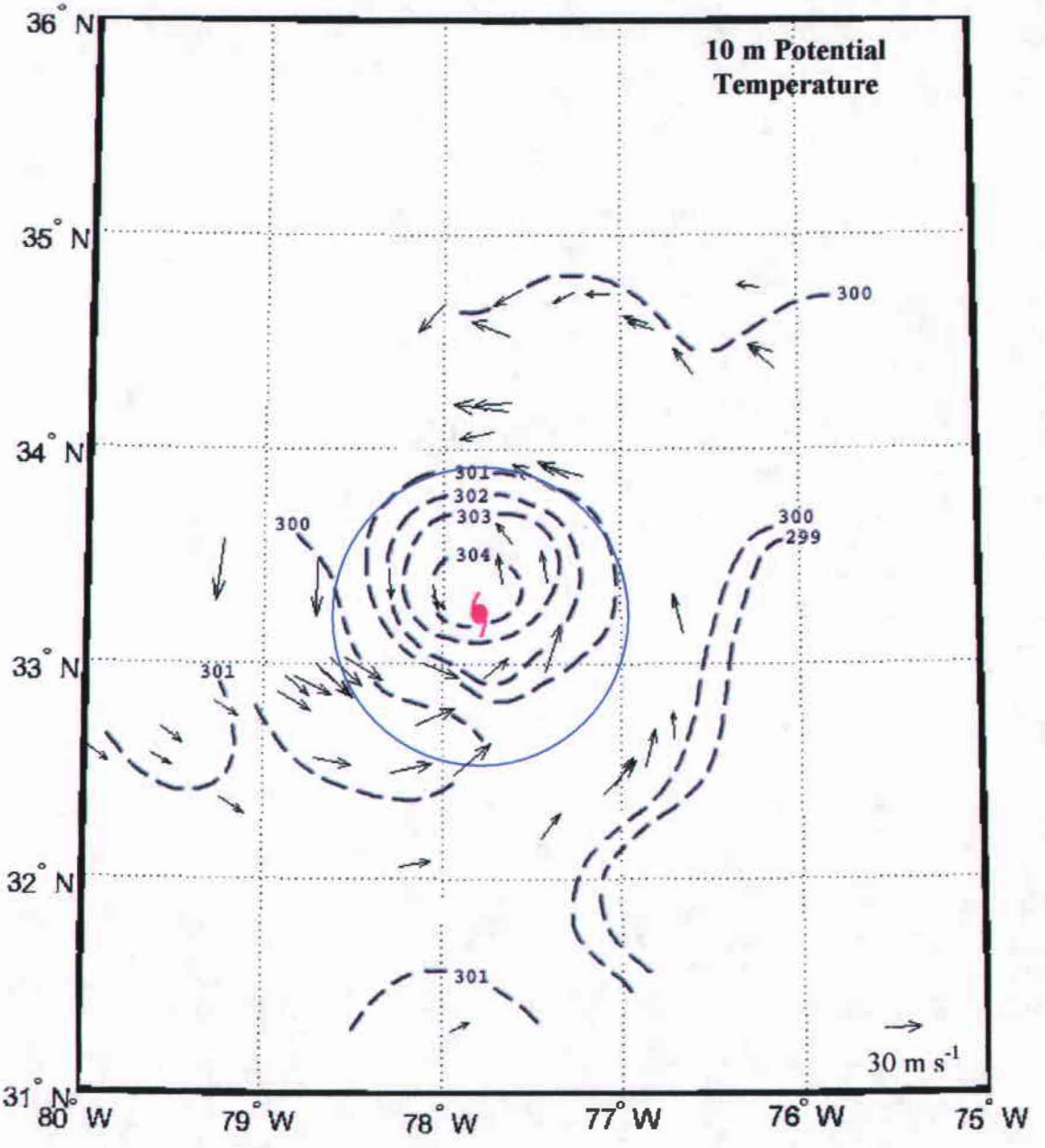

B.3.1. Storm-relative composite of Bonnie's potential temperature (K) at 10 m. The red symbol denotes the storm center and the blue ring is Bonnie's approximate eyewall location at 1730 Z, the time of this composite. The black arrows represent the wind speed and direction at 10 m. The scale is indicated to the lower right side of the image.

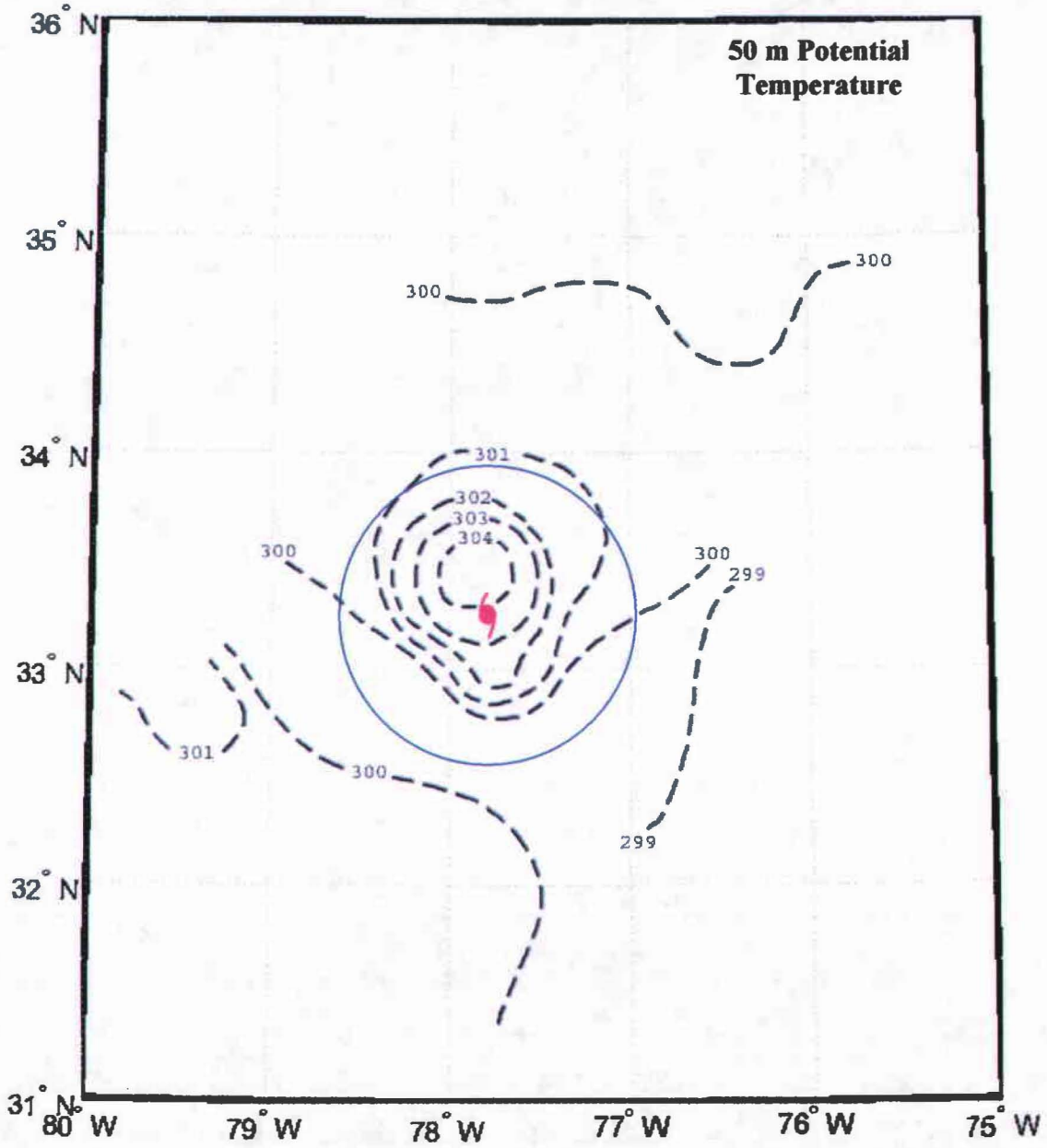

B.3.2. Similar to B.3.1., but at 50 m.

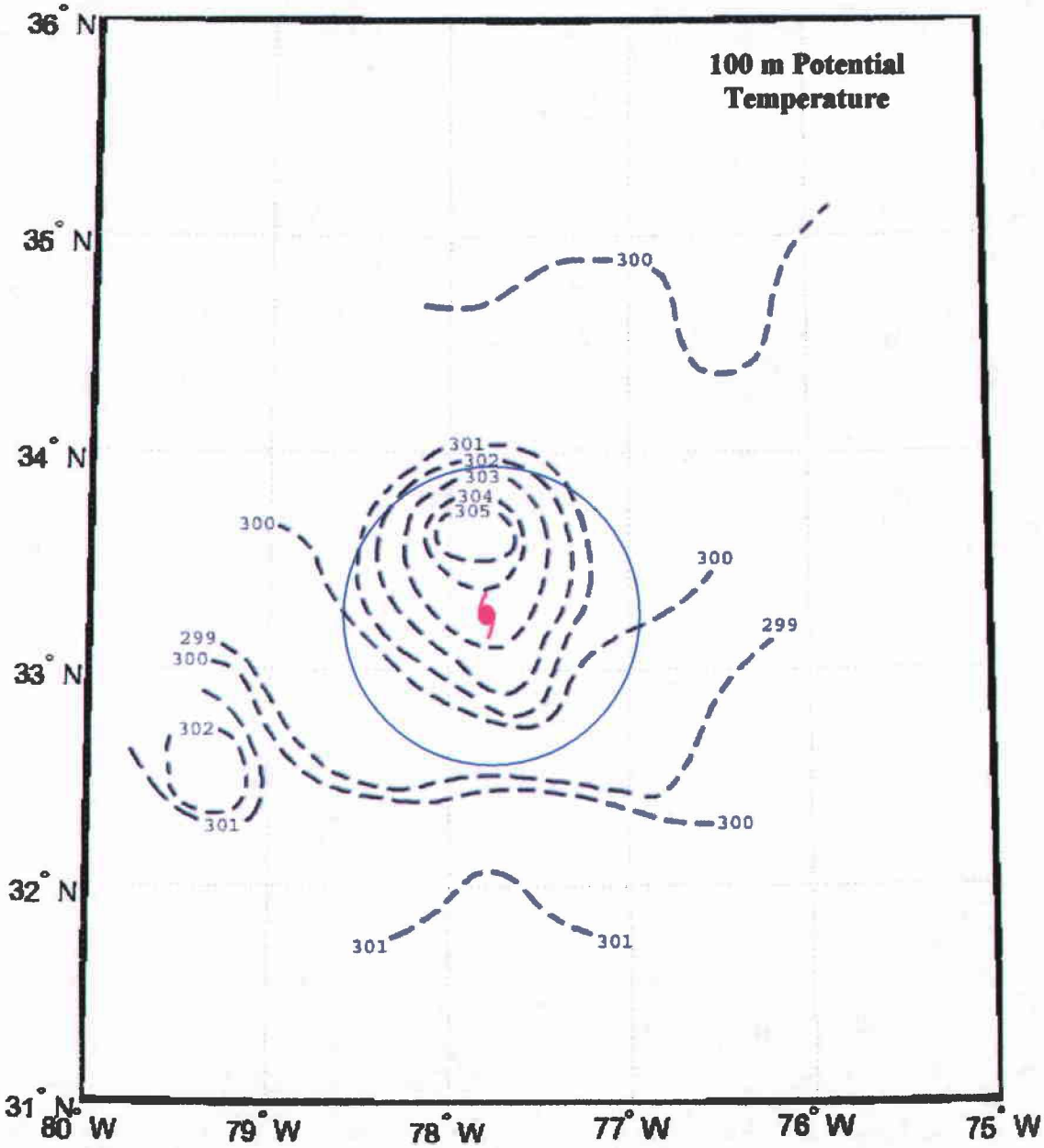

B.3.3. Similar to B.3.1., but at 100 m.

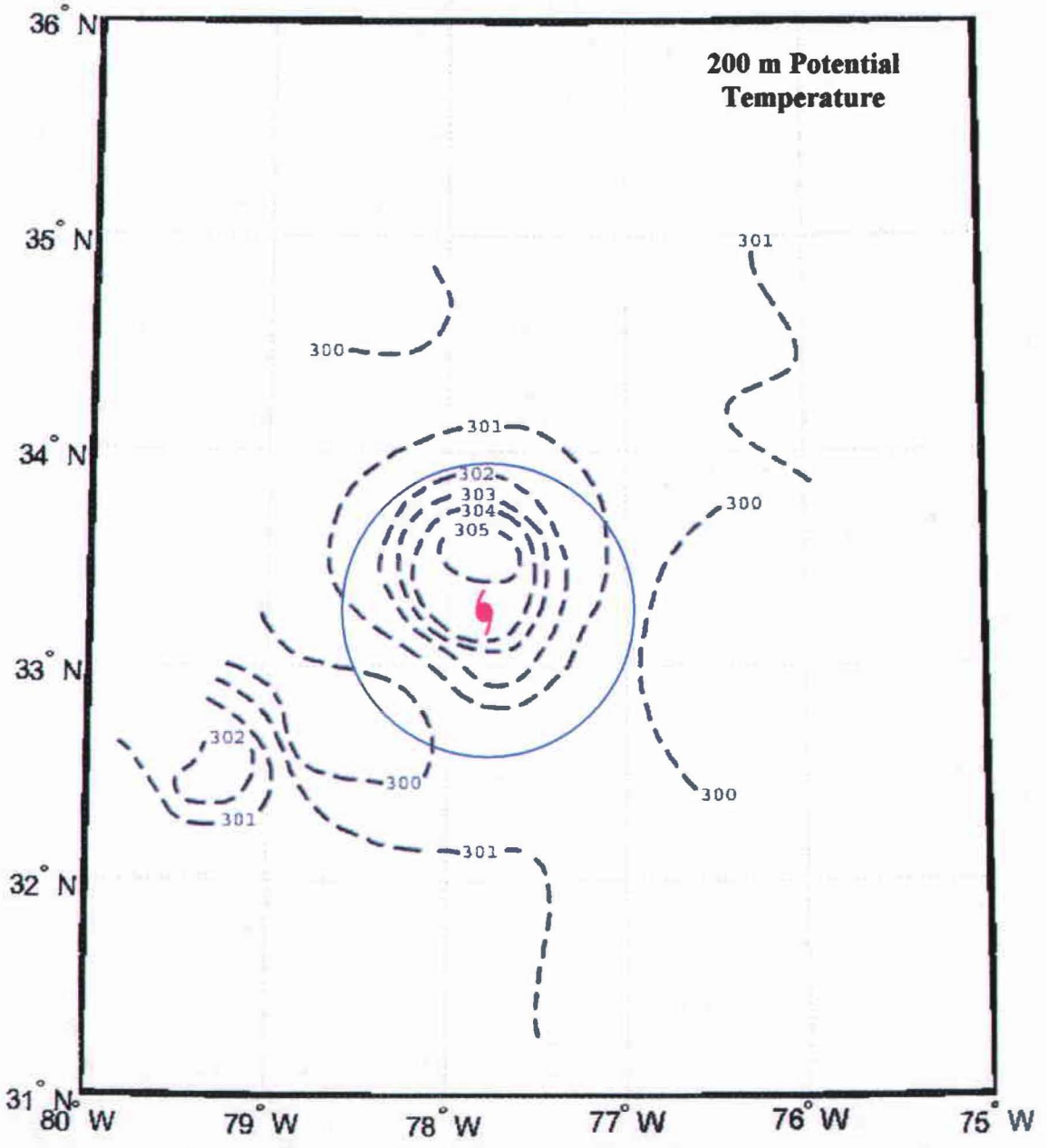

B.3.4. Similar to B.3.1., but at 200 m.

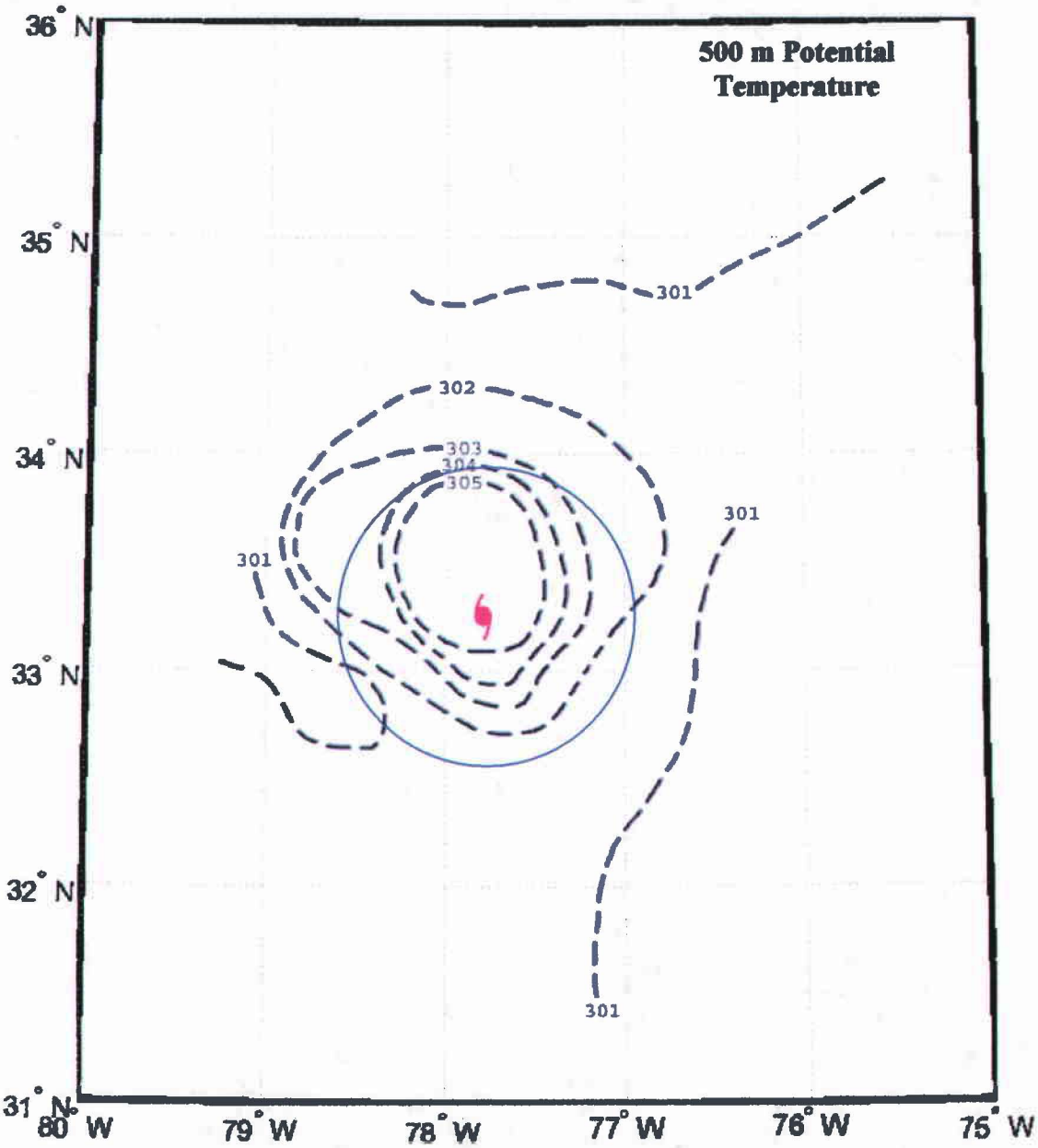

B.3.5. Similar to B.3.1., but at 500 m.

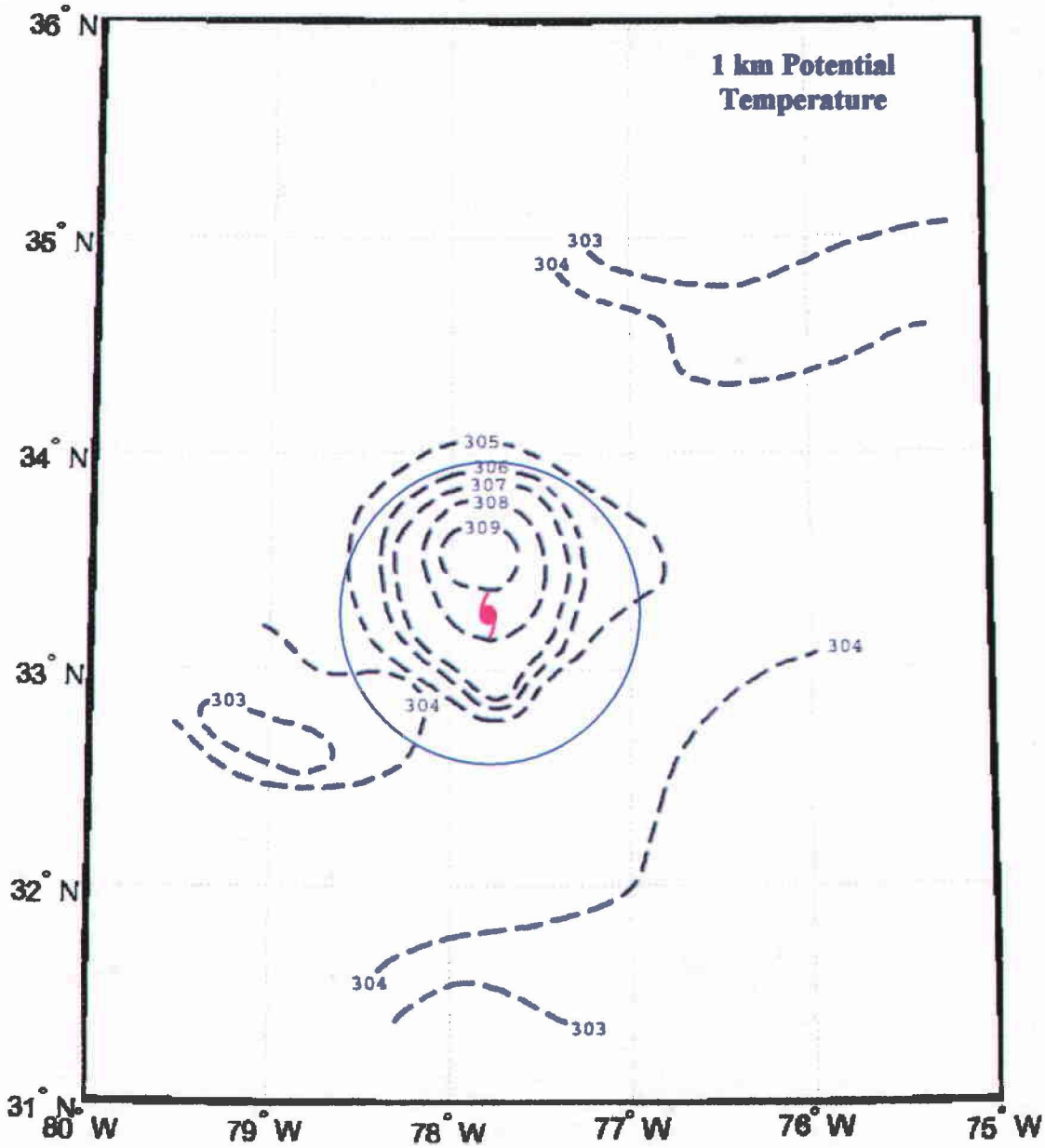

B.3.6. Similar to B.3.1., but at 1 km.

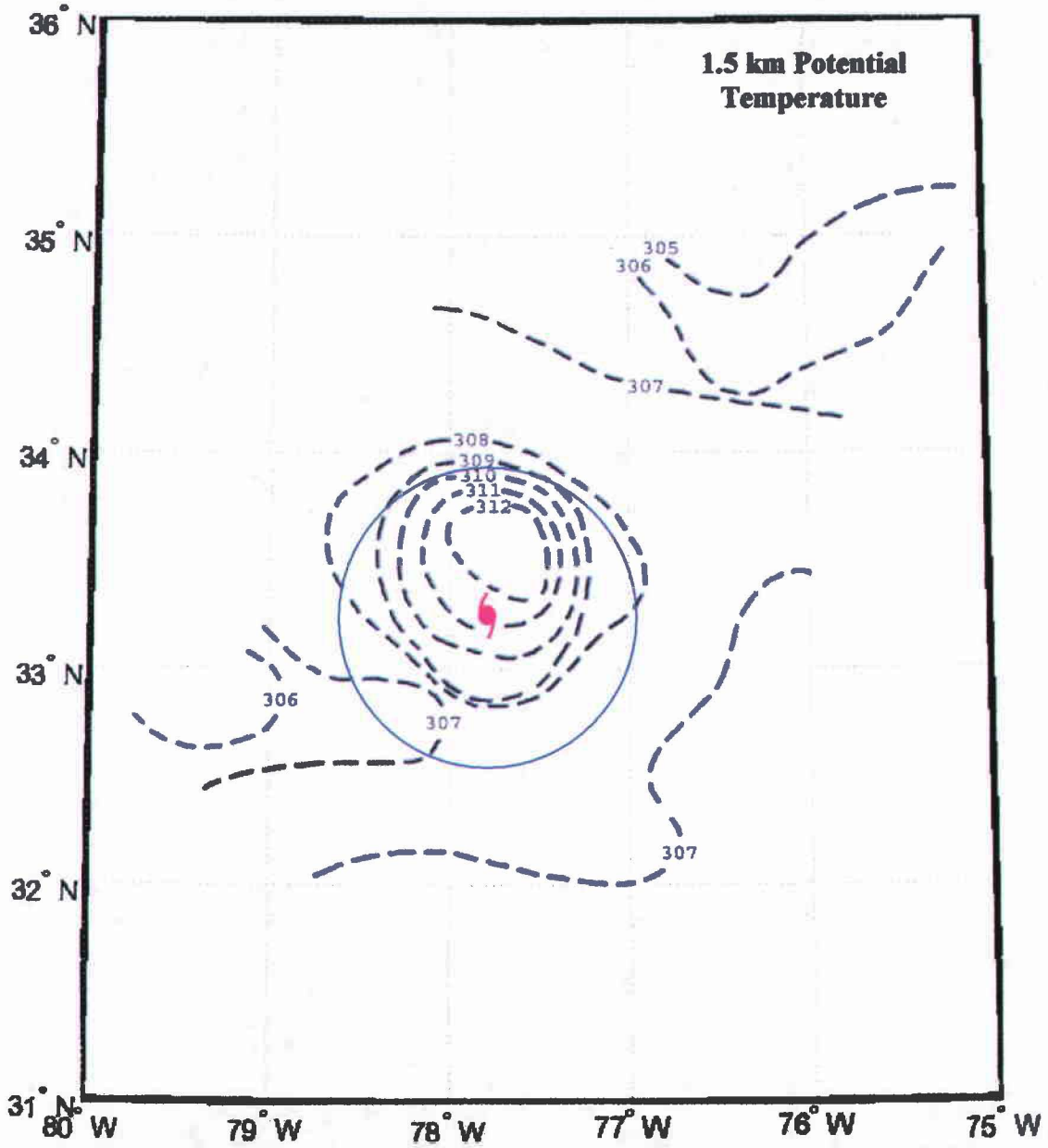

B.3.7. Similar to B.3.1., but at 1.5 km.

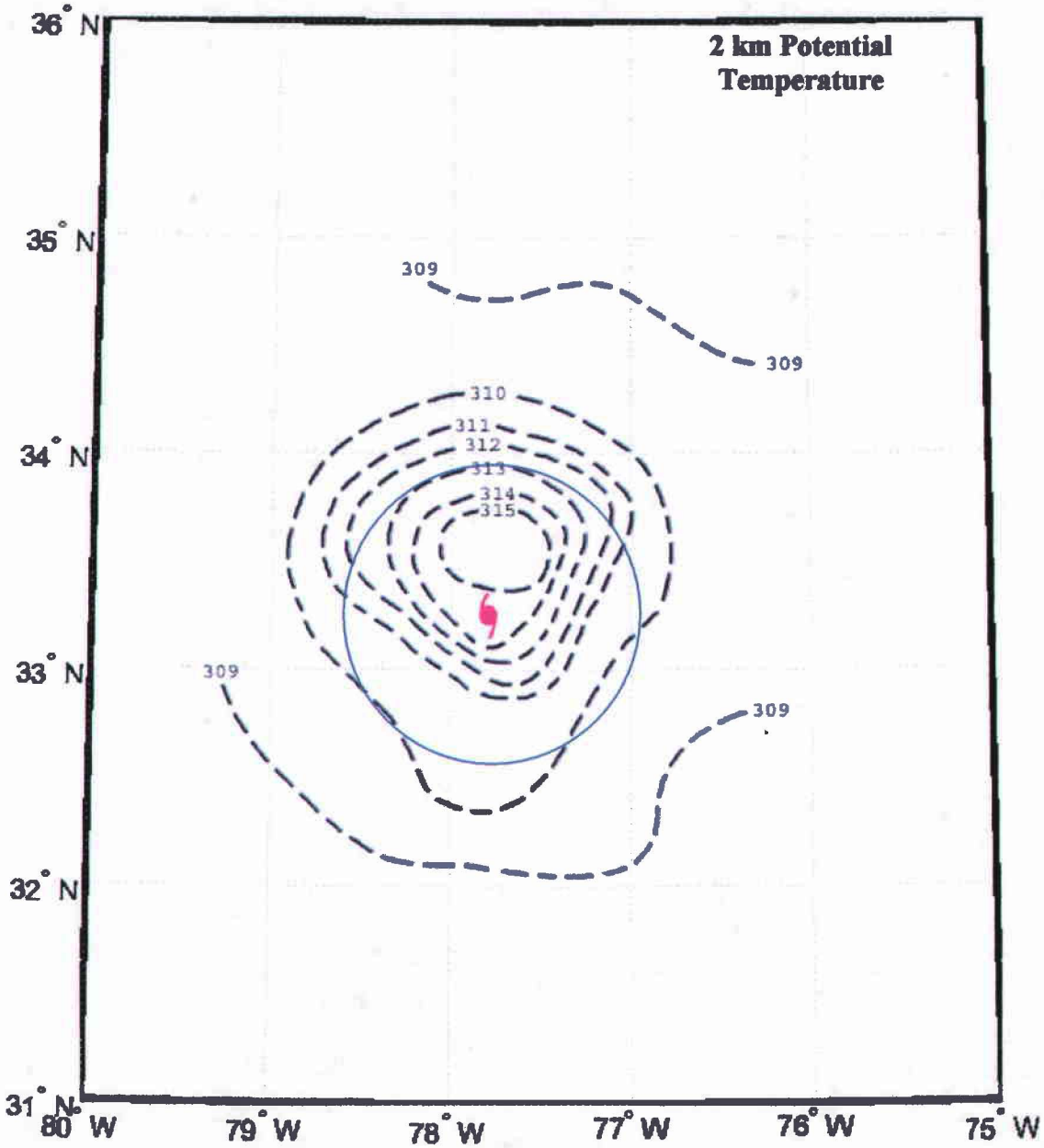

B.3.8. Similar to B.3.1., but at 2 km.

B.4. Equivalent Potential Temperature (K)

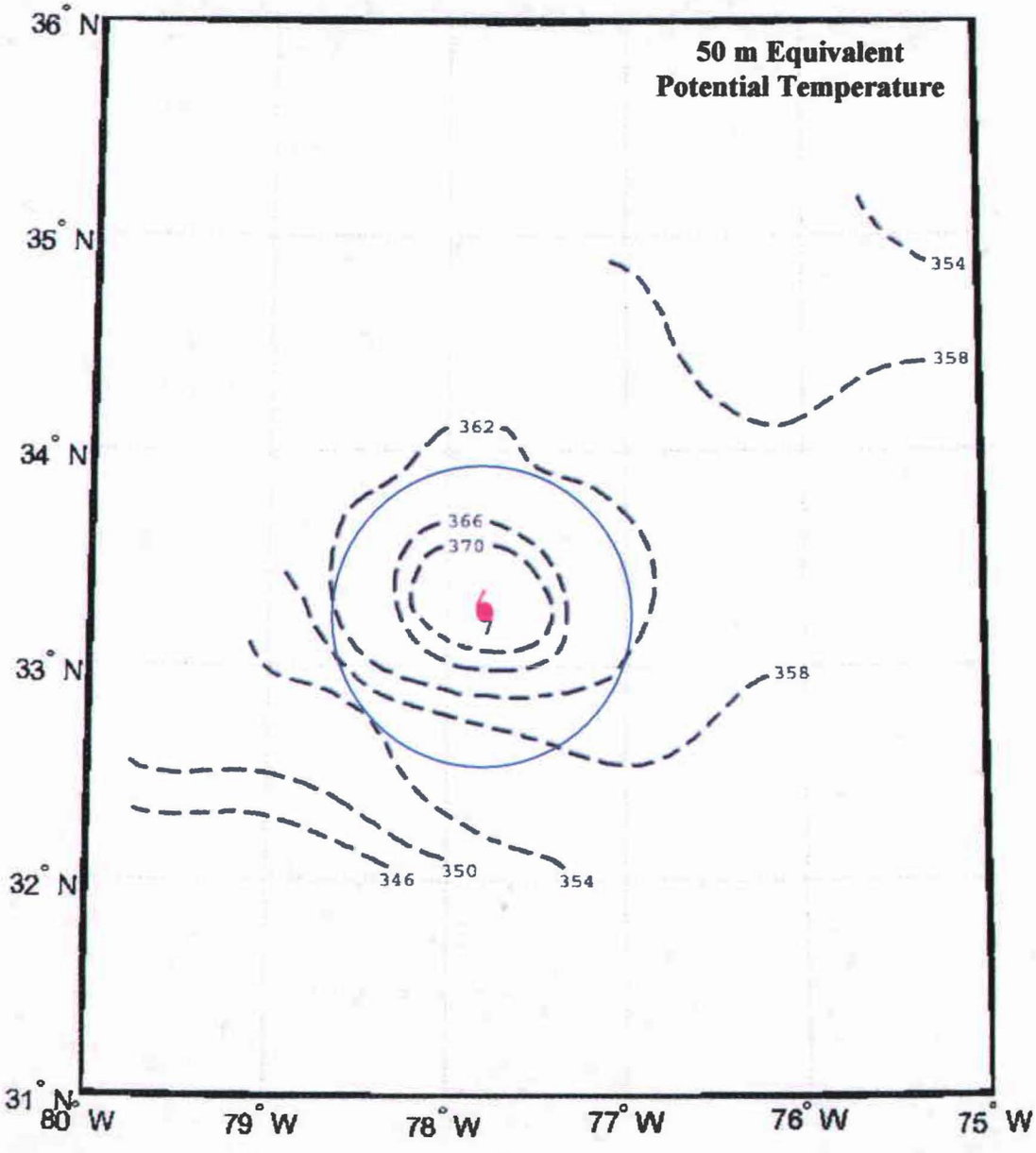

B.4.1. Storm-relative composite of Bonnie's equivalent potential temperature (K) at 50 m. The red symbol denotes the storm center and the blue ring is Bonnie's approximate eyewall location at 1730 Z, the time of this composite.

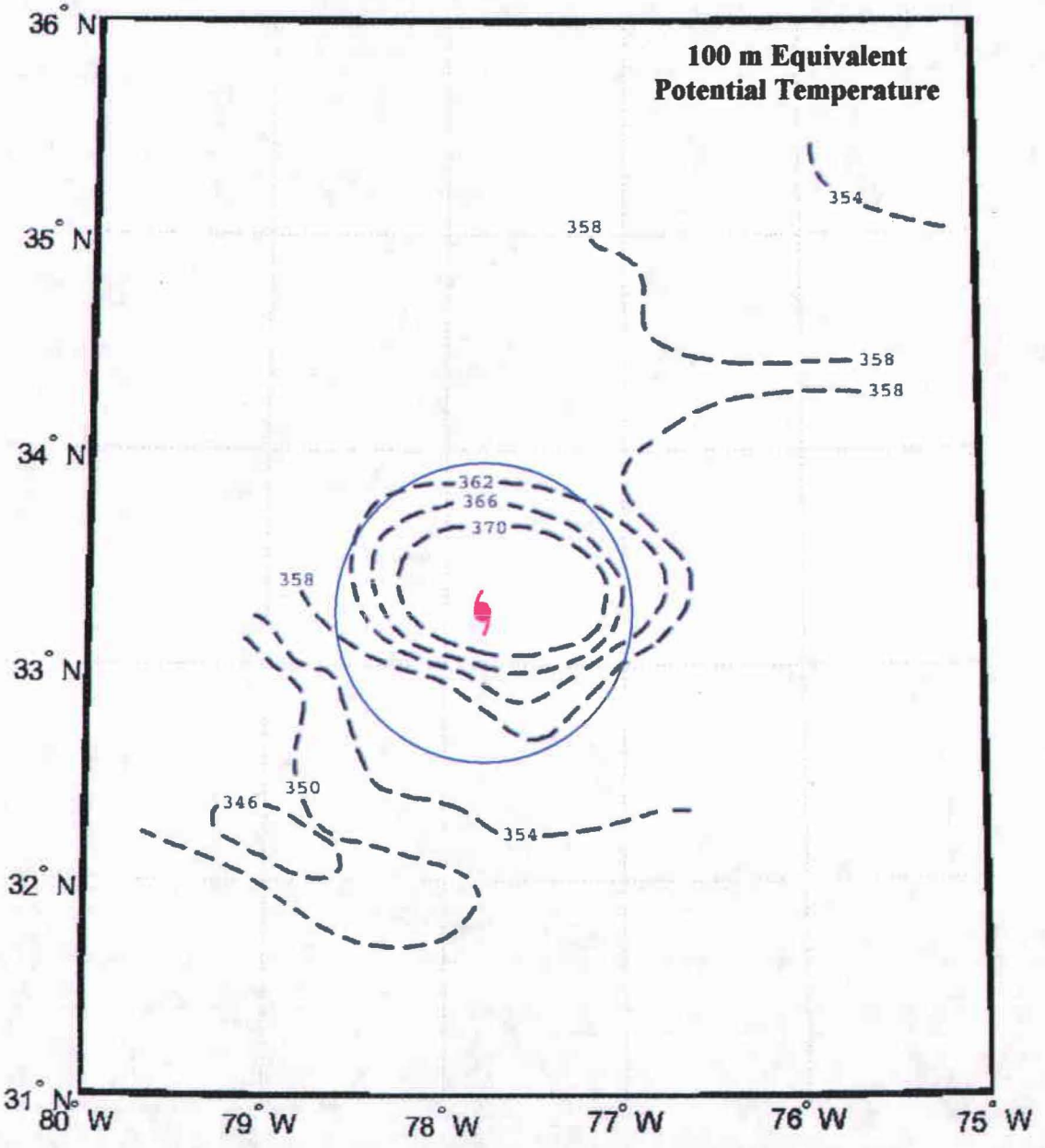

B.4.2. Similar to B.4.1., but at 100 m.

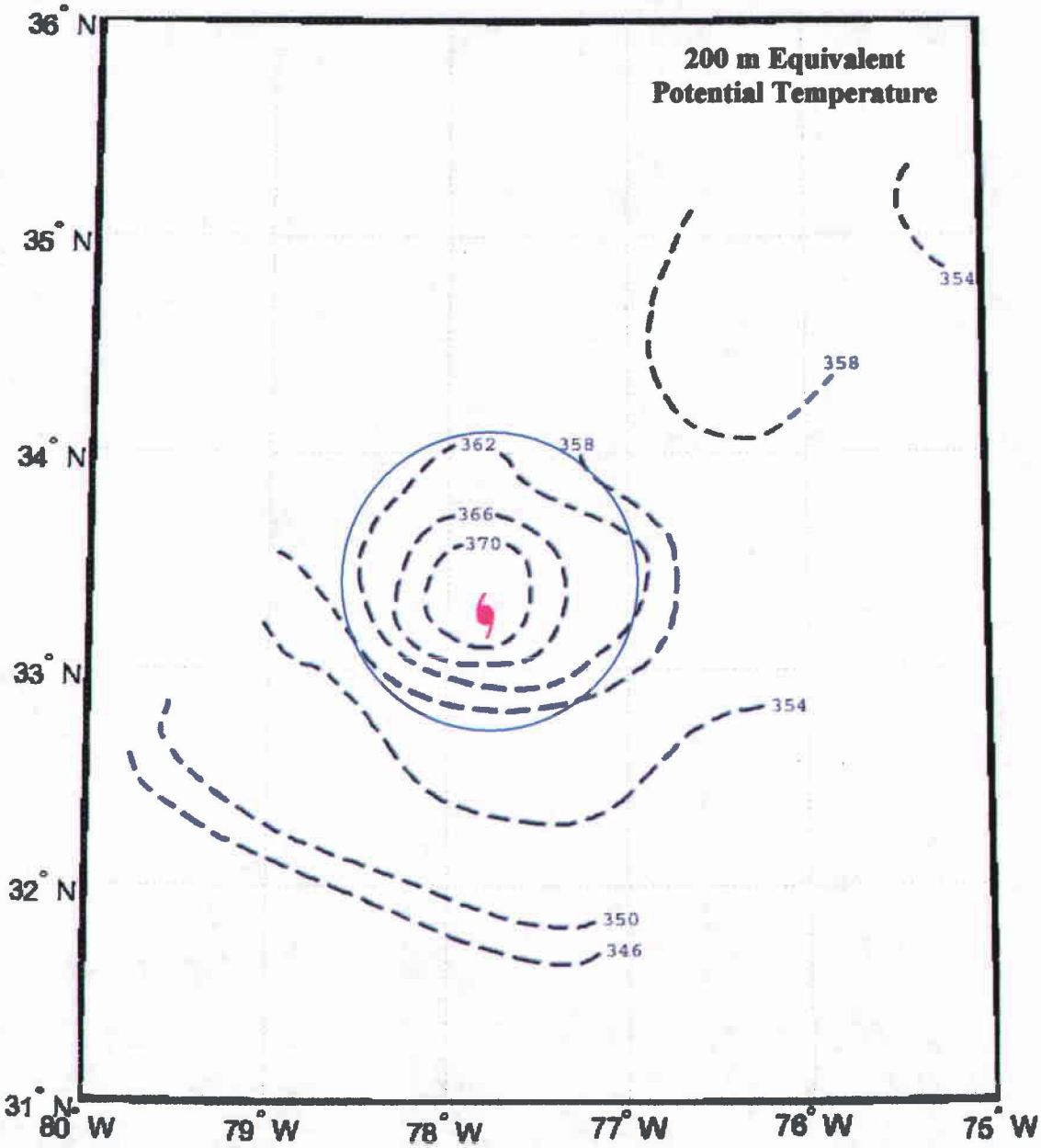

B.4.3. Similar to B.4.1., but at 200 m.

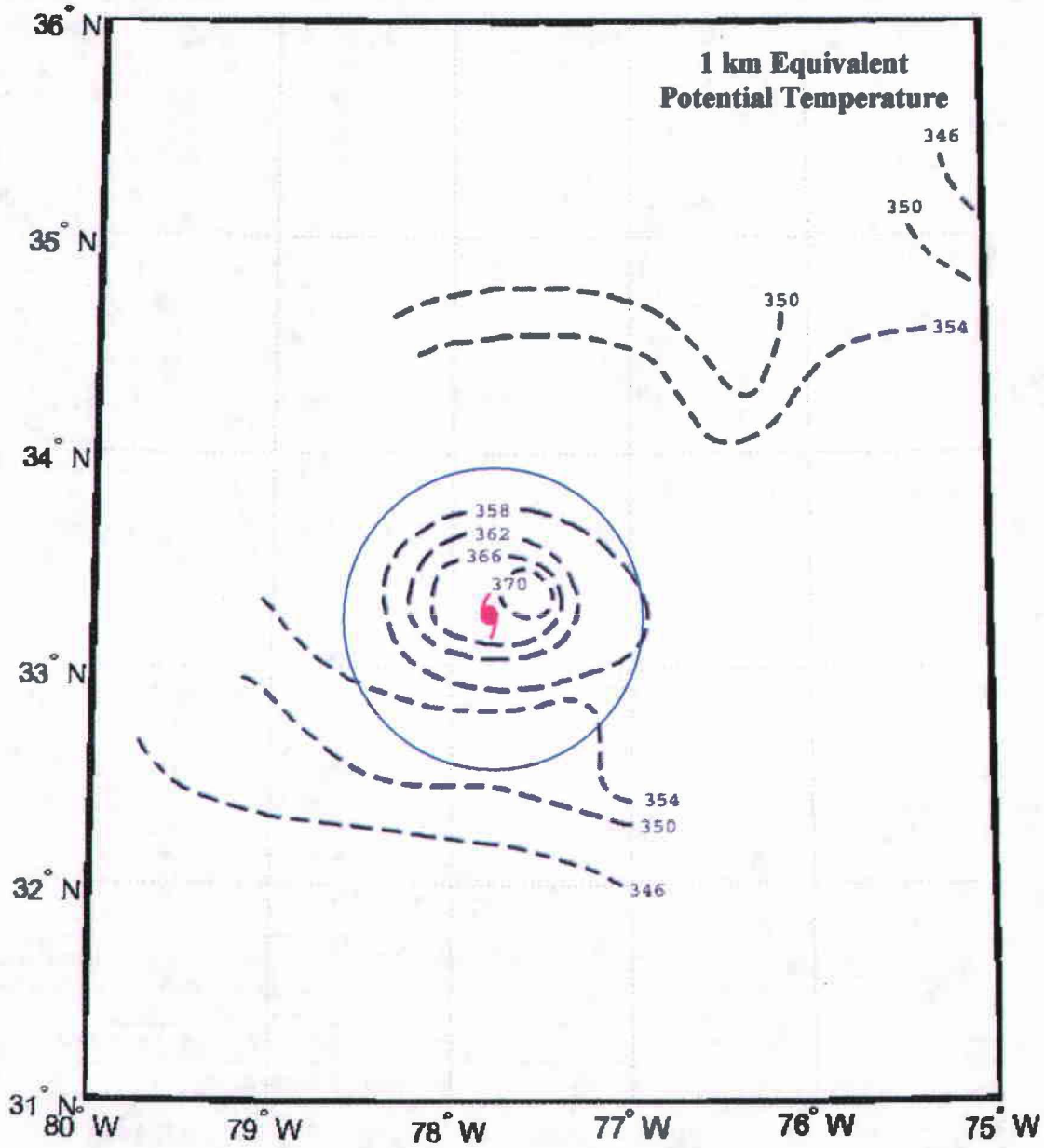

B.4.4. Similar to B.4.1., but at 1 km.

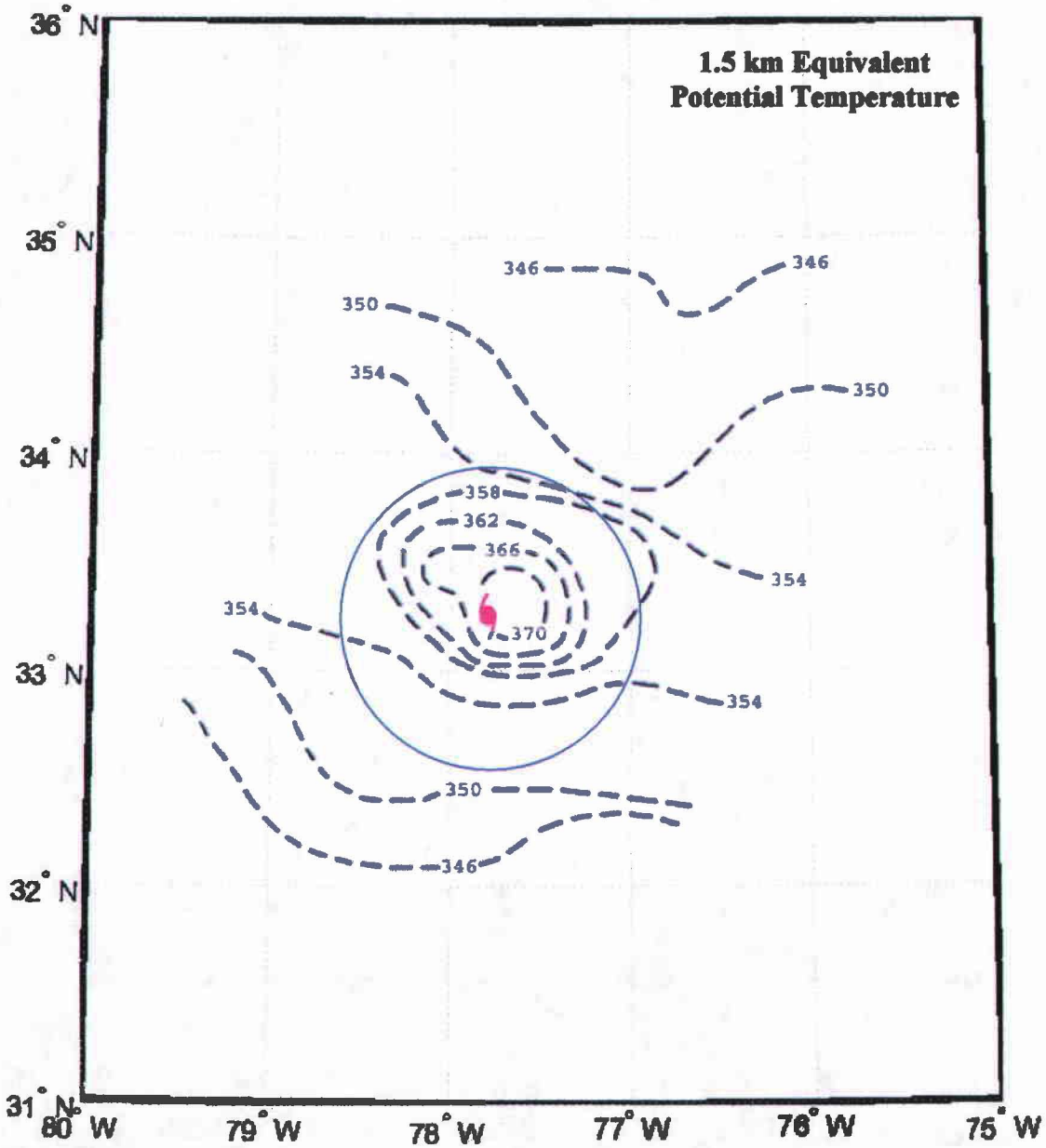

B.4.5. Similar to B.4.1., but at 1.5 km.

B.5. Radial Wind Speed (m s^{-1})

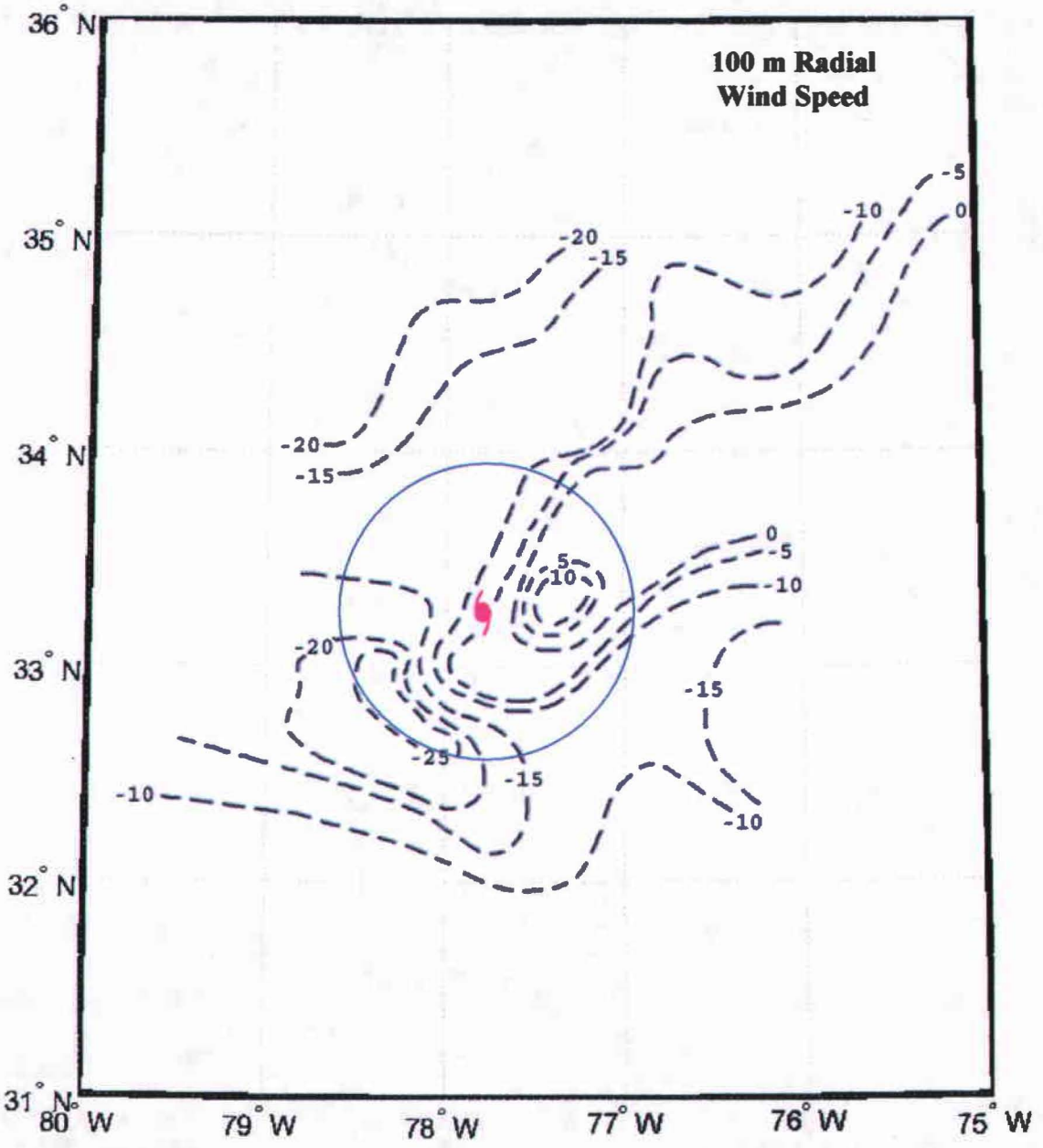

B.5.1. Storm-relative composite of Bonnie's radial wind speed (m s^{-1}) at 100 m. The red symbol denotes the storm center and the blue ring is Bonnie's approximate eyewall location at 1730 Z, the time of this composite. Negative values imply inflow.

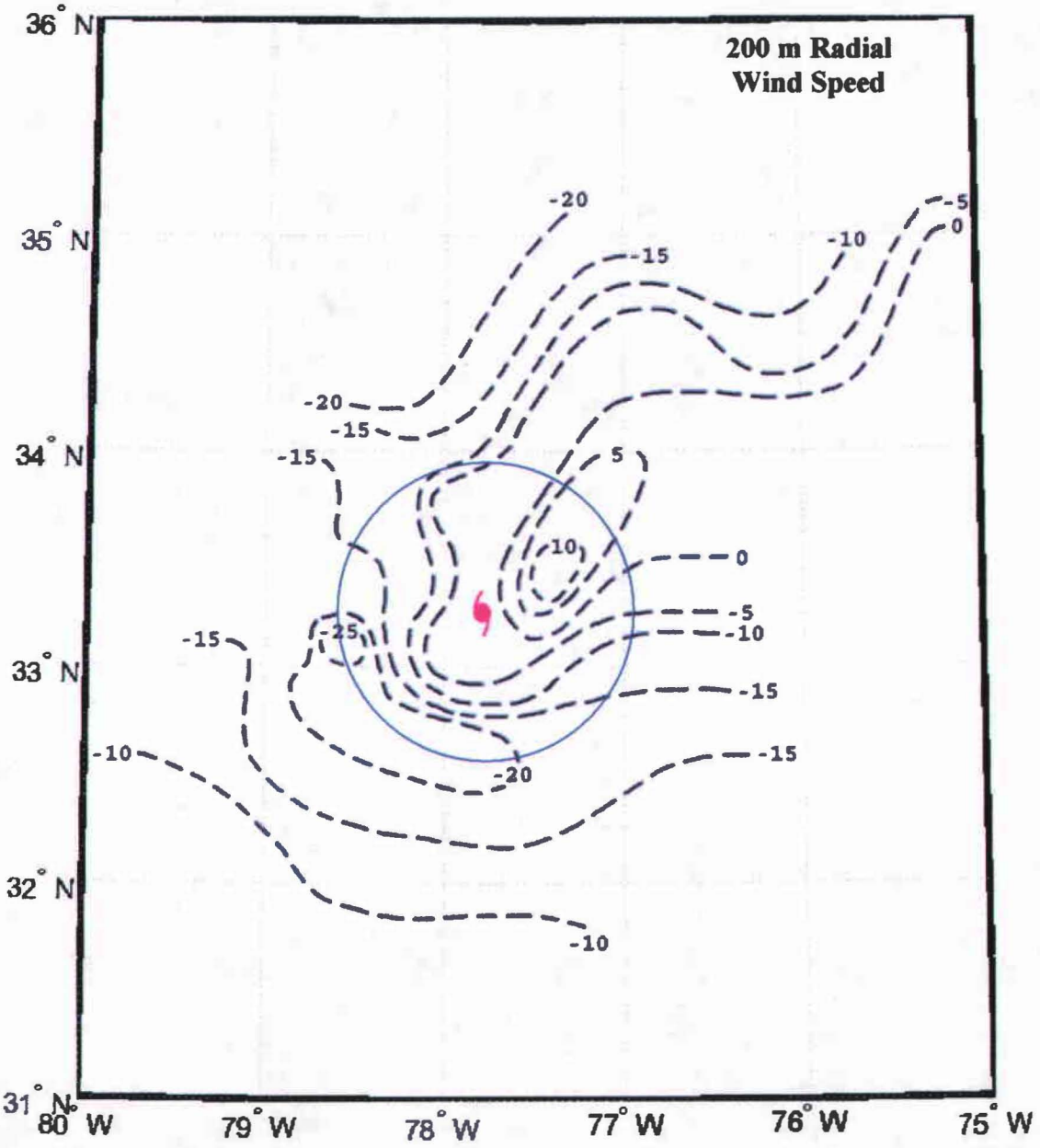

B.5.2. Similar to B.5.1., but at 200 m.

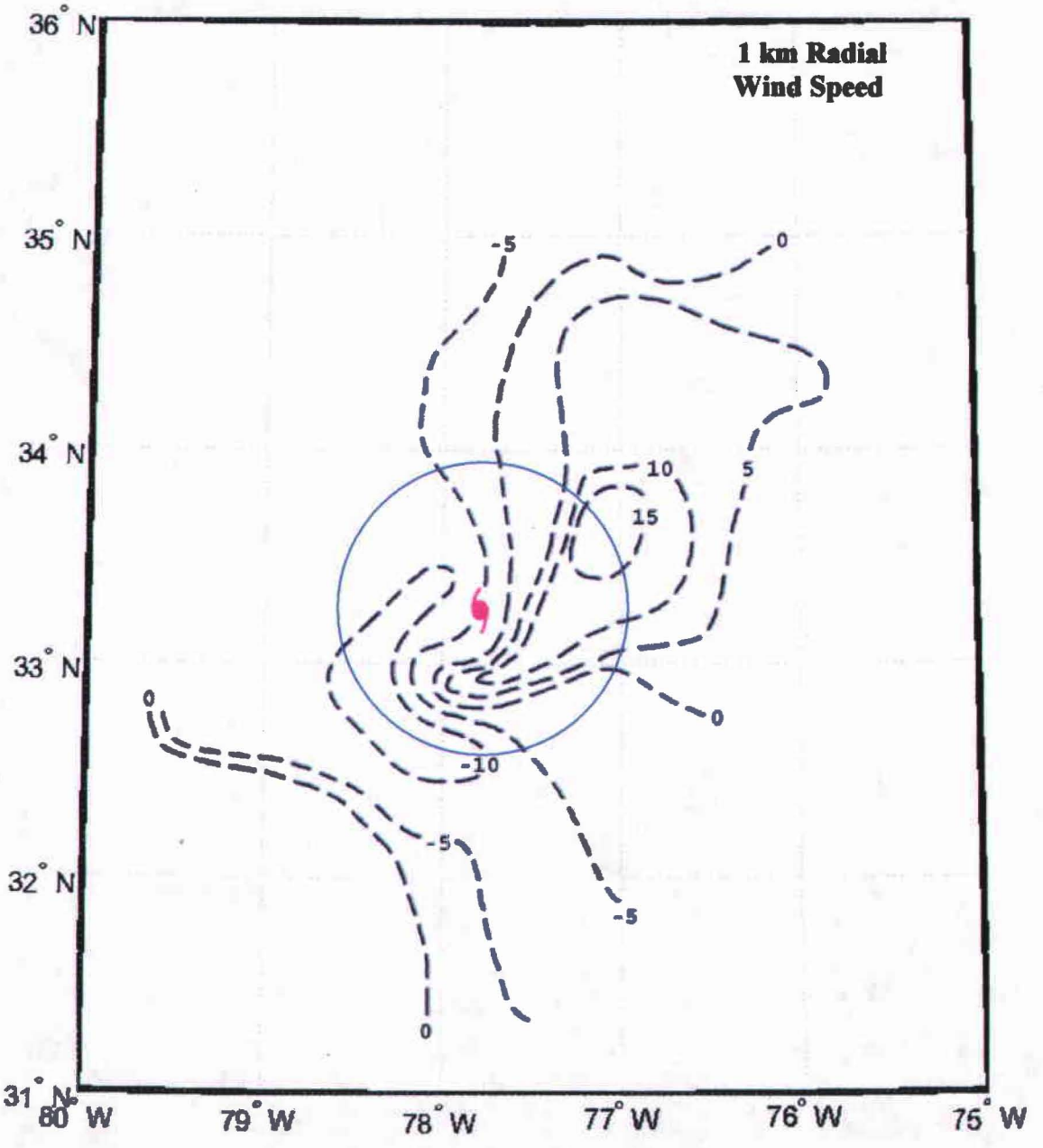

B.5.3. Similar to B.5.1., but at 1 km.

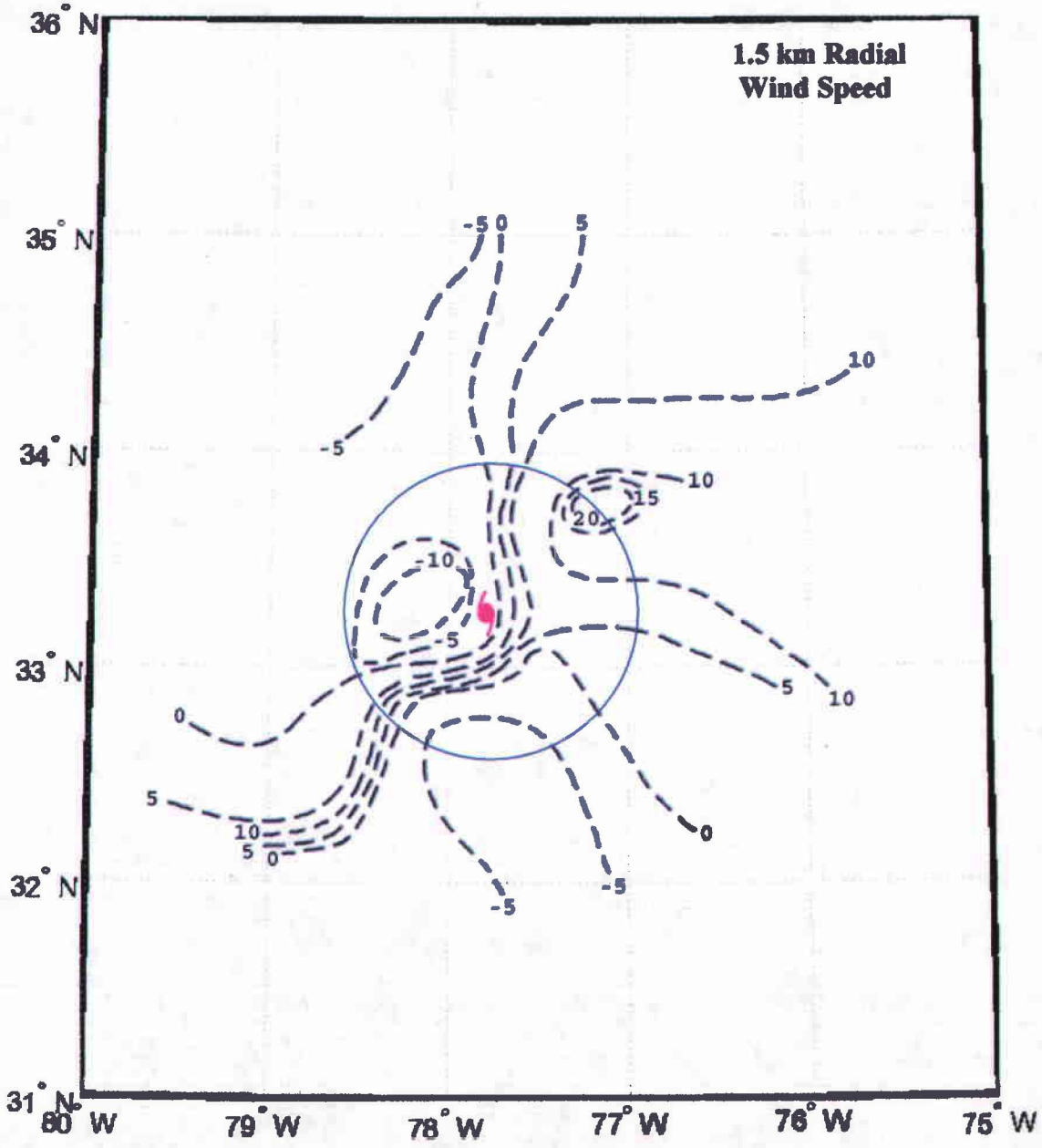

B.5.4. Similar to B.5.1., but at 1.5 km.

B.6. Tangential Wind Speed (m s^{-1})

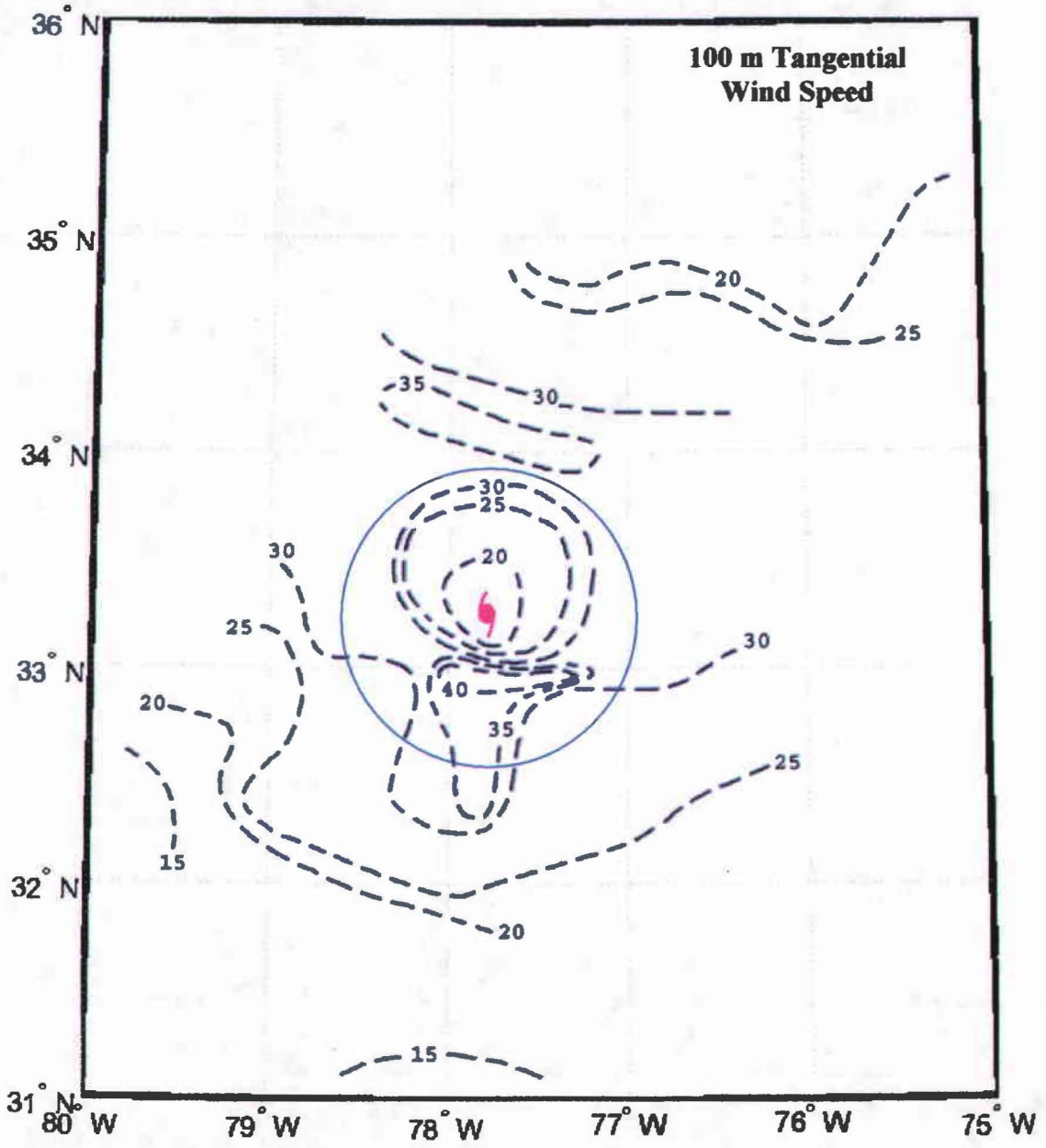

B.6.1. Storm-relative composite of Bonnie's tangential wind speed (m s^{-1}) at 100 m. The red symbol denotes the storm center and the blue ring is Bonnie's approximate eyewall location at 1730 Z, the time of this composite.

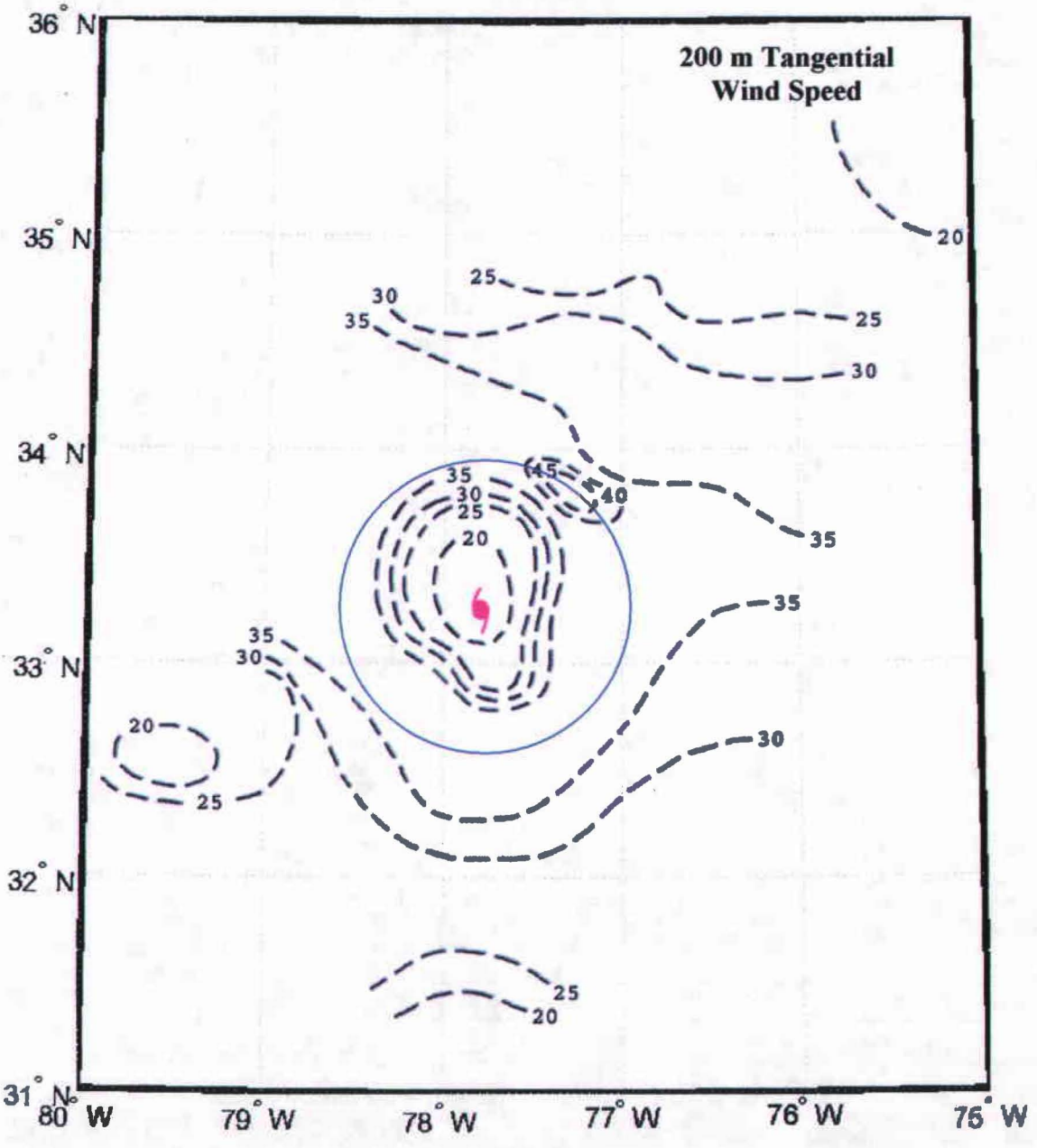

B.6.2. Similar to B.6.1., but at 200 m.

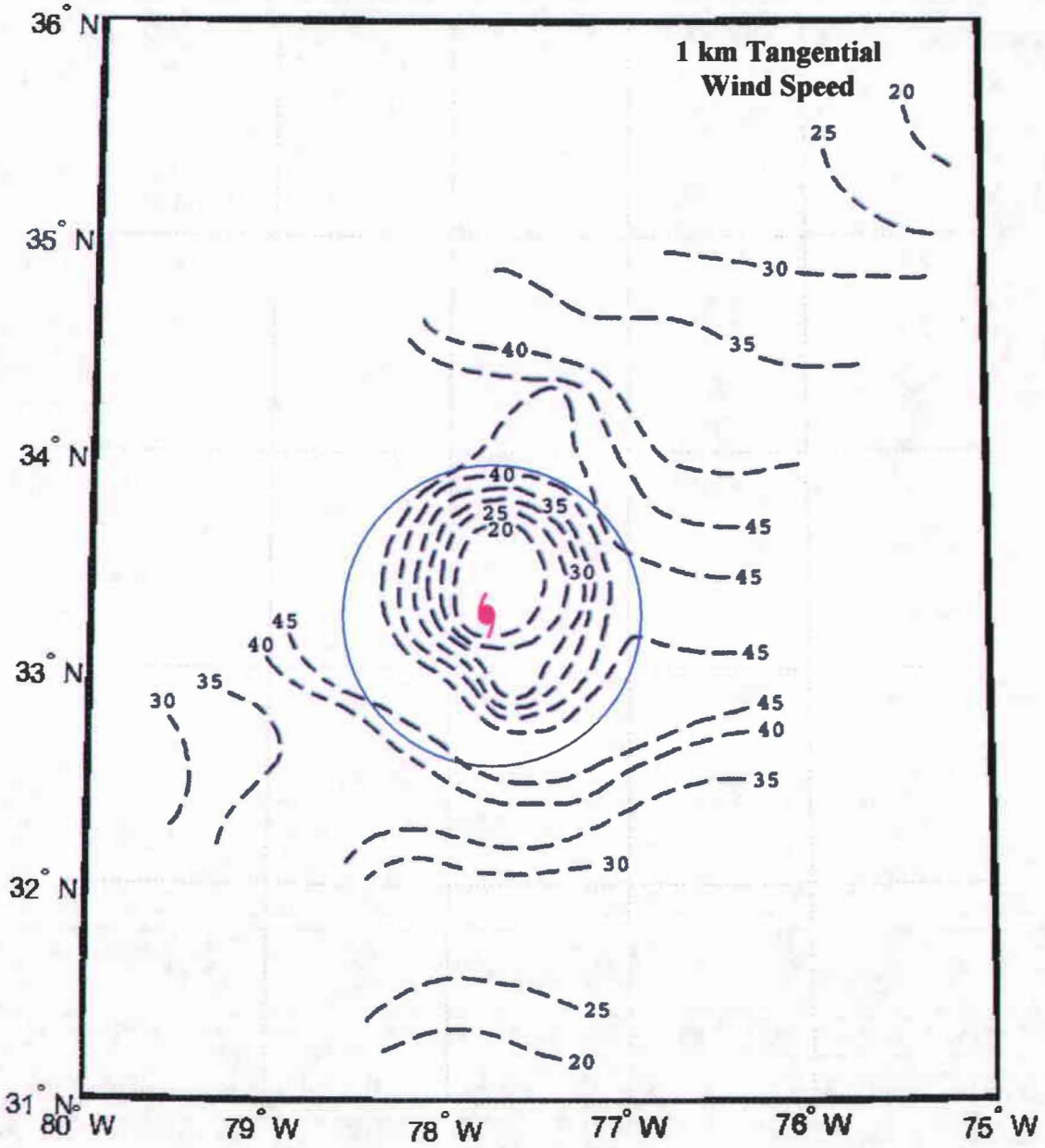

B.6.3. Similar to B.6.1., but at 1 km.

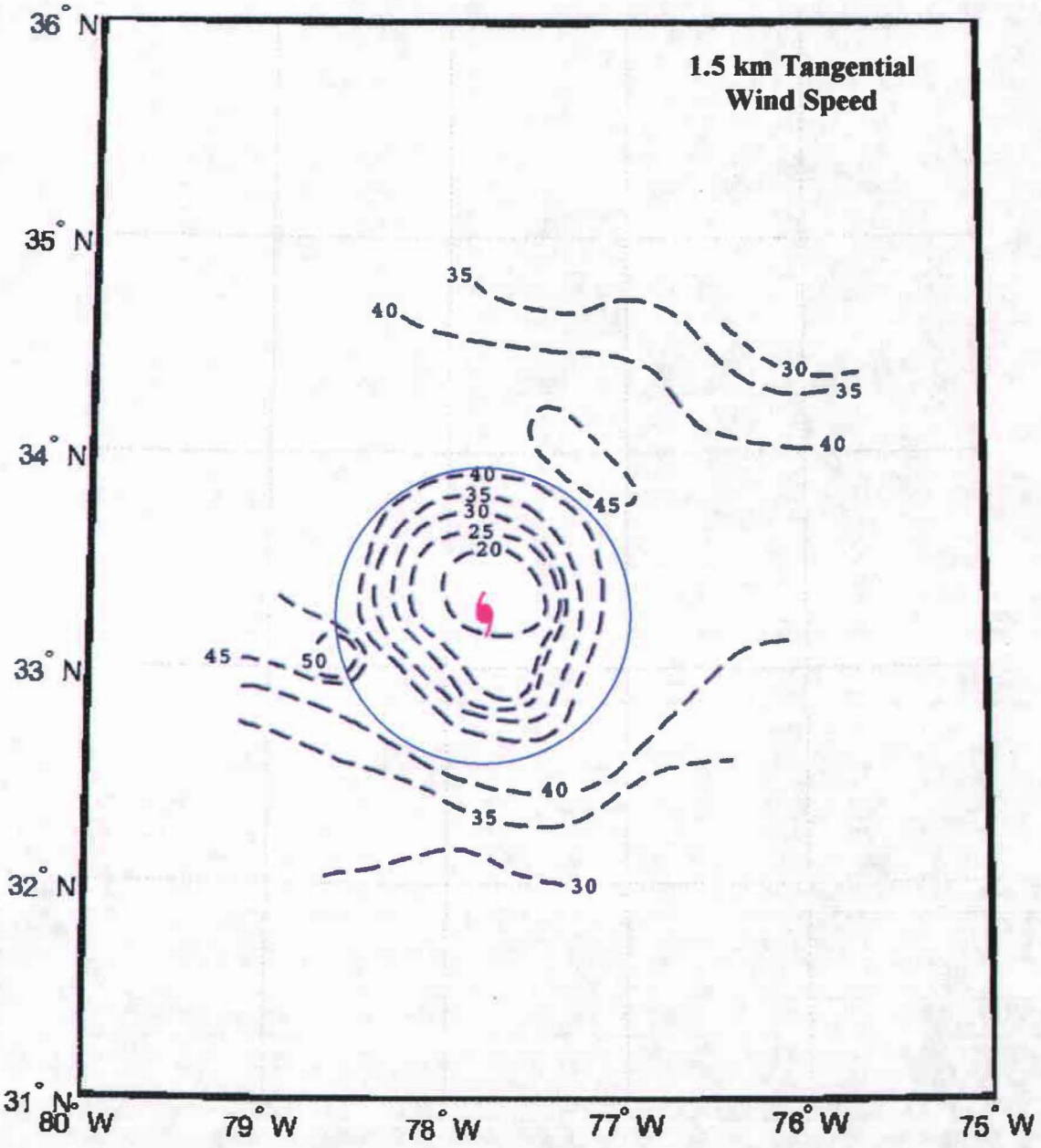

B.6.4. Similar to B.6.1., but at 1.5 km.

REFERENCES

Andreas, Edgar L., 1995: The temperature of evaporating sea spray droplets. *J. Atmos. Sci.*, **52**, 852-862.

Barnes, G. M., and P. B. Bogner, 2001: Comments on "Surface observations in the hurricane environment". *Mon. Wea. Rev.*, **129**, 1267-1269.

Black, P. G., and G. J. Holland, 1995: The boundary layer of Tropical Cyclone Kerry (1979). *Mon. Wea. Rev.*, **123**, 2007-2028.

Bogner, P. B., G. M. Barnes, and J. L. Franklin, 2000: Conditional instability and shear for six hurricanes over the Atlantic Ocean. *Wea. Forecasting*, **15**, 192-207.

Bolton, D., 1980: The computation of equivalent potential temperature. *Mon. Wea. Rev.*, **108**, 1046–1053.

Cione, J. J., P. G. Black, and S. H. Houston, 2000: Surface observations in the hurricane environment. *Mon. Wea. Rev.*, **128**, 1550-1561.

Dunion, J.P., C. W. Landsea, S. H. Houston, and M.D. Powell, 2003: A reanalysis of the surface winds for Hurricane Donna of 1960. *Mon. Wea. Rev.*, **131**, 1992-2011.

Emanuel, K. A., 1986: An air-sea interaction theory for tropical cyclones. Part I: Steady-state maintenance. *J. Atmos. Sci.,* **43**, 585–605.

Hanley, D., J. Molinari, and D. Keyser, 2001: A composite study of the interactions between tropical cyclones and upper-tropospheric troughs. *Mon. Wea. Rev.*, **129**, 2570-2584.

Hawkins, H. F., and S. M. Imbembo, 1976: The structure of a small, intense hurricane, Inez (1966). *Mon. Wea. Rev.*, **104**, 418-442.

Hock, T.F., and J.L. Franklin, 1999: The NCAR GPS dropwindsonde. *Bull. Amer. Meteor. Soc.*, **80**, 407-420.

Houston, S.H., and M.D. Powell, 2003: Surface wind fields for Florida Bay Hurricanes. *J. Coastal Res.*, **19**, 503-513.

Jarvinen, B.R., C. J. Neumann, and M.A.S. Davis, 1984: *A tropical cyclone data tape for the North Atlantic Basin, 1886-1983: Contents, limitations, and uses*. Miami, Florida: Tropical Prediction Center, NOAA Technical Memorandum, NWS-NHC-22, 21p.

Jordan, C. L., 1958: Mean soundings for the West Indies area. *J. Meteor.*, **15**, 91-97.

Jorgensen, D. P., 1984b: Mesoscale and convective-scale characteristics of mature hurricanes. Part II: Inner core structure of Hurricane Allen (1980). *J. Atmos. Sci.*, **41**, 1287-1311.

Kepert, J.D., 2002: The wind-field structure of the tropical cyclone boundary layer. Ph.D. thesis, Dept. of Mathematics and Statistics, Monash University, 350 pp. [Available from Dept. of Mathematics and Statistics, Monash University, Vic 3800, Australia.]

Korolev, V.S., S. A. Petrichenko, and V.D. Pudov, 1990: Heat and moisture exchange between the ocean and atmosphere in tropical storms Tess and Skip. *Meteorologiya i Gidrologiya*, **2**, 108-111. (English translation in *Soviet Meteorology and Hydrology*, **2**, 92-94.)

Marks, F. D., Jr., 1985: Evolution of the structure of precipitation in Hurricane Allen (1980). *Mon. Wea. Rev.*, **113**, 909-930.

Miller, B. I., 1964: A study of the filling of Hurricane Donna (1960) over land. *Mon. Wea. Rev.*, **92**, 389-406.

Powell, M. D., 1980: Evaluations of diagnostic marine boundary layer models applied to hurricanes. *Mon. Wea. Rev.*, **108**, 757-766.

——, 1982: The transition of the Hurricane Frederic boundary layer wind field of the open Gulf of Mexico to landfall. *Mon. Wea. Rev.*, **110**, 1912-1932.

——, 1987: Changes in the low-level kinematic and thermodynamic structure of Hurricane Alicia (1983) at landfall. *Mon. Wea. Rev.*, **115**, 75-99.

——, P. P. Dodge, and M. L. Black, 1991: The landfall of Hurricane Hugo in the Carolinas: Surface wind distribution. *Wea. Forecasting*, **6**, 379-399.

——, and S. H. Houston, 1996: Hurricane Andrew's landfall in south Florida. Part II: Surface wind fields and potential real-time applications. *Wea. Forecasting*, **11**, 329-349.

Riehl, H., 1963: Some relations between the wind and thermal structure of steady state hurricanes. *J. Atmos. Sci.*, **20**, 276-287.

Samsury, C. E., and E. J. Zipser, 1995: Secondary Wind Maxima in Hurricanes: Airflow and Relationship to Rainbands. *Mon. Wea. Rev.*, **123**, 3502–3517.

Sethu Raman, S., 1979: Atmospheric turbulence and storm surge due to Hurricane Belle (1976). *Mon. Wea. Rev.*, **107**, 314-321.

Shapiro, Lloyd J., 1983: The asymmetric boundary layer flow under a translating hurricane. *J. Atmos. Sci.*, **40**, 1984-1998.

Shea, D. J., and W. M. Gray, 1973: The hurricane's inner core region. I. Symmetric and asymmetric structure. *J. Atmos. Sci.*, **30**, 1544–1564.

Tuleya, R. E., 1994: Tropical storm development and decay: Sensitivity to surface boundary conditions. *Mon. Wea. Rev.*, **122**, 291-304.

——, and Y. Kurihara, 1978: A numerical simulation of the landfall of tropical cyclones. *J. Atmos. Sci.*, **35**, 242-257.

Willoughby, H.E., J.A. Clos, and M.G. Shoreibah, 1982: Concentric eye walls, secondary wind maxima, and the evolution of the hurricane vortex. *J. Atmos. Sci.*, **39**, 395-411.

Wroe, D.R., and G. M. Barnes 2001: Inflow layer energetics of Hurricane Bonnie (1998) near landfall. *Mon. Wea. Rev.*, **131**, 1600-1612.